الجمهورية الجزائرية الديمقراطية الشعبية

People's Democratic Republic of Algeria

وزارة التعليم العالي والبحث العلمي

Ministry of Higher Education and Scientific Research

جامعة عين تموشنت - بلحاج بوشعيب

Ain Témouchent University – Belhadj Bouchaib

Faculty of Science and Technology

Department of Mechanical Engineering

End-of-Study Project

For the award of the Master degree

Field: Science and Technology

Major: Mechanical Engineering

Specialty: Mechanical Construction

Topic:

Finite Element Analysis of Crack and Scratch Defect Interaction in a Buried API X80 Pipeline

Prepared by:

– LAMRI SIDAHMED EL MAHDI

Before the jury composed of:

Mr. BAHRAM KADDOUR	UAT.B.B (Ain Témouchent)	President
Mr. BELHENINI SOUFYANE	UAT.B.B (Ain Témouchent)	Examiner
Mm. BELGHOUL HAKIMA	UAT.B.B (Ain Témouchent)	Examiner
Mr. OUDAD WAHID	UAT.B.B (Ain Témouchent)	Supervisor

2025/2026

Acknowledgments

We would like to first express our deepest gratitude to Almighty God for granting us the strength and courage to complete this work.

We also extend my sincere appreciation to my parents for their encouragement, support, and the sacrifices they have endured for us.

Our thanks also go to all the professors of the Department of Mechanical Engineering who contributed to our education and training.

.

Dedication

I dedicate this work to my beloved parents, whose support, sacrifices, and encouragement have been the foundation of my success throughout my academic journey.

To my family, for their patience, understanding, and constant motivation during the completion of this work.

To my teachers and professors, whose guidance and knowledge have contributed greatly to my education and personal development.

To my friend 7 and colleagues, who provided support, encouragement, and valuable assistance throughout this project.

Finally, I dedicate this work to everyone who contributed, directly or indirectly, to the realization of this dissertation.

Sidahmed EL Mahdi

Abstract

The structural integrity of oil and gas pipelines is strongly influenced by the presence of defects that may develop during manufacturing, installation, or service. Among these defects, cracks and scratches are considered critical because they create stress concentrations that can reduce the load-carrying capacity of the pipeline and increase the risk of failure. Understanding the interaction between such defects is therefore essential for ensuring safe and reliable pipeline operation.

This work investigates the interaction between crack and scratch defects in a buried API 5L X80 steel pipeline using the Finite Element Method (FEM). Numerical simulations were performed with ABAQUS to analyze the influence of defect geometry, including crack depth, crack width, scratch depth, scratch width, and scratch orientation. The distributions of Von Mises stress, equivalent plastic strain (PEEQ), and J-integral were evaluated to characterize the mechanical and fracture behavior of the pipeline.

The results show that increasing defect dimensions leads to higher stress concentration and plastic deformation levels. Furthermore, the J-integral values increase with crack size, indicating a greater tendency for crack propagation. The study also highlights the influence of repair configurations on reducing the crack driving force and improving structural integrity.

The findings contribute to a better understanding of defect interaction mechanisms in high-strength pipeline steels and provide useful information for pipeline integrity assessment and maintenance strategies.

Résumé

L'intégrité structurelle des pipelines pétroliers et gaziers est fortement influencée par la présence de défauts pouvant apparaître lors de la fabrication, de l'installation ou de l'exploitation. Parmi ces défauts, les fissures et les rayures sont particulièrement critiques, car elles génèrent des concentrations de contraintes susceptibles de réduire la capacité portante du pipeline et d'augmenter le risque de rupture. La compréhension de l'interaction entre ces défauts est donc essentielle pour garantir la sécurité et la fiabilité des réseaux de transport.

Ce travail porte sur l'étude de l'interaction entre une fissure et une rayure dans un pipeline enterré en acier API 5L X80 à l'aide de la méthode des éléments finis (FEM). Les simulations numériques ont été réalisées sous ABAQUS afin d'analyser l'influence des paramètres géométriques des défauts, notamment la profondeur et la largeur de la fissure, ainsi que la profondeur, la largeur et l'orientation de la rayure. Les distributions de la contrainte de Von Mises, de la déformation plastique équivalente (PEEQ) et de l'intégrale J ont été évaluées afin de caractériser le comportement mécanique et la résistance à la rupture du pipeline.

Les résultats montrent que l'augmentation des dimensions des défauts entraîne une élévation des concentrations de contraintes et des déformations plastiques. De plus, les valeurs de l'intégrale J augmentent avec la taille de la fissure, indiquant une plus grande tendance à la propagation de celle-ci. L'étude met également en évidence l'effet bénéfique de certaines configurations de réparation, qui permettent de réduire la force motrice de propagation de la fissure et d'améliorer l'intégrité structurelle du pipeline.

Les résultats obtenus contribuent à une meilleure compréhension des mécanismes d'interaction entre défauts dans les aciers à haute résistance destinés aux pipelines et fournissent des informations utiles pour l'évaluation de l'intégrité et la mise en œuvre des stratégies de maintenance.

الملخص

تتأثر السلامة الهيكلية لخطوط أنابيب النفط والغاز بشكل كبير بوجود العيوب التي قد تظهر أثناء مراحل التصنيع أو التركيب أو خلال فترة التشغيل.

وتُعد الشقوق والخدوش من أخطر هذه العيوب، إذ تؤدي إلى تركيز الإجهادات وتقليل قدرة الأنبوب على تحمل الأحمال، مما يزيد من احتمالية حدوث الفشل أو الانهيار لذلك، فإن دراسة التفاعل بين هذه العيوب تُعد ضرورية لضمان التشغيل الآمن والموثوق لخطوط الأنابيب.

يهدف هذا العمل إلى دراسة التفاعل بين الشقوق والخدوش في أنبوب مدفون مصنوع من فولاذ (5 ل اكس 80) باستخدام طريقة العناصر المحددة. وقد أُنجزت المحاكاة العددية بواسطة برنامج أباكوس لتحليل تأثير الخصائص الهندسية للعيوب، بما في ذلك عمق الشق وعرضه، وكذلك عمق الخدش وعرضه واتجاهه.

وتم تقييم توزيع إجهاد فون ميزس، والانفعال اللدن المكافئ، والتكامل (جي) من أجل توصيف السلوك الميكانيكي ومقاومة الكسر للأنبوب.

أظهرت النتائج أن زيادة أبعاد العيوب تؤدي إلى ارتفاع مستويات تركيز الإجهادات والانفعالات اللدنة. كما تبين أن قيم التكامل جي تزداد مع زيادة أبعاد الشق، مما يدل على ارتفاع قابلية انتشار الشق وحدوث الكسر. كذلك أبرزت الدراسة الدور الإيجابي لبعض تقنيات الإصلاح في تقليل القوة الدافعة لانتشار الشق وتحسين السلامة الهيكلية للأنبوب.

تساهم هذه النتائج في تحسين فهم آليات التفاعل بين العيوب في الفولاذ عالي المقاومة المستخدم في خطوط الأنابيب، كما توفر معطيات مفيدة لتقييم السلامة الهيكلية ووضع استراتيجيات فعالة للصيانة وإدارة سلامة الأنابيب.

Table of contents

Table of contents

Table of contents

List of Figures

List of Figures

List of tables

General Introduction

Pipelines play a vital role in the transportation of oil, natural gas, and petroleum products over long distances. Due to their safety, reliability, and economic efficiency, they are widely used throughout the world. As energy demand continues to grow, ensuring the integrity and safe operation of pipeline systems has become a major challenge for the oil and gas industry.

Modern pipelines are commonly manufactured from high-strength steels such as API 5L X80, which offer excellent mechanical properties and high resistance to operating loads. However, during service, pipelines may develop various defects caused by corrosion, fatigue, manufacturing imperfections, or mechanical damage. Among these defects, cracks and scratches are particularly critical because they can create stress concentrations that reduce the structural strength of the pipeline and increase the risk of failure.

Fracture mechanics provides effective tools for studying the behavior of structures containing defects and for predicting crack growth and failure conditions. In addition, the Finite Element Method (FEM) has become an essential technique for analyzing complex defect geometries and evaluating their effects on pipeline integrity.

The objective of this work is to investigate the interaction between crack and scratch defects in a buried API 5L X80 pipeline using finite element simulations performed with ABAQUS. The study focuses on the influence of defect geometry on stress distribution, plastic deformation, and fracture behavior through the analysis of the J-integral and other mechanical parameters.

This dissertation is organized into three chapters. The first chapter presents the fundamentals of fracture mechanics for pipelines. The second chapter discusses pipeline integrity and defect assessment methods. The third chapter focuses on the numerical modeling and simulation of crack and scratch defects, as well as the evaluation of their effects on the structural integrity of the pipeline.

1. Chapter I: Fracture Mechanics for Pipelines

1.1. Generalities on Pipelines

1.1.1 Role of pipelines in hydrocarbon transportation

Pipelines constitute the most reliable, economical, and safest means for the long-distance transportation of hydrocarbons, including crude oil, refined petroleum products, and natural gas. According to the U.S. Energy Information Administration and the data compiled by the International Energy Agency, more than two-thirds of the world energy supply transits through pipeline networks, with a total length exceeding 3.5 million kilometers worldwide [Mohitpour et al., 2003; EIA, 2021]. Unlike road or rail transportation, pipelines operate continuously, with very low energy consumption per unit of transported product, and they are largely unaffected by weather conditions because the majority of them are buried.

In the petroleum industry, the term 'pipeline' generally designates a steel structure consisting of welded cylindrical segments (line pipes), connected by elbows, tees, reducers, valves and other fittings, and supplied with auxiliary equipment such as pumping or compression stations, cathodic-protection systems, and measurement or monitoring devices. The internal pressure can range from a few bars in low-pressure distribution networks to more than 150 bars in modern high-pressure gas transmission lines. The operating temperature varies between -40 °C and +80 °C depending on the fluid transported and the climatic environment [Hopkins, 2007].

Algeria, which is the host country of this study, owns one of the most extensive pipeline networks in Africa. The national company SONATRACH operates a transmission system of more than 22,000 km that connects the oil and gas fields of the Sahara to the Mediterranean export terminals and to several European countries through underwater pipelines such as Medgaz, Transmed and the Maghreb-Europe Gas Pipeline [Sonatrach, 2020]. The continuous extension of this network and the gradual aging of its older sections, some of which were built during the 1960s and 1970s, make pipeline integrity a key strategic and economic issue for the country, and motivate the kind of fracture-mechanics-based analyses that constitute the subject of the present work.

1.1.2 Classification and types of line pipes

Line pipes are classified, on one hand, according to their manufacturing process and, on the other hand, according to the steel grade defined by the American Petroleum Institute (API)

Specification 5L [API 5L, 2018]. Three main families of line pipes are encountered in industrial practice: seamless pipes (SMLS) obtained by piercing and hot-rolling a solid billet; longitudinally welded pipes manufactured by submerged-arc welding (SAWL) or by high-frequency electric resistance welding (ERW/HFW); and helically (spirally) welded pipes (SAWH). Each process gives rise to specific metallurgical features and to characteristic defect populations that strongly influence the in-service behavior of the line.

The steel grade in API 5L is designated by a letter and a number, such as X42, X52, X60, X65, X70, X80 or X100, where the number refers to the specified minimum yield strength (SMYS) expressed in kilopounds per square inch (ksi). Therefore, an API 5L X80 pipeline steel has a specified minimum yield strength of 80 ksi, approximately 555 MPa. Higher steel grades such as X80, X100 and even X120 belong to the family of high-strength low-alloy (HSLA) steels developed since the 1980s thanks to the introduction of thermo-mechanical control processing (TMCP) and to microalloying with niobium, vanadium and titanium [Hillenbrand et al., 2002; Hashemi, 2011].

The X80 grade, which is at the core of the present work, is characterized by a fine-grained ferrite-bainite microstructure that combines high yield strength (typically between 555 MPa and 690 MPa), high ultimate tensile strength (between 625 MPa and 825 MPa), and a remarkable upper-shelf Charpy V-notch energy that often exceeds 250 J at 0 °C [Shin et al., 2007]. The use of X80 in new gas transmission projects, including the Bolivia-Brazil GASBOL line, the West-East Pipeline II in China, the Cheyenne Plains Gas Pipeline in the United States, and the Nordstream system in Europe, has allowed designers to increase the operating pressure up to 12-15 MPa while reducing the wall thickness and the total mass of steel installed [Liessem & Erdelen-Peppler, 2004].

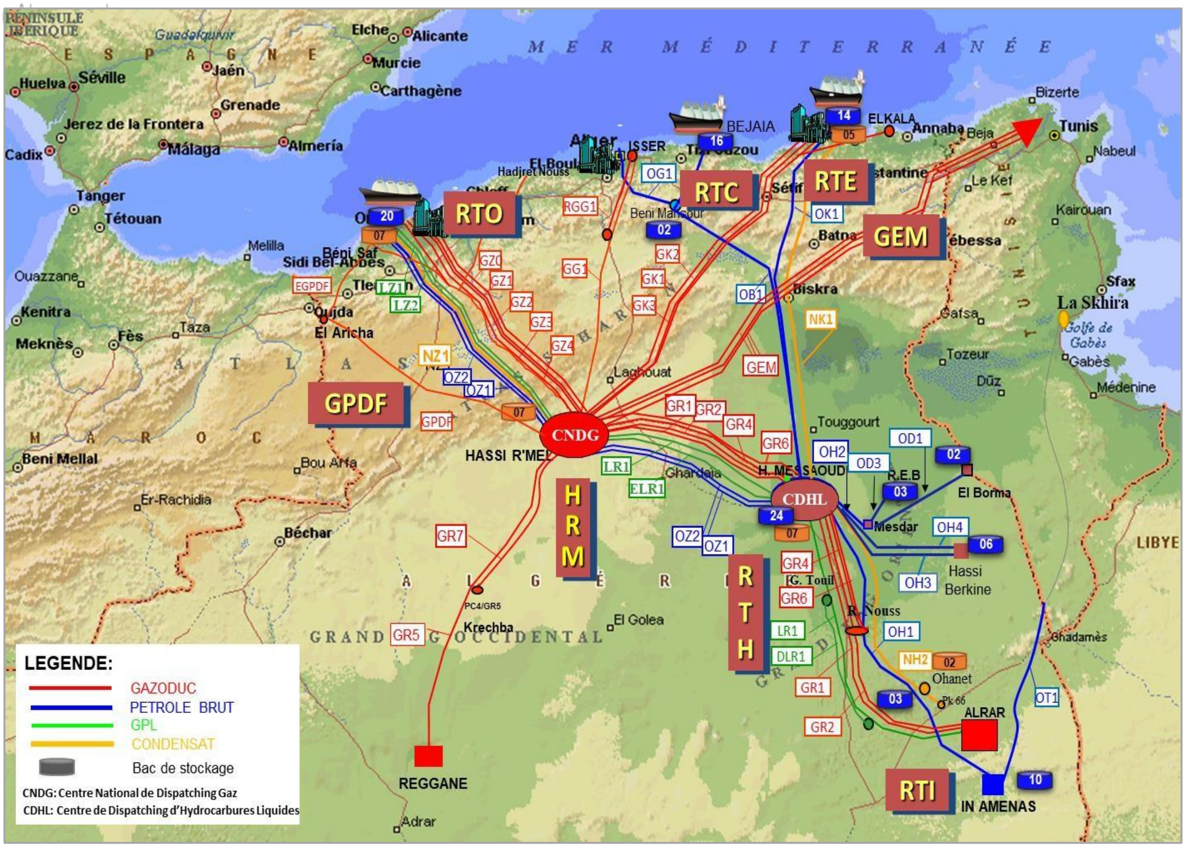

Figure 4: Transportation Network Map [Anon., AVRIL 2022]

1.1.3 Design parameters and operating conditions

The mechanical design of a transmission pipeline is governed by international codes such as ASME B31.4 for liquid pipelines, ASME B31.8 for gas pipelines, ISO 13623, and the Canadian standard CSA Z662 [ASME B31.4, 2019; ASME B31.8, 2020; CSA Z662, 2019]. The wall thickness of a straight pipe section subjected to internal pressure is calculated using a Barlow-type formula derived from the thin-shell theory:

$$t = (\,p \times D)\,(p \times D)/(2 \times S \times F \times E \times T) \quad (1)$$

where t is the required wall thickness, P is the design internal pressure, D is the outer diameter, S is the specified minimum yield strength, F is the design factor (typically 0.72 for class-1 locations and reduced to 0.40 in densely populated areas), E is the longitudinal joint factor, and T is the temperature de-rating factor. This deterministic approach, although still widely used, is now complemented by limit-state design and reliability-based approaches that explicitly account for material variability, defect populations and operational uncertainties [Zhou & Nessim, 2011].

Buried pipelines are subjected to a combination of loads: the hoop and axial stresses generated by internal pressure; the soil overburden; the surface traffic loads transmitted through the soil; thermal expansion stresses due to temperature differences between the operating fluid and the surrounding ground; and possible secondary loads such as differential settlement, seismic activity or third-party interference [O'Rourke & Liu, 2012]. The hoop stress σh is generally dominant and is given by the well-known thin-walled-cylinder expression $\sigma h = P \times D/(2 \times t)$, which is the equation that motivates the choice of high-grade steels for high-pressure operation.

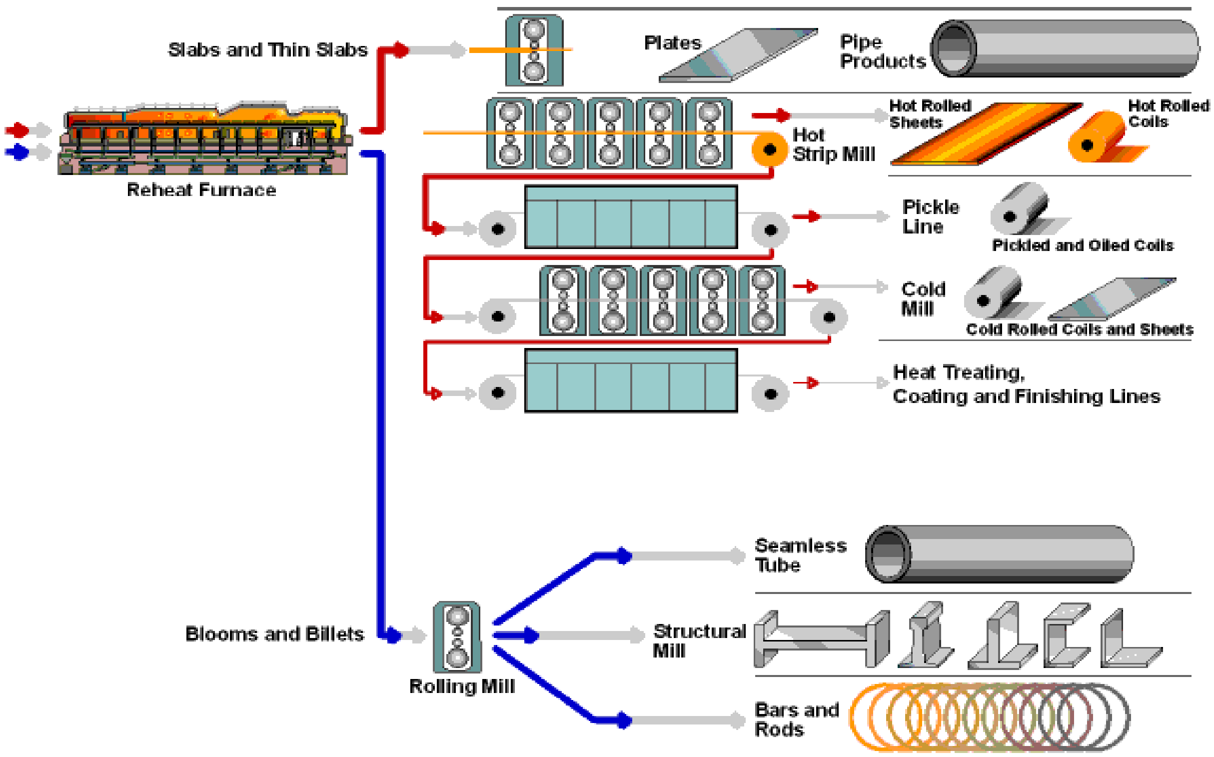

Figure 5 : Steel making flow chart [Sir Rashid Fiaz, 26 April 2011]

1.1.4 Mechanical and metallurgical properties of API 5L X80 steel

The API 5L X80 steel is produced by hot-rolling followed by accelerated cooling, which yields an acicular ferrite or fine ferrite-bainite microstructure with grain sizes typically in the range of 3 to 10 µm. Microalloying elements such as Nb, V and Ti form fine carbonitride precipitates that pin the austenite grain boundaries during rolling and provide additional strengthening through precipitation hardening [DeArdo, 2003]. Compared to earlier grades such as X52 or X60, the X80 steel offers a higher strength-to-weight ratio, improved weldability through low carbon content (typically C < 0.07 %), and excellent low-temperature toughness.

The chemical composition of a typical X80 steel involves carbon contents below 0.08 %, manganese around 1.7-1.9 %, silicon between 0.20 % and 0.40 %, and microalloying additions of Nb (0.03-0.06 %), Ti (0.01-0.02 %) and sometimes Mo (up to 0.30 %) and Cr (up to 0.25 %) to enhance hardenability and bainite formation [Gray, 2002]. The resulting carbon equivalent (CE), evaluated through the International Institute of Welding formula, is generally kept below 0.43 to guarantee good field weldability. The yield-to-tensile ratio (Y/T), which is a critical parameter for the strain capacity of the pipeline, usually lies between 0.85 and 0.93 for X80 steel.

The fracture behavior of X80 exhibits a sharp ductile-to-brittle transition between -60 °C and -100 °C, but at room temperature the steel is fully ductile and fractures by microvoid coalescence. The plane-strain fracture toughness KIC of X80 base metal at 20 °C is typically in the range of 130-200 MPa·m^0.5, and the corresponding J-integral at initiation (J0.2/BL) is between 200 kJ/m² and 500 kJ/m² [Kim et al., 2007; Hwang et al., 2011]. The crack-tip opening displacement (CTOD) measured according to ASTM E1820 ranges from 0.20 to 0.40 mm, indicating that the material has a substantial energy-absorption capability before unstable fracture, which is essential for arresting running ductile fractures in long high-pressure gas lines.

1.2. Fundamentals of Fracture Mechanics

1.2.1 Historical perspective and motivation

Fracture mechanics emerged as a scientific discipline in the early twentieth century, driven by the observation that real engineering structures often fail at stress levels much lower than the yield stress of the constituent material. The pioneering work of Griffith on glass rods, published in 1921, established the first energy-based fracture criterion, postulating that a crack will propagate when the strain energy released exceeds the surface energy required to create new crack surfaces [Griffith, 1921]. Although Griffith's theory was originally limited to brittle materials, it laid the conceptual foundation for all subsequent developments.

After the catastrophic failures of the Liberty ships during the Second World War, when nearly 1500 out of 2700 welded cargo ships suffered significant brittle fractures, the need for a quantitative fracture-toughness criterion applicable to metals became urgent [Anderson, 2017]. The fundamental contribution of Irwin in 1957 extended Griffith's theory to ductile materials by introducing the concept of the stress-intensity factor K and of the energy release rate G, thereby creating the field of Linear Elastic Fracture Mechanics (LEFM) [Irwin, 1957].

During the 1960s, the limits of LEFM became apparent for materials and geometries in which significant plastic deformation occurs at the crack tip. Wells introduced the crack-tip opening displacement (CTOD) parameter in 1961, and Rice formulated in 1968 the path-independent integral known as the J-integral, which constitutes the cornerstone of Elastic-Plastic Fracture Mechanics (EPFM) [Wells, 1961; Rice, 1968]. These two parameters, CTOD and J, remain to this day the most widely used in the integrity assessment of ductile structures such as modern high-toughness pipelines.

1.2.2 The three modes of fracture

From a kinematic standpoint, three independent loading modes are recognized at the tip of a crack. Mode I, also called the opening mode, corresponds to tensile stress acting perpendicular to the crack plane and produces a symmetric opening of the crack faces. Mode II, the in-plane shear or sliding mode, results from shear stress acting parallel to the crack plane and perpendicular to the crack front. Mode III, the out-of-plane shear or tearing mode, corresponds to shear stress acting parallel to the crack plane and parallel to the crack front [Anderson, 2017].

In pipeline applications, Mode I is by far the most relevant because the dominant loading is the hoop stress generated by internal pressure, which acts perpendicular to the plane of longitudinal surface flaws — the most common defect orientation observed in service. Mixed-mode loading may occur for inclined cracks or when the pipeline experiences combined pressure and bending, but its quantitative treatment requires more elaborate fracture parameters that go beyond the scope of standard assessments.

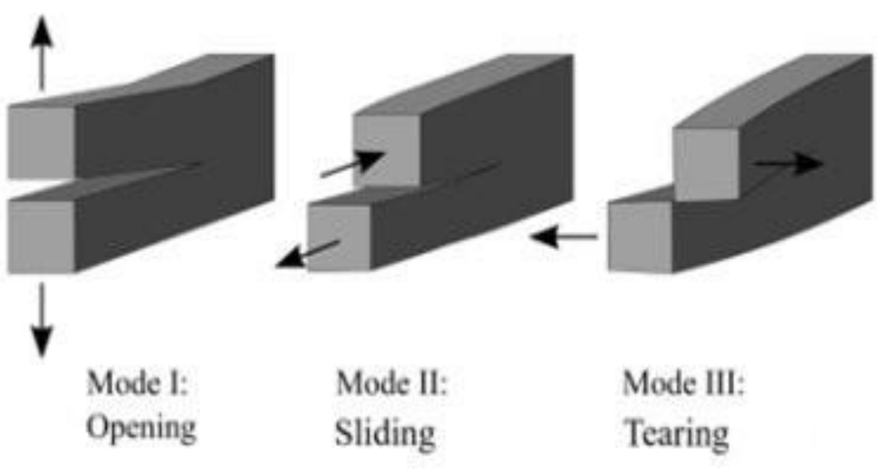

Figure 6: the three modes of fracture [Anon., s.d.]

1.2.3 Linear elastic fracture mechanics: the stress-intensity factor

In the framework of Linear Elastic Fracture Mechanics, the singular stress field near the tip of a sharp crack in an isotropic homogeneous elastic body is governed by the stress-intensity factor K. For Mode I, the stress components in the vicinity of the crack tip are given by the Westergaard-Irwin asymptotic expressions:

$$\sigma ij(r,\theta) = k.I/\sqrt{(2\pi r\,)} \times fij(\theta) + \textit{higher-order terms} \quad (2)$$

where r and θ are the polar coordinates centered at the crack tip and fij are dimensionless angular functions [Westergaard, 1939; Irwin, 1957]. The stress-intensity factor KI depends on the applied load, on the geometry of the cracked body, and on the crack size. For a through-thickness crack of length 2a embedded in an infinite plate under remote tensile stress σ, KI is simply σ√(πa). For more complex configurations such as semi-elliptical surface cracks in pipes, finite-geometry correction factors are introduced and tabulated in handbooks such as those compiled by Murakami and by Tada, Paris and Irwin [Tada et al., 2000; Murakami, 1987].

The fracture criterion in LEFM is expressed by comparing the applied stress-intensity factor to a critical value of the material, namely the plane-strain fracture toughness KIC, which is a material property measured according to standardized procedures such as ASTM E399 [ASTM E399, 2020]. Brittle fracture is predicted when KI reaches KIC. However, the strict validity conditions of plane-strain fracture toughness require that both the thickness of the specimen and the crack length be larger than 2.5(KIC/σy)^2, which is rarely the case for ductile high-toughness materials such as pipeline steels. This limitation motivated the development of elastic-plastic parameters.

1.2.4 Elastic-plastic fracture mechanics: CTOD and the J-integral

When the plastic zone at the crack tip becomes comparable to or larger than the in-plane dimensions of the cracked body, the LEFM concepts lose their validity and elastic-plastic fracture parameters must be used. The Crack-Tip Opening Displacement (CTOD), introduced by Wells, is defined geometrically as the relative displacement of two points originally located at the crack tip after blunting takes place [Wells, 1961]. CTOD can be related to KI in the small-scale-yielding regime by the relation $\delta = K\_I^2 / (m \times \sigma y \times E')$, where m is a constraint factor and E' equals E in plane stress and $E / (1 - \nu^2)$ in plane strain.

The J-integral, introduced by Rice in 1968, is a path-independent contour integral that quantifies the energy release rate per unit of crack extension for both elastic and elastic-plastic material behavior [Rice, 1968]. It is defined by:

$$J = \int \Gamma (w\, dy - Ti.\partial ui/\partial x \cdot ds) \quad (3)$$

where Γ is an arbitrary contour starting from the lower crack face and ending on the upper crack face, W is the strain-energy density, Ti are the components of the traction vector acting on the contour, ui are the displacement components, and ds is the arc length along the contour. The path-independence of J — valid under monotonic, proportional loading and for materials without body forces or thermal strains — makes the J-integral particularly attractive for numerical implementation in finite element codes, since the contour can be chosen sufficiently far from the singular crack tip to avoid the numerical difficulties associated with the strong gradients in that region.

From a physical viewpoint, J can be interpreted as the rate of change of potential energy with respect to crack extension for a non-linear elastic body, and it is identical to the energy release rate G in the linear elastic case. Hutchinson, Rice and Rosengren (HRR) demonstrated in 1968 that for a power-law hardening material, the stresses and strains in the vicinity of the crack tip follow a singular distribution governed by J:

$$\sigma ij = \sigma y \times (J/(\alpha\, \sigma y\, \varepsilon y \ln r))^{(1/(n+1))} \times \tilde{\sigma} ij(\theta,n) \quad (4)$$

where α is the Ramberg-Osgood coefficient, n is the strain-hardening exponent, In is a dimensionless integration constant, and σ̃ij are the angular functions tabulated by Hutchinson and by Rice & Rosengren [Hutchinson, 1968; Rice & Rosengren, 1968]. This HRR solution generalizes the K-field of LEFM to the elastic-plastic regime and provides the theoretical basis for the use of J as a one-parameter characterization of the crack-tip stress and strain fields under conditions of high constraint.

The critical value of J at the onset of stable crack growth, denoted Jc or JIC depending on the specific test procedure (ASTM E1820), is a material property that, together with the resistance curve J-Δa, characterizes the fracture toughness of a ductile material. For modern pipeline steels such as API X80, JIC at 20 °C generally lies between 200 and 500 kJ/m², with significant scatter related to microstructural inhomogeneity, especially in the heat-affected zone of welded joints [Hwang et al., 2011; Sumpter & Forbes, 1992].

1.2.5 Two-parameter fracture mechanics and constraint effects

In the framework of single-parameter fracture mechanics, either K or J completely characterizes the crack-tip state. This idealization, however, fails when the geometry or loading does not produce the highly-constrained conditions assumed by the asymptotic K- and HRR-fields. To account for the so-called 'constraint effect' — i.e. the dependence of the apparent fracture toughness on geometry and loading — two-parameter approaches such as J-T, J-Q and J-A2 have been developed [O'Dowd & Shih, 1991; Yang et al., 1993].

In the J-Q approach of O'Dowd and Shih, the actual stress field at the crack tip is decomposed into the reference HRR field, multiplied by a constraint parameter Q that quantifies the deviation of the local hydrostatic stress from the high-constraint reference state. Low-constraint geometries (shallow cracks, thin sections, predominantly tensile loading) exhibit negative Q values and apparently higher toughness than the standard high-constraint specimens used for the determination of JIC. For pipeline applications, where surface flaws are usually shallow with respect to the wall thickness, two-parameter approaches lead to less conservative integrity predictions and have been incorporated in the most recent revisions of the BS 7910 and API 579-1/ASME FFS-1 standards [BS 7910, 2019; API 579-1, 2021].

1.3. Crack Initiation and Propagation

1.3.1 Mechanisms of crack initiation in pipelines

Crack initiation in pipelines results from a complex interaction between the metallurgical state of the steel, the applied mechanical loading, and the operating environment. From a phenomenological point of view, three categories of initiation mechanisms are usually distinguished: mechanical initiation under monotonic or cyclic loading, environmentally-assisted initiation, and thermally or radiation-induced initiation, the latter being marginal for pipeline applications. Mechanical initiation is generally associated with stress concentrators such as inclusions, second-phase particles, surface scratches, dents, weld defects, or geometric discontinuities introduced during manufacturing or during in-service operations [Mohitpour et al., 2003; Cosham & Hopkins, 2007].

At the microscopic scale, the initiation of ductile cracks proceeds through nucleation, growth, and coalescence of microvoids around hard inclusions (typically MnS, Al2O3, or carbide particles) under the action of high local hydrostatic stresses. The classical Rice and Tracey model, complemented by the more recent Gurson-Tvergaard-Needleman (GTN) constitutive law, captures the kinetics of void nucleation and growth in ductile metals and has been calibrated for several pipeline steels [Rice & Tracey, 1969; Tvergaard & Needleman, 1984]. For X80 steel in particular, parametric studies of the GTN model have shown that the initial volume fraction of voids f0 lies between 0.0005 and 0.002, while the critical fraction fc at the onset of coalescence is approximately 0.05 [Oh et al., 2007].

In welded sections, microcrack initiation is often favored by the local heterogeneity of the heat-affected zone (HAZ), where the rapid thermal cycle of welding produces a mixture of martensite, bainite and untempered ferrite with very different yield strengths. Hydrogen-induced cracking (HIC) and sulphide stress cracking (SSC) constitute additional initiation mechanisms in sour service, governed by the diffusion of atomic hydrogen toward zones of high triaxiality and by the precipitation of hydrogen at non-metallic inclusions or grain boundaries [Carneiro et al., 2003; ANSI/NACE MR0175, 2015].

1.3.2 Stable and unstable crack propagation

Once a crack has been initiated, its propagation can be either stable or unstable depending on the loading mode, on the geometry, and on the material's resistance curve. In a load-controlled experiment with monotonically increasing load, a crack of length a is stable if the increase in the applied driving force (K or J) with a is smaller than the increase in the material's resistance (Kc(Δa) or J-R curve), and unstable in the opposite case. This stability criterion is expressed graphically by the tangency condition between the applied driving force curve and the material's resistance curve, and analytically by the inequality dJappl/da < dJR/da.

In pipeline operation, the most catastrophic scenario is the so-called running ductile fracture (RDF), which can propagate over kilometers in gas pipelines at velocities of 200-300 m/s, driven by the depressurization wave behind the crack front. The Battelle Two-Curve Method (BTCM), developed at the Battelle Memorial Institute in the 1970s, predicts the arrest length of a running ductile fracture by comparing the crack-propagation velocity to the decompression-wave velocity in the gas [Maxey, 1974; Eiber et al., 2004]. Modern high-grade steels such as X80 and X100 require an upper-shelf Charpy energy of at least 100-150 J to guarantee fracture arrest under typical operating pressures, while propagation in lower-grade steels can occur at much lower toughness values.

1.3.3 Fatigue crack growth

Pipelines in operation are subjected to cyclic loading that originates from internal pressure fluctuations, from periodic pumping cycles, from temperature variations, and from external causes such as traffic loads or wave action in offshore pipelines. These cyclic loads can drive a pre-existing flaw to propagate by fatigue until it reaches a critical size and triggers final failure. Paris and Erdogan formulated in 1963 the well-known empirical law that relates the fatigue crack growth rate da/dN to the range of the stress intensity factor ΔK [Paris & Erdogan, 1963]:

$$\frac{da}{dN} = C \times (\Delta K)^{m} \quad (5)$$

where C and m are material constants depending on the steel grade, the load ratio R, the environment, and the loading frequency. For typical pipeline steels and air environment, m lies between 2.5 and 3.5, and C is of the order of 10^-12 (m/cycle)/(MPa·m^0.5)^m. The standard BS 7910 [BS 7910, 2019] provides recommended values for assessment purposes and distinguishes the upper-bound mean and 95 % confidence Paris parameters as a function of the material category and the environment.

In aggressive environments such as those involving CO2, H2S, or near-neutral pH soil electrolytes, the fatigue crack growth rate can increase by one or two orders of magnitude compared to air, due to the synergistic action of hydrogen embrittlement and active dissolution at the crack tip [Chen et al., 2007]. Furthermore, the threshold stress intensity factor range ΔKth, below which no measurable crack growth occurs, decreases with environmental aggressiveness and load ratio. In typical X80 pipeline service, ΔKth values lie in the range of 4-8 MPa·m^0.5 [Beretta et al., 2013].

1.3.4 Stress corrosion cracking

Stress corrosion cracking (SCC) is a long-recognized degradation mechanism for buried gas pipelines, especially under disbonded coatings and in alkaline soil environments. Two main SCC categories are distinguished: high-pH or 'classical' SCC, occurring in carbonate-bicarbonate environments at pH values around 9-11, and near-neutral pH SCC, occurring in dilute groundwater environments at pH 5.5-7.5. Both forms produce colonies of intergranular or transgranular cracks oriented predominantly along the longitudinal direction of the pipe, perpendicular to the maximum hoop stress [Parkins, 2000; Beavers & Harle, 2001].

The initiation of SCC requires the simultaneous presence of three factors: a susceptible material, a corrosive environment, and a sufficient tensile stress (sustained or fluctuating). Once initiated, SCC can grow at rates of 10^{-9} to 10^{-7} m/s, leading to coalescence of adjacent cracks and to the eventual formation of a single critical defect that can cause failure either by leak or by rupture, depending on the relationship between defect size and critical fracture parameters of the steel [Parkins et al., 2003]. Major SCC-related incidents have occurred on transmission pipelines in the United States, Canada, Russia, and Iran, prompting the development of dedicated in-line inspection (ILI) and integrity-management programs.

1.4. Factors Influencing Pipeline Rupture

1.4.1 Geometric factors: defect dimensions and shape

The failure of a pipeline section containing a defect depends primarily on the dimensions and shape of the defect. For a longitudinal surface flaw of depth a, length 2c, and located in a pipe of wall thickness t and outer diameter D, the most relevant geometric parameters are the relative depth a/t, the aspect ratio a/c, and the dimensionless flaw length $2c/\sqrt{(Dt)}$ introduced by Folias [Folias, 1965]. These three parameters appear in nearly all empirical and semi-empirical failure assessment equations, including the original ASME B31G, the modified B31G, the RSTRENG, and the DNV-RP-F101 methods, which will be discussed in section 1.5.

The geometry of dents and gouges has also a strong influence on the failure pressure. Empirical observations and laboratory experiments have shown that the residual strength of a dented pipeline decreases rapidly when the dent depth exceeds 2-3 % of the pipe outer diameter, especially when the dent contains a stress concentrator such as a scratch or a notch produced by the indentation tool [Cosham & Hopkins, 2007; Macdonald & Cosham, 2005]. The interaction between a dent and a co-located gouge is particularly severe because the dent introduces residual stresses and strain hardening locally, while the gouge acts as a crack initiator that subsequently propagates under the cyclic loading of pressure fluctuations.

1.4.2 Material factors: strength, toughness and microstructure

The mechanical and metallurgical properties of the steel constitute the second family of parameters that govern the rupture behavior of pipelines. The most relevant material properties are the yield strength σ_y, the ultimate tensile strength σ_u, the work-hardening exponent n, the flow stress σ_f (often defined as the average between σ_y and σ_u), and the fracture toughness expressed by KIC, JIC, or CTOD. The strain capacity, which is the maximum tensile strain that the material can sustain before localization and necking, is also crucial for pipelines subjected to ground movements, frost heave or thaw settlement [Glover et al., 2003].

For a given defect geometry, increasing the steel grade from X52 to X80 raises the burst pressure by approximately 50 %, but it also reduces the strain capacity and the upper-shelf toughness for the same plate thickness. This trade-off between strength and ductility is a classic dilemma in pipeline design and motivates the use of advanced micro-alloyed steels with optimized Y/T ratio and high toughness. The microstructure also plays a key role: acicular ferrite microstructures generally exhibit higher toughness than polygonal ferrite-pearlite ones for the same yield strength, due to the larger density of high-angle grain boundaries that act as crack-arrest barriers [Krauss, 2005].

1.4.3 Environmental factors

Environmental conditions, both internal and external, exert a major influence on the long-term integrity of pipelines. Internally, the presence of CO2, H2S, oxygen, chlorides or sulfate-reducing bacteria can accelerate the corrosion and the cracking processes, while externally the soil resistivity, moisture content, pH and microbiological activity govern the rate of external corrosion in the case of coating defects and inadequate cathodic protection. The combined effect of mechanical loading and corrosive environment, known as corrosion fatigue or environmentally-assisted cracking, is responsible for a significant fraction of pipeline failures recorded in the European Gas pipeline Incident data Group (EGIG) and the U.S. Pipeline and Hazardous Materials Safety Administration (PHMSA) databases [EGIG, 2018; PHMSA, 2020].

Temperature also plays a role through the ductile-to-brittle transition behavior of ferritic steels: a pipeline operating in arctic conditions can experience a drop in toughness of one or two orders of magnitude during cold spells, leading to brittle fracture initiation from otherwise sub-critical defects. Modern X80 steels have been specifically designed to retain high toughness down to -40 °C or -60 °C through grain refinement, microalloying and accelerated cooling. The temperature dependence of the fracture toughness can be described by the Master Curve approach proposed by Wallin and standardized in ASTM E1921 [Wallin, 1991; ASTM E1921, 2021].

1.4.4 Operational and human factors

The fourth class of factors that contribute to pipeline failures encompasses operational and human factors, including third-party interference (excavation by external parties without due notification), errors during construction or repair, deviation from operating procedures, and insufficient inspection or maintenance practices. According to EGIG statistics covering the period 1970-2019, third-party interference accounts for approximately one-third of the total incidents on European gas transmission pipelines, while construction defects and material flaws together represent another 25 % of the incidents [EGIG, 2018]. The relative importance of human and operational factors highlights the need for risk-based integrity management programs that combine quantitative engineering assessments with effective surveillance and damage-prevention measures.

1.5. Evaluation and Rupture Criteria

1.5.1 The Failure Assessment Diagram (FAD) approach

The Failure Assessment Diagram (FAD) approach is the most widely accepted method for the structural integrity assessment of cracked components, including pipelines. It was originally developed in the United Kingdom by the Central Electricity Generating Board under the form of the R6 procedure [R6, 2013], and has since been adopted and refined in international standards such as BS 7910, API 579-1/ASME FFS-1, and SINTAP/FITNET [BS 7910, 2019; API 579-1, 2021; Koçak et al., 2008]. The FAD approach is based on the simultaneous consideration of two failure modes: brittle fracture, characterized by the ratio Kr = KI/Kmat (6) (or √(Je/J)), and plastic collapse, characterized by the ratio $Lr = \sigma ref/\sigma y$ (7)

The assessment point of coordinates (Lr, Kr) is plotted on the FAD diagram, which is bounded by an assessment curve (also called the failure assessment line) and by a vertical cut-off Lr,max corresponding to the limit-load condition. If the assessment point lies inside the region delimited by the curve and the axes, the cracked component is judged safe under the considered loading; otherwise, the assessment indicates an unacceptable risk of failure. Different levels of FAD analysis are defined, from the basic Option 1 curve (using only the yield strength) to advanced Option 3 curves based on the material-specific stress-strain curve.

1.5.2 Empirical methods for corroded pipelines

For corrosion defects, where the loss of material is gradual and the defect can be approximated as a longitudinal blunt flaw rather than as a sharp crack, several semi-empirical failure equations have been developed, mostly during the 1970s-1990s, on the basis of full-scale burst tests on pipes containing artificially machined defects. The pioneer equation was published by ASME under the form B31G [ASME B31G, 1984], and was later refined into the Modified B31G (also called B31G-Modified or 0.85 dL) by Kiefner and Vieth [Kiefner & Vieth, 1989]:

$$Pf = \sigma flow \times \left(\frac{2t}{D}\right) \times \left(\frac{1-0.85\frac{a}{t}}{1-0.85\frac{a}{t\cdot M}}\right) \quad (8)$$

where Pf is the predicted failure pressure, σflow = SMYS + 69 MPa, and M is the Folias bulging factor that depends on the dimensionless flaw length $z = c^2 / (Dt)$. The Modified B31G equation has been widely used in the industry and is the default method recommended by the U.S. Department of Transportation. More recent methods such as RSTRENG, DNV-RP-F101, PCORRC (developed by Battelle), and the LPC-1 method developed by Andrew Cosham at Penspen have refined the geometry definition and the failure criterion, and they typically provide less conservative predictions for ductile materials [Cosham et al., 2007; DNV-RP-F101, 2019; Stephens & Leis, 2000].

1.5.3 Specific assessment methods for dents and gouges

The assessment of dents, gouges and combined dent-gouge defects requires specific methods, since the geometry of these defects and their underlying mechanical behavior depart significantly from those of corrosion defects. The Pipeline Defect Assessment Manual (PDAM), developed by Cosham and Hopkins as a comprehensive synthesis of the open literature, presents specific equations for plain dents, kinked dents, gouges, and combined dent-gouge defects [Cosham & Hopkins, 2007]. For a plain dent of depth H/D measured at zero pressure, the fatigue life under cyclic internal pressure can be estimated by the equation:

$$N = 562.2 \times \left(\frac{2\sigma u}{Sa}\right)^{5.26} \times \left(\frac{1}{\frac{H_0}{D}}\right) \quad (9)$$

where Sa is the stress range, σu is the ultimate tensile strength, and H0 is the dent depth at zero pressure. This equation, which is based on the work of the European Pipeline Research Group (EPRG), provides a conservative estimate of the fatigue life of plain dents and is recommended in BS 7910. For dent-gouge combinations, the EPRG criterion, calibrated against more than one hundred full-scale burst tests, combines the dent depth and the gouge depth in a single failure-pressure equation, with the inclusion of the 2/3 Charpy V-notch energy ratio as a toughness parameter [Lyons et al., 2020; Cosham & Hopkins, 2007].

1.5.4 Numerical methods: finite element analysis and J-integral computation

Numerical methods, and in particular the finite element method, are increasingly used for the rigorous integrity assessment of pipelines containing complex defects, and they constitute the methodological backbone of the present work. The finite element computation of the J-integral relies either on the contour integral originally defined by Rice or, more commonly in three-dimensional analyses, on the equivalent domain integral formulation that converts the line integral into an area or volume integral over a domain surrounding the crack front [Shih et al., 1986]. The domain integral formulation is implemented in all major commercial finite element codes (Abaqus, Ansys, Code_Aster, MSC.Marc) and provides path-independent J values with high numerical accuracy when a sufficient number of contours (typically five to ten rings of elements around the crack front) are evaluated.

In the case of stationary cracks under monotonic loading, the J-integral computed by finite elements can be compared directly to the experimentally-measured JIC or J-R curve of the material to predict the onset of stable crack growth. In the presence of additional defects in the vicinity of the main crack, such as dents or scratches, the J-integral becomes a sensitive indicator of the interaction between defects, and its evaluation as a function of geometric parameters (separation distance, relative orientation, depth of the secondary defect) provides quantitative criteria for the assessment of defect interaction effects. This is precisely the scope of the analyses described in the subsequent chapters of this work, where the interaction of a crack with a co-located dent and with a remote scratch in an X80 pipeline is investigated using three-dimensional finite element models with elastic-plastic material behavior.

Recent contributions have shown that interaction between defects can either be detrimental — when the secondary defect amplifies the local stress and strain fields acting on the primary crack — or beneficial, when the secondary defect locally redistributes the load and shields the crack tip. Allouti et al. [Allouti et al., 2012, 2014] investigated the interaction between a dent and a crack-like gouge in X52 pipeline steel and showed that the burst pressure decreases by up to 50 % when the gouge depth exceeds 10 % of the wall thickness. Similar studies on X65, X70 and X80 grades by Pluvinage and co-workers [Pluvinage et al., 2014, 2018] confirmed the strong interaction between dents, gouges and corrosion defects, and pointed to the J-integral as the most discriminating fracture parameter for the assessment of such combined-defect configurations.

1.2.7 Stress-intensity factor solutions for surface cracks in pipes

The accurate evaluation of stress-intensity factors for semi-elliptical surface cracks in cylindrical shells is essential for the integrity assessment of pipelines and pressure vessels. Compilations of such solutions are provided in the major fracture-mechanics handbooks: Tada, Paris and Irwin compiled the most comprehensive collection for plane geometries and simple shells; Newman and Raju developed widely-used empirical equations for semi-elliptical surface cracks in finite-thickness plates and in pressurized cylinders [Newman & Raju, 1981; Tada et al., 2000]. The Newman-Raju solution, in particular, expresses the stress-intensity factor along the elliptical crack front as a function of the relative depth a/t, the aspect ratio a/c, the angle along the crack front, the loading mode (membrane or bending), and the ratio of inner to outer radius for cylindrical geometries. The expressions are valid up to $a/t \approx 0.8$ and have been validated against more than fifty independent numerical or experimental data sets.

For pipelines specifically, the API 579-1/ASME FFS-1 standard and the BS 7910 procedure provide K-solutions that account for the pressurization of the crack faces (which is relevant for through-thickness cracks but not for surface cracks), for the global hoop bending due to the curvature of the cylinder, and for the redistribution of stresses around the defect. The R6 procedure and the SINTAP/FITNET procedure provide equivalent solutions with slightly different conventions. Modern industry practice typically combines these analytical or semi-empirical K-solutions for routine assessments with detailed three-dimensional finite element analyses for critical configurations or for cases where the analytical solutions are not directly applicable [BS 7910, 2019; API 579-1, 2021].

1.5.5 The Failure Assessment Diagram: options and constraint corrections

The Failure Assessment Diagram (FAD) is constructed by plotting an assessment curve (also called the failure assessment line) and a vertical cut-off $L_{r,max}$ in the (L_r, K_r) plane. The shape of the assessment curve depends on the level of refinement chosen by the analyst, and BS 7910 distinguishes three main 'Options' of increasing accuracy and decreasing conservatism [BS 7910, 2019].

Option 1 corresponds to a generic curve applicable to any material for which only the yield strength and the ultimate tensile strength are known. The Option 1 curve has a simple analytical form: $f(L_r) = (1 + 0.5 L_r^2)^{-0.5} \times [0.3 + 0.7 \exp(-0.6 L_r^6)]$, with a cut-off at $L_{r,max} = (\sigma_y + \sigma_u)$

/ (2 σy). The Option 1 curve is the most conservative of the three, and is used when minimal material data are available.

Option 2 uses the actual stress-strain curve of the material, integrated numerically from the origin to the current strain corresponding to Lr. The Option 2 curve provides a less conservative assessment than Option 1 because it accounts explicitly for the work-hardening behavior of the material. It is the preferred option for modern pipeline steels with significant work-hardening capability such as X65, X70, and X80, for which the Option 1 curve tends to be excessively conservative.

Option 3 is based on a J-based or J-Lr relationship derived from a detailed finite element analysis of the specific cracked configuration of interest. Option 3 is the most accurate of the three options, but it requires substantial computational effort and is typically reserved for safety-critical assessments or for configurations that are not adequately covered by the standard K-solutions. The construction of an Option 3 FAD constitutes one of the natural application areas of the kind of finite element analyses performed in the present work.

In addition to the choice of the FAD option, modern assessment procedures account for the constraint effect on the apparent fracture toughness through two-parameter approaches (J-Q, J-T, J-A2). The constraint correction is particularly important for shallow surface cracks ($a/t < 0.3$), for which the constraint at the crack tip is reduced compared to the standard deep-crack laboratory specimens, and where the apparent fracture toughness can be significantly higher than the conventional plane-strain KIC or JIC. The integration of constraint corrections into the FAD-based assessment procedure leads to a substantial reduction of the conservatism in the prediction of the failure pressure for typical pipeline defects [Yang et al., 1993; O'Dowd & Shih, 1991].

1.6. Complementary Considerations on Pipeline Fracture Mechanics

1.6.1 The Algerian transmission network and the case for X80 steel

The Algerian gas transmission system, operated by the national company SONATRACH, is among the oldest and largest in Africa. The backbone of the system consists of the GR1, GR2, GR3 and GR4 trunk lines (48-inch diameter, X60-X70 steel grades, designed for 70-80 bar), which transport gas from the Hassi R'Mel hub to the Mediterranean LNG terminals of Arzew, Skikda and Bethioua. Three submarine pipelines (Transmed, Medgaz and the now-decommissioned GME) carry Algerian gas to the European market through Tunisia, Spain, and Morocco. The total length of the system exceeds 22,000 km, and several major projects (GR5 line, Hassi R'Mel-Hassi Messaoud crude line) have been implemented with API 5L X70 and X80 grades during the last decade [Sonatrach, 2020].

The adoption of X80 steel for new high-pressure gas transmission projects in Algeria is motivated by the same considerations as in other major gas-producing countries: a 30 % reduction in steel weight for the same operating pressure compared to X65, a 15-20 % reduction in the total project cost, a higher transmission capacity for a given pipe diameter, and improved compatibility with hydrogen-blended natural gas in view of future energy-transition scenarios. The technical challenges associated with X80 — strict control of the rolling and cooling parameters, qualification of low-hydrogen welding consumables, refinement of girth-weld inspection methods — have been addressed by an active research community in the Algerian universities and by international collaborations, in particular through joint projects involving research groups in Metz, Toulouse, and London [Hadj Meliani et al., 2010; Bouledroua et al., 2017].

The aging of the older sections of the Algerian network — some of which were installed in the 1960s in regions with active soil corrosion or seismic activity — has prompted the development of national integrity-management programs, supported by the procurement of in-line inspection capabilities, the training of integrity engineers, and the issuance of dedicated technical specifications. The present work, focused on the interaction of mechanical-damage defects in an X80 pipeline, is intended to provide a contribution to the assessment methodology of multi-defect configurations encountered on the Algerian and international transmission networks.

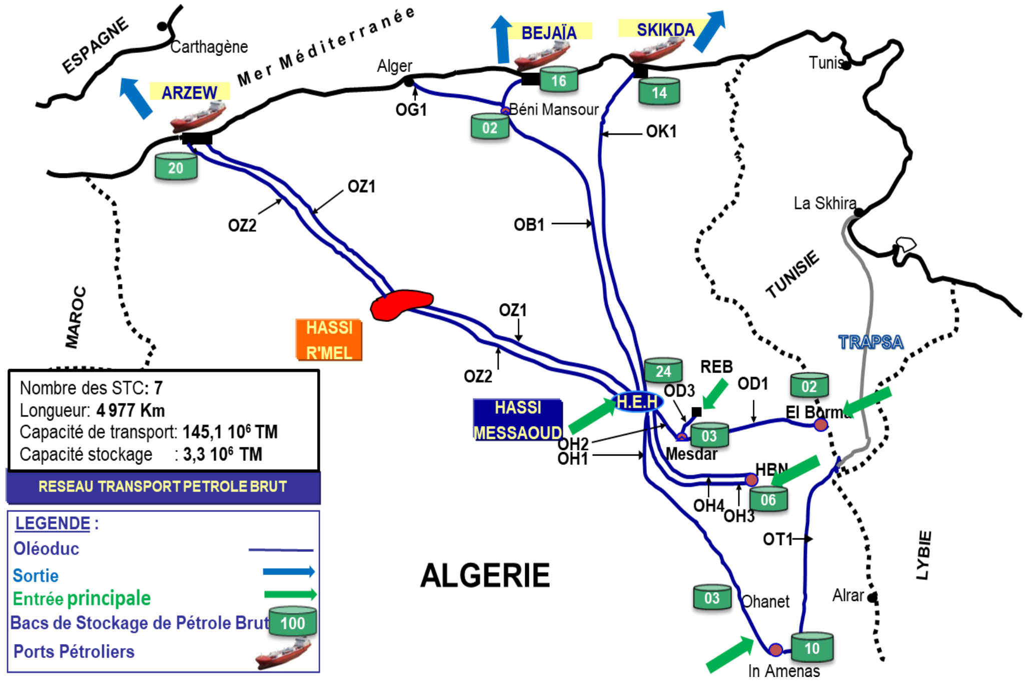

Figure 4: Map of the Crude Oil Transport Network [Anon., AVRIL 2022]

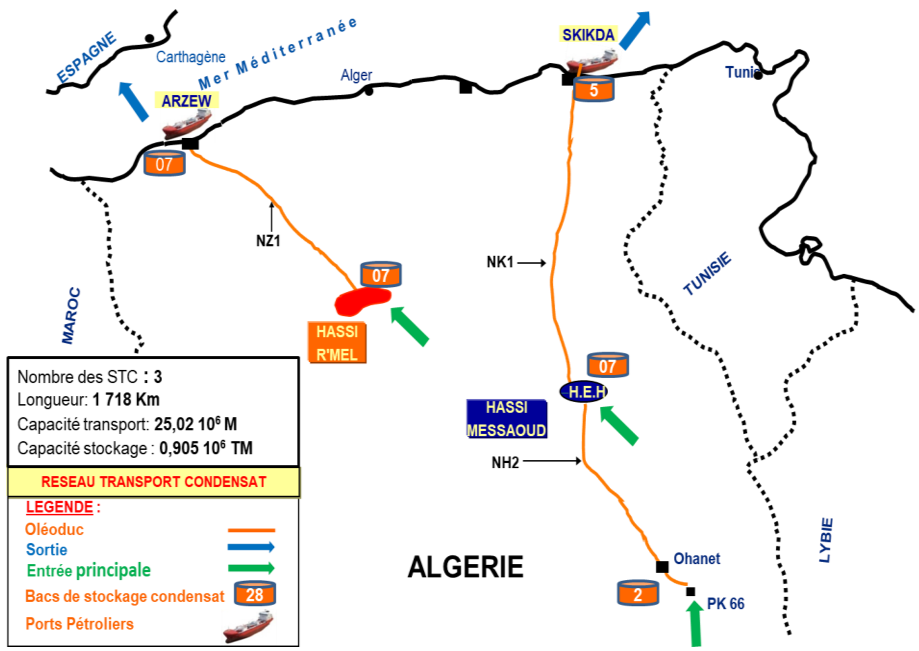

Figure 5: Network Map of Condensate Transport [Anon., AVRIL 2022]

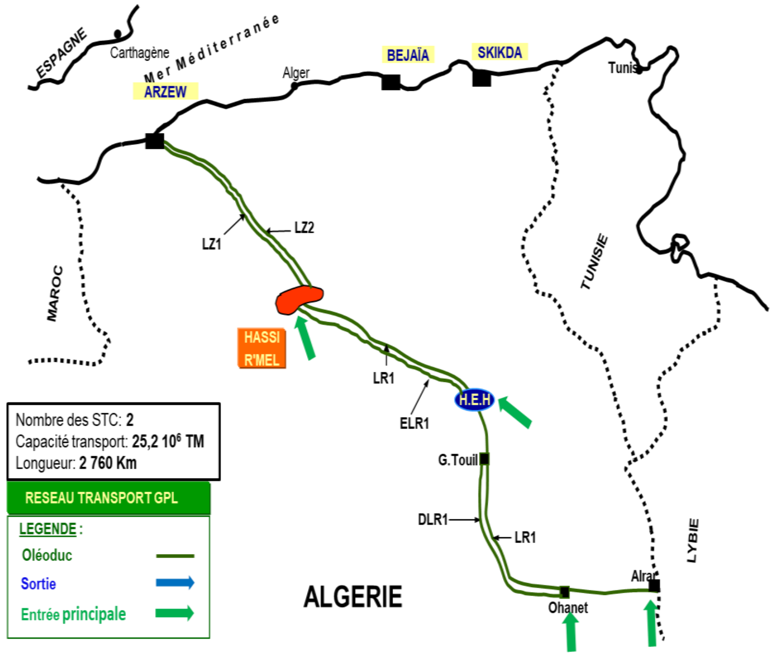

Figure 6:Map of the LPG Transport Network [Anon., AVRIL 2022]

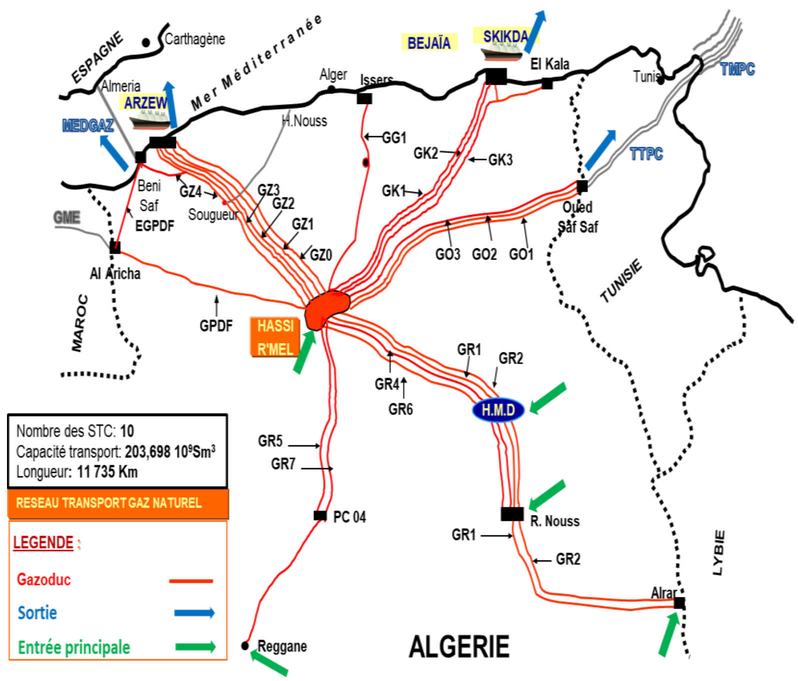

Figure 7: Map of the natural Gas Transport Network [Anon., AVRIL 2022]

1.6.2 Numerical computation of the J-integral in finite elements

The accurate computation of the J-integral in three-dimensional finite element models is a non-trivial task that requires careful attention to several technical issues. The first issue is the formulation of the integral itself. While the original Rice integral was defined as a line integral on a contour Γ around the crack tip, three-dimensional implementations typically use the equivalent domain integral formulation, in which the line integral is converted into an area or volume integral over a domain surrounding the crack front [Shih et al., 1986; Nikishkov & Atluri, 1987]. The equivalent domain integral is given by:

$$J(s) = \int V \left(\sigma ij \times \frac{\partial ui}{\partial x} - W\delta ij\right) \times \frac{\partial q}{\partial xi} dV \ (10)$$

where q is a smooth scalar field that takes the value 1 on the inner boundary of the integration domain and 0 on its outer boundary, and where the derivative ∂q/∂xi is non-zero only in a thin ring of elements surrounding the crack front. This formulation is much better suited to numerical implementation than the original contour integral, because the integration is performed at the Gauss points of the finite elements and benefits from the natural high accuracy of finite element integration.

The second issue is the choice of the finite element mesh in the vicinity of the crack tip. For elastic-plastic problems with high mesh refinement near the crack tip, a focused mesh in which the elements collapse to the crack tip and have quarter-point nodes is generally preferred for two-dimensional models, while three-dimensional models use brick or wedge elements forming concentric rings around the crack front. The smallest element size at the crack tip is typically of the order of CTOD/20 to CTOD/50, which for a typical pipeline geometry translates to element dimensions of 10-50 µm. This high level of refinement is required to capture the strong gradients of stress and strain in the singular zone, and to ensure the path-independence of the computed J values [Brocks & Scheider, 2003].

The third issue is the verification of path independence. In a well-posed numerical problem, the value of J computed on different integration domains (concentric rings of elements at increasing distance from the crack tip) should be identical within numerical accuracy. In practice, the value of J computed on the smallest ring (i.e., the elements immediately adjacent to the crack tip) is sensitive to the modeling details and is generally discarded; the values computed on rings at intermediate distances are taken as the reference. Variations of more than 5 % between different rings indicate a problem with the mesh refinement, the material model, or the loading definition, and should trigger a re-examination of the model.

The fourth issue is the influence of plasticity-induced effects. The original derivation of J assumes a non-linear elastic material with proportional loading, and the path-independence breaks down in the presence of unloading, of finite strains, or of large rotations. Modifications of the J formulation — such as the J* of Atluri, the Tˆ integral of Stonesifer-Atluri, or the energy-domain integral of Moran-Shih — have been proposed to extend the validity of J to general elastic-plastic situations [Atluri, 1986; Moran & Shih, 1987]. For pipeline applications under quasi-static monotonic loading, the standard J formulation implemented in commercial codes is generally adequate, provided that the displacements remain small with respect to the wall thickness and that the geometric non-linearities are properly accounted for in the model.

1.6.3 The Charpy V-notch impact test and the transition curve

The Charpy V-notch (CVN) impact test, although it is not a fracture-mechanics test in the strict sense, remains the most widely used qualification test for pipeline steels because of its simplicity, low cost, and decades of correlation with operating experience. In a CVN test, a small notched specimen (10 × 10 × 55 mm with a 2 mm-deep notch of 0.25 mm radius) is broken by the impact of a pendulum hammer, and the energy absorbed in the fracture is measured. By repeating the test at different temperatures, the temperature dependence of the absorbed energy is mapped out, producing the well-known ductile-to-brittle transition curve.

API 5L specifies minimum CVN energy values for line pipes of different grades and wall thicknesses, with typical values of 27-40 J for the base metal of X52-X70 steels at the design minimum temperature, and 80-100 J for the base metal of X80-X100 steels [API 5L, 2018]. The corresponding minimum values for the weld metal and the heat-affected zone are usually slightly lower (typically 60-80 % of the base-metal value). The temperature at which the fracture surface is 50 % brittle and 50 % ductile (the FATT, Fracture Appearance Transition Temperature) is also recorded, and should be significantly below the lowest service temperature to guarantee fully ductile fracture during all operating conditions.

Correlations have been established between CVN energy and fracture-mechanics parameters such as KIC, JIC, and CTOD. The most widely used correlation is the Rolfe-Novak-Barsom correlation for the upper-shelf region, the Wallin Master Curve for the transition region, and the lower-bound Sailors-Corten correlation for conservative estimates. These correlations, while useful for preliminary estimates, are no substitute for direct measurement of the fracture-mechanics parameters in cases where a rigorous integrity assessment is required [Rolfe & Barsom, 1999; Wallin, 1991].

1.6.4 Damage tolerance and the leak-before-break concept

Damage tolerance is the design philosophy according to which a pipeline is engineered to safely operate in the presence of a population of pre-existing flaws of sizes smaller than the critical size that would lead to immediate failure. The damage-tolerance approach involves three steps: assumption of a maximum credible initial defect size, prediction of the defect growth under operational loading, and verification that the defect remains below the critical size during the entire operational life. The defect growth predictions are based on Paris-law fatigue analysis, SCC growth-rate data, or corrosion-rate distributions, depending on the active degradation mechanism.

The leak-before-break (LBB) concept, originally developed for nuclear pressure vessels in the 1970s, postulates that a growing crack will first propagate through the pipe wall thickness and produce a detectable leak before reaching the critical length that would cause a catastrophic rupture. The LBB concept is particularly important for high-pressure gas pipelines, where a leak (smaller, slower release) is much less consequential than a rupture (massive, rapid release). The achievement of LBB conditions depends on the relationship between the critical length of a through-wall crack at the operating pressure and the through-wall crack length corresponding to a detectable leak (typically defined by a minimum leak rate or by the sensitivity of the leak-detection system) [Wilkowski, 2000].

For modern X80 transmission pipelines, the LBB margin (ratio of critical through-wall length to detectable through-wall length) is typically in the range of 2 to 5 for representative operating pressures, indicating that the LBB concept is broadly applicable. However, this conclusion can be challenged in the presence of interacting defects, of localized embrittlement (e.g. in welds), or of low-temperature service conditions. The detailed J-integral analyses presented in the subsequent chapters of this work are intended, among other objectives, to evaluate whether the LBB margin is preserved when a fatigue crack interacts with a co-located dent and/or with a remote scratch.

1.6.5 Statistical analysis of pipeline failures

The statistical analysis of pipeline failures provides essential input for the development of risk-based integrity management programs and for the validation of fitness-for-service methods.

Several international databases collect data on pipeline incidents: the European Gas pipeline Incident data Group (EGIG) covers more than 140,000 km of European gas transmission pipelines since 1970; the Concawe database covers European cross-country oil pipelines since 1971; the U.S. PHMSA database is the most extensive and includes incidents on gas and liquid pipelines in the United States since 1970; the Canadian Energy Regulator (CER, formerly NEB) maintains a similar database for Canadian transmission pipelines [EGIG, 2018; Concawe, 2020; PHMSA, 2020; CER, 2019].

According to the EGIG 10th report, covering the period 1970-2016 on European gas transmission pipelines, the overall incident frequency is 0.32 per 1000 km·year, with a clear decreasing trend over the last two decades thanks to the implementation of integrity-management programs and the deployment of in-line inspection technologies. The distribution of incidents by cause is as follows: external interference (third-party damage) 26 %, construction defects and material flaws 26 %, corrosion 19 %, ground movement 6 %, hot tap made by error 4 %, other causes 19 %. The relative weight of construction and material defects has decreased significantly with the improvement of manufacturing quality and welding procedures, while the relative weight of corrosion-related incidents has decreased thanks to the systematic deployment of ILI tools.

PHMSA statistics for U.S. natural gas transmission pipelines over the period 2010-2019 show an overall incident frequency of approximately 0.07 per 1000 km·year for significant incidents (those causing fatalities, injuries, or property damage above $50,000), substantially lower than the European figure but with a different distribution of causes: equipment failures 33 %, corrosion 25 %, material/weld defects 17 %, external force 14 %, incorrect operations 6 %, and other 5 %. These statistics support the prioritization of corrosion management and material defect assessment as the two most important elements of modern integrity-management programs [PHMSA, 2020; Lam & Zhou, 2016].

1.6.6 Hydrogen effects and the implications for future X80 service

The progressive emergence of hydrogen as a key vector of the energy transition has revived a long-standing concern of the pipeline industry: the susceptibility of high-strength steels to hydrogen-induced degradation. When dissolved in the metal, atomic hydrogen accumulates at microstructural traps (dislocations, grain boundaries, second-phase interfaces, voids) and modifies the mechanical response of the material in several ways: a reduction of the apparent ductility (hydrogen embrittlement, HE), a decrease of the fracture toughness, an acceleration of the fatigue crack growth rate, and the possible initiation of hydrogen-induced cracking (HIC) at sites of high triaxial stress. The magnitude of these effects depends on the hydrogen partial pressure, on the operating temperature, on the chemical composition and microstructure of the steel, on the rate of loading, and on the presence of cathodic poisoning species such as H2S [Capelle et al., 2008; San Marchi & Somerday, 2012].

For X80 steel specifically, an active research effort has been undertaken in the last decade to characterize the influence of hydrogen on the mechanical and fracture-mechanics properties. The general conclusions of these studies are that X80 retains adequate strength and ductility under low-pressure hydrogen (e.g. for the blending of hydrogen with natural gas at concentrations up to 10-20 % vol), but that significant degradation can occur at higher hydrogen partial pressures or in the presence of localized cold-worked regions (typical of dents and gouges). The fatigue crack growth rate is the most sensitive property, with acceleration factors of 5 to 10 commonly reported for X80 under hydrogen pressures of 5-10 MPa compared to air. These findings have direct implications for the assessment of multi-defect configurations in pipelines intended for future hydrogen service, since the local cold-working at the bottom of dents and gouges can be expected to act as a preferential hydrogen-accumulation site and to amplify the local degradation of the fracture-mechanics properties [Slifka et al., 2018].

The integration of hydrogen-effect models into the J-integral-based assessment of multi-defect configurations is one of the most active research frontiers in pipeline fracture mechanics. Three modeling approaches are currently being developed: (i) phenomenological reduction factors applied to the air-environment J-R curve to account for the hydrogen-induced toughness loss; (ii) micro-mechanical models based on the local hydrogen concentration at the crack tip, computed from the diffusion equation with hydrostatic-stress-driven trapping; and (iii) cohesive-zone or phase-field models in which the cohesive strength is locally reduced as a function of the hydrogen concentration. The present work does not include hydrogen effects explicitly, but the methodology developed here can be extended to hydrogen service through any of these three modeling approaches, provided that the relevant material parameters are characterized through dedicated experimental campaigns.

1.7. Chapter Summary and Conclusions

This first chapter has reviewed the fundamentals of fracture mechanics with specific emphasis on their application to buried high-pressure transmission pipelines made of API 5L X80 steel.

Starting from the general context of the world hydrocarbon transportation infrastructure, with its 3.5 million kilometers of operating pipelines and its hundreds of billions of dollars of annual economic activity, the chapter has progressively introduced the technical concepts and the analytical tools that constitute the discipline of pipeline fracture mechanics.

The historical development of fracture mechanics, from the pioneering work of Griffith on brittle fracture in glass (1921) to the modern J-integral and CTOD methodologies of Rice (1968), Hutchinson (1968) and Wells (1961), has been outlined, with particular emphasis on the contributions that have specifically targeted the assessment of pressure-containing structures and pipelines. The two main families of fracture-mechanics parameters — the linear-elastic K and the elastic-plastic J and CTOD — have been defined, their relationships have been established for typical pipeline configurations, and their experimental determination through the ASTM E399, E1820 and E1921 standardized tests has been described.

The mechanisms of crack initiation and propagation have been examined in the four main families relevant to pipeline operation: brittle cleavage under low-temperature conditions, ductile fracture through microvoid nucleation, growth and coalescence (Rice-Tracey, Gurson-Tvergaard-Needleman models), fatigue propagation under cyclic loading (Paris law and its refinements), and environmentally-assisted cracking, including the two main forms of stress corrosion cracking in pipelines (high-pH SCC and near-neutral-pH SCC) and hydrogen-induced cracking under sour service conditions.

The factors that influence the fracture behavior of pipeline steels have been analyzed in three categories: material-related factors (chemical composition, microstructure, mechanical properties, including the specific properties of X80 steel), loading-related factors (internal pressure, temperature, residual stresses, dynamic effects), and environmental factors (corrosive species, hydrogen environments). The discussion has highlighted the specific advantages of X80 steel — high yield strength combined with excellent ductile toughness — but also its specific challenges, including the strict control of the rolling and cooling parameters and the qualification of low-hydrogen welding consumables.

Finally, the evaluation methods and rupture criteria currently used in industrial practice have been reviewed: the empirical equations for corrosion defects (B31G family, DNV-RP-F101, PCORRC), the Failure Assessment Diagram (FAD) approach with its three Options (BS 7910, API 579-1, R6), the J-integral and CTOD methods for crack-like defects, and the specific approaches developed for dent-gouge configurations (EPRG criterion). The numerical computation of the J-integral in three-dimensional finite element models has been discussed in some detail, since it constitutes the methodological core of the present work.

Section 1.6 has provided complementary considerations specifically relevant to the present research: the context of the Algerian transmission network and the strategic case for X80 steel, the numerical implementation of the J-integral computation through the equivalent domain integral, the role of the Charpy V-notch impact test as a qualification tool, the damage-tolerance and leak-before-break design philosophies, and the statistical analysis of pipeline failures based on the EGIG and PHMSA databases. These considerations frame the present numerical study within the broader context of pipeline-integrity research and practice.

On the basis of this overview, several conclusions can be drawn that orient the methodology of the subsequent numerical study. First, the elastic-plastic J-integral is the most appropriate fracture-mechanics parameter for the assessment of ductile high-toughness pipeline steels such as X80, for which the linear-elastic stress-intensity factor K is generally insufficient. Second, the accurate computation of J in the presence of multiple interacting defects (crack, dent, scratch) requires detailed three-dimensional finite element analyses with non-linear material behavior, proper mesh refinement around the crack front (element size of CTOD/20 to CTOD/50), and verification of path-independence. Third, the relevant material characterization includes not only the conventional tensile properties (E, σy, σu, ε_uniform) but also the J-R curve obtained from SE(B) or C(T) specimens, the Charpy transition curve, and ideally the constraint-corrected fracture toughness for the relevant crack geometries. Fourth, the results of the numerical analyses should be presented in non-dimensional form, in terms of interaction factors or amplification ratios, to enable their generalization beyond the specific configurations analyzed.

These conclusions provide the methodological foundation for the numerical study presented in the subsequent chapters, where the J-integral behavior of a longitudinal surface crack interacting with a co-located dent and with a remote scratch in an API X80 transmission pipeline will be investigated in detail through systematic parametric finite element simulations.

2. Chapter II: Pipeline Integrity

2.1. Introduction to Pipeline Integrity

2.1.1 Definition and scope of pipeline integrity

Pipeline integrity can be defined as the ability of a pipeline system to safely and reliably perform its intended function — namely, the continuous transportation of a fluid between two points — without releasing its content into the environment and without endangering people, property, or surrounding ecosystems. From an engineering point of view, pipeline integrity encompasses the structural integrity of the steel pipe and of all associated components (welds, fittings, valves, supports), the integrity of the protective coating and cathodic-protection system, and the integrity of the operational control system (pressure-relief devices, leak-detection systems, communication and SCADA infrastructure).

Pipeline integrity management has evolved from a reactive, inspection-driven discipline in the 1960s and 1970s into a proactive, risk-based discipline embodied in modern Integrity Management Programs (IMP). The U.S. Pipeline Safety Improvement Act of 2002 and the subsequent issuance of 49 CFR Part 192 (gas pipelines) and Part 195 (liquid pipelines) by the Department of Transportation made the implementation of formal IMP mandatory for operators of pipelines passing through High-Consequence Areas (HCAs) [PHMSA, 2002]. Equivalent regulations were adopted in Canada (CSA Z662), in the European Union (PEMSA), and in many other producing countries. International standards such as API 1160 for liquid pipelines and ASME B31.8S for gas pipelines provide detailed guidance on the elements of an Integrity Management Program [API 1160, 2019; ASME B31.8S, 2018].

From a system perspective, an IMP comprises six main components: identification of threats and hazards, risk assessment, integrity assessment (through inspection, testing or evaluation), implementation of mitigation measures, performance evaluation through Key Performance Indicators (KPIs), and continuous improvement through periodic management reviews. The interaction between these components forms a closed-loop quality system inspired by the Plan-Do-Check-Act (PDCA) cycle of ISO 9001. The successful implementation of an IMP requires a deep technical understanding of the failure mechanisms, of the inspection and surveillance technologies, and of the fitness-for-service assessment methods, which are the subject of the present chapter.

2.1.2 Economic and societal stakes

The economic and societal stakes associated with pipeline integrity are very high. The total replacement value of the world pipeline network is estimated at more than 1500 billion US dollars, and the loss of even a single pipeline section can cost tens of millions of dollars in lost production, environmental damage and legal liabilities. Major pipeline failures, such as the Belo Oriente accident in Brazil (2000), the Carlsbad explosion in New Mexico (2000), the Ghislenghien gas-pipeline rupture in Belgium (2004), the Enbridge Line 6B oil spill in Michigan (2010), and the San Bruno gas-pipeline explosion in California (2010) have caused dozens of fatalities, billions of dollars of damages, and have profoundly shaken public confidence in the pipeline industry [NTSB, 2011, 2012; Lam & Zhou, 2016].

These accidents have triggered substantial regulatory reforms, with notable strengthening of integrity-assessment frequencies, increased reliance on in-line inspection technologies, and stricter requirements for the qualification of inspection personnel and the documentation of integrity-assessment processes. They have also reinforced the role of fracture mechanics and computational methods as scientific bases for fitness-for-service assessments, since the empirical failure equations developed in the 1970s and 1980s prove insufficient for the assessment of complex defect interactions or for the prediction of failure under novel operating conditions such as hydrogen transportation or low-temperature service.

2.1.3 The defense-in-depth concept

Pipeline integrity management relies on the concept of defense-in-depth, in which multiple independent barriers are deployed to prevent the occurrence of a leak or rupture and, in case of failure of one or more barriers, to mitigate its consequences. The first barrier is the structural integrity of the pipe wall itself, ensured by careful design, quality of manufacturing, and rigorous Fitness-For-Service assessment of any detected defect. The second barrier is the protective coating and the cathodic-protection system, which prevent external corrosion. The third barrier consists in the operating procedures and the SCADA control system, which limit the pressure, monitor the operating conditions, and detect anomalies in real time. The fourth barrier is constituted by the leak-detection systems and the emergency-response procedures, which limit the consequences of any release.

The robustness of the defense-in-depth approach has been confirmed by extensive statistical analyses showing that most major accidents involve the simultaneous failure of two or more barriers, rather than the failure of a single isolated barrier. The systematic identification, monitoring, and reinforcement of all barriers is therefore the cornerstone of modern pipeline integrity management, in line with the recommendations of the International Energy Agency, the European Commission, and the United Nations Sustainable Development Goals related to safe and reliable energy infrastructure [IEA, 2019].

2.2. Types of Defects and Degradation Mechanisms

2.2.1 Classification of pipeline defects

Pipeline defects can be classified in several ways. From an origin point of view, three categories are usually distinguished: manufacturing defects, which originate in the steelmaking process or in the welding operations performed during pipe fabrication; construction defects, introduced during transportation, handling and installation of the pipe in the field; and in-service defects, which appear during operation under the combined effect of mechanical, environmental and operational factors. From a geometrical point of view, defects can be planar (cracks, lack of fusion, lack of penetration), volumetric (corrosion patches, dents, gouges, inclusions), or geometric (out-of-roundness, ovality, misalignment of welds). From a kinematic point of view, defects can be static (their size remains constant over time) or active (their size evolves with time, as is the case for corrosion, fatigue cracking, or stress corrosion cracking).

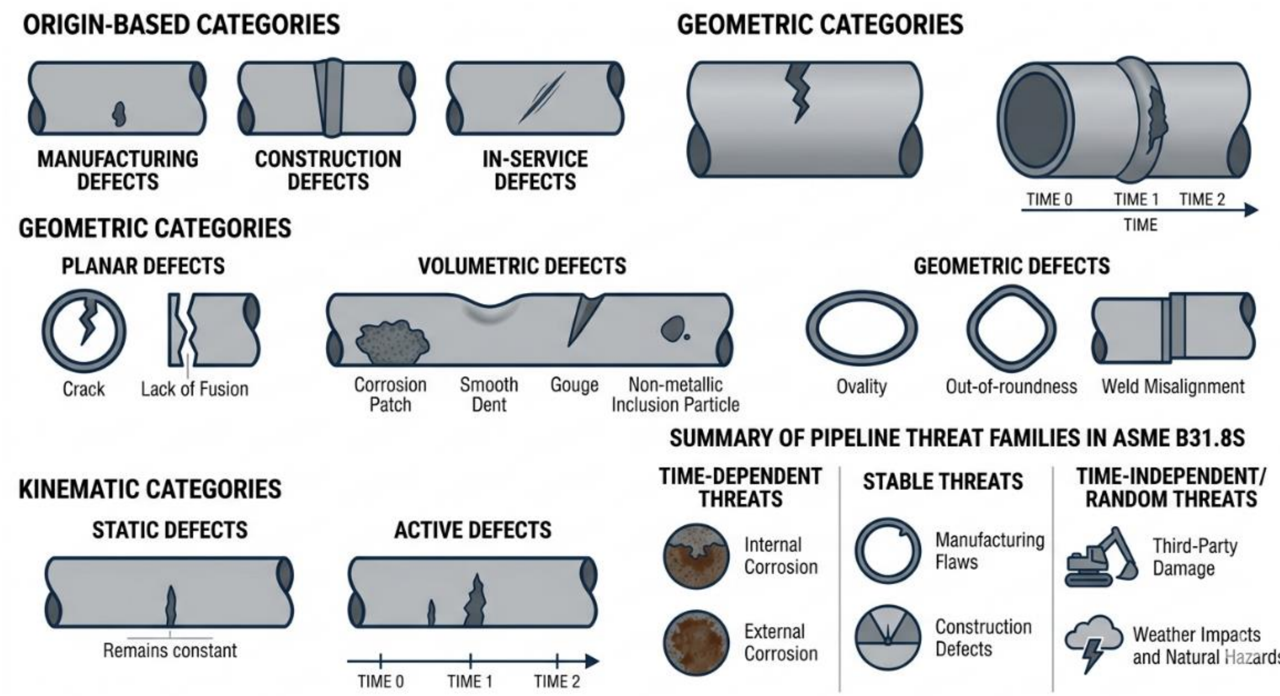

Figure 8: Pipeline Defect Classification and Threat Families in ASME B31.8S

The ASME B31.8S standard distinguishes nine families of threats, grouped into three categories: time-dependent threats (external corrosion, internal corrosion, stress corrosion cracking), stable threats (manufacturing defects, construction defects, equipment defects), and time-independent or random threats (third-party damage, incorrect operations, weather and outside-force damage) [ASME B31.8S, 2018]. This classification provides a useful framework for the design of an Integrity Management Program, since each family of threats calls for specific inspection technologies, surveillance procedures, and mitigation strategies.

2.2.2 Metal-loss defects: corrosion and erosion

Metal-loss defects, encompassing external corrosion, internal corrosion, and erosion, are by far the most frequent threat to onshore and offshore pipelines. External corrosion is the localized or generalized electrochemical degradation of the outer surface of the pipe, caused by the contact between the bare steel and the surrounding soil electrolyte. The corrosion rate depends on the soil resistivity, moisture content, pH, redox potential, dissolved oxygen concentration, and the presence of sulfate-reducing or iron-oxidizing bacteria. Coating defects (holidays, disbondments) and inadequate cathodic protection are usually necessary conditions for external corrosion to develop [Beavers & Thompson, 2006].

Internal corrosion, on the other hand, results from the chemical interaction between the transported fluid and the internal surface of the pipe. The main agents are CO2 (sweet corrosion), H2S (sour corrosion), oxygen, organic acids, and chlorides, often in combination with bacterial activity. Sweet corrosion follows the well-known de Waard-Milliams model, while sour corrosion can produce, in addition to general thinning, hydrogen-induced cracking (HIC), sulphide stress cracking (SSC), and stepwise cracking [de Waard & Lotz, 1993; Carneiro et al., 2003]. Erosion corrosion is observed in pipelines transporting multi-phase flows containing sand particles, water droplets, or gas bubbles, and is concentrated in bends, tees and reducers.

Assessment of metal-loss defects is the most mature topic of pipeline integrity, with a long tradition of full-scale burst tests, dedicated assessment methods (B31G, Modified B31G, RSTRENG, DNV-RP-F101, PCORRC, LPC-1, SHELL92), and in-line inspection technologies (magnetic flux leakage, ultrasonic wall-thickness measurement, electromagnetic acoustic transducers). Recent research has focused on the assessment of interacting corrosion clusters, on the influence of complex profiles, and on the integration of probabilistic models accounting for the uncertainty in the corrosion rate and in the defect dimensions [Cosham et al., 2007; Shuai et al., 2017].

2.2.3 Crack-like defects: SCC, fatigue, hydrogen and weld cracks

Crack-like defects represent the most severe threat to pipeline integrity because their small thickness, sharp tip and propensity to propagate under cyclic or environmental loading make them difficult to detect and to characterize. Four main classes of crack-like defects are encountered in service: stress-corrosion cracks (high-pH and near-neutral-pH SCC), fatigue cracks (initiated at stress concentrators such as toes of girth welds, dents or seam welds), hydrogen-induced cracks (HIC, SOHIC, and stepwise cracking in sour service), and weld defects (lack of fusion, lack of penetration, slag inclusions, undercuts, hot cracking) [Parkins, 2000; Beavers, 2014].

SCC is particularly insidious because it tends to develop in colonies of parallel cracks that can coalesce and form a critical defect rapidly. Operating experience accumulated over the past four decades has revealed that the most susceptible pipelines are those operating above 60 % of SMYS, in soils with disbonded asphalt coating, and in regions where the temperature fluctuations promote the formation of carbonate-bicarbonate electrolytes under the disbonded coating. The Pipeline Research Council International (PRCI) has compiled detailed databases of SCC occurrences and has developed specific assessment methods based on the modified ln-secant equation and on the J-integral approach [Leis & Thomas, 2001].

Fatigue cracking is mainly observed in pipelines subjected to substantial pressure cycles, such as liquid pipelines with frequent shutdown-restart cycles, or in offshore pipelines subjected to wave action and vortex-induced vibration. The fatigue life of a pipeline section containing a flaw can be predicted by integration of the Paris law from the initial flaw size to the critical flaw size determined by FAD or J-based assessment. For X80 pipeline steel, dedicated experimental campaigns have been carried out to determine fatigue crack growth rates in air and in simulated near-neutral-pH soil environments [Beretta et al., 2013; Chen et al., 2007].

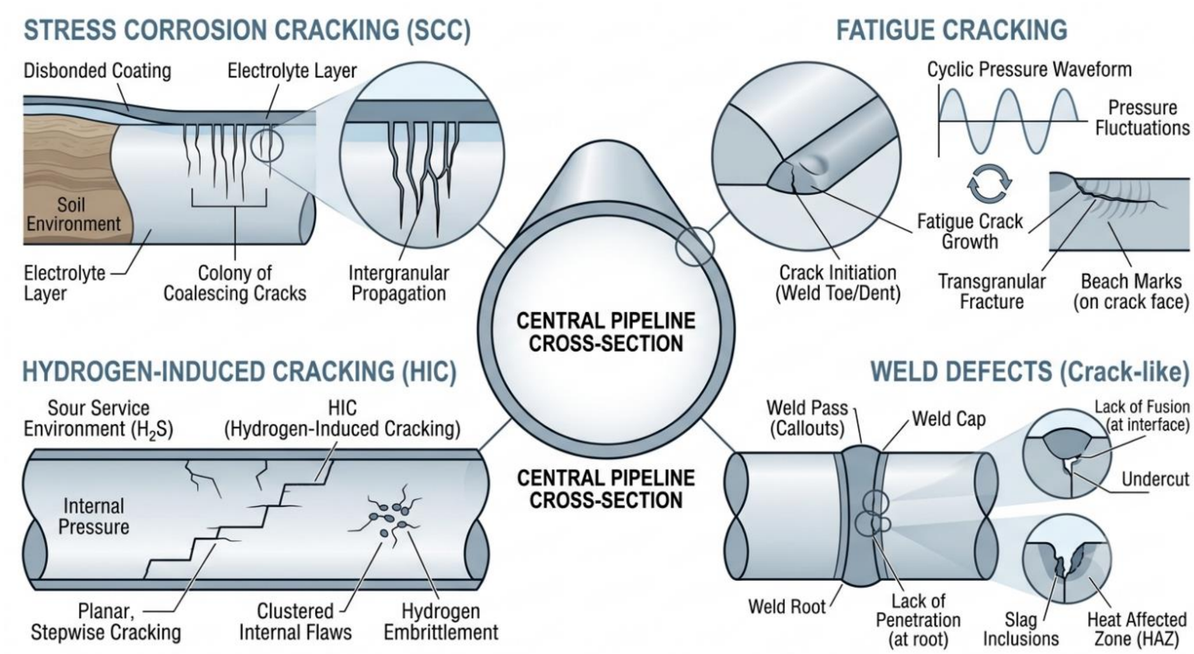

Figure 9: Crack-Like Pipeline Defects: SCC, Fatigue Cracking, HIC, and Weld Defects

2.2.4 Mechanical damage: dents, gouges, and scratches

Mechanical damage encompasses all the defects caused by external mechanical contact with the pipe, including dents, gouges, scratches, grooves and arc burns. These defects are most frequently produced by excavation equipment (backhoes, augers) operated by third parties, and they account for a significant fraction of major pipeline failures recorded worldwide. A dent is a permanent plastic deformation of the pipe wall that produces a change of curvature and does not necessarily involve loss of material; a gouge is a loss of material caused by mechanical scraping, often accompanied by cold-working and microstructural alteration of the underlying steel; a scratch is a shallow gouge with limited depth (typically less than 10 % of the wall thickness).

The structural significance of mechanical damage depends on the geometry of the defect (depth, length, shape, orientation), on the presence or absence of co-located stress concentrators, and on the operational history of the pipeline after the damage event. Plain dents (i.e., dents without gouge, scratch or weld interaction) tend to re-round under the action of internal pressure, but they introduce residual stresses, strain hardening and a local stress concentration that can promote fatigue crack initiation under cyclic loading. Dent-gouge combinations are particularly dangerous because the gouge acts as an initial flaw that can propagate by fatigue under the cyclic stress concentration induced by the dent [Macdonald & Cosham, 2005; Cosham & Hopkins, 2007].

The interaction between a crack-like defect (such as a fatigue crack or a SCC colony) and a co-located dent, gouge, or scratch is the central topic of the present work. Experimental and numerical studies have shown that this interaction can lead to a significant amplification of the local fracture parameters (J-integral, CTOD), well beyond the values predicted by single-defect assessments. The amplification factor depends on the relative position of the defects, on their respective depths, on the level of internal pressure, and on the elastic-plastic constitutive behavior of the steel. Quantitative characterization of this interaction is essential for the safe operation of high-pressure transmission pipelines, and it can only be achieved through detailed three-dimensional finite element simulations including non-linear material behavior, contact between the indenter and the pipe wall, and accurate computation of the J-integral along the crack front.

2.2.5 Geometric defects and weld imperfections

In addition to the three main families of defects described above, several other classes of imperfections can compromise pipeline integrity. Geometric defects include ovality, out-of-roundness, wrinkles, buckles, and misalignment of girth welds; their main effect is the introduction of localized bending stresses and the modification of the elastic-plastic response of the pipe under combined pressure and bending. Wrinkles, in particular, can develop into low-cycle fatigue cracks if the pipeline is subjected to repeated thermal cycles, as encountered in steam injection lines or in arctic environments [Souza & Murray, 1999].

Weld imperfections are a heterogeneous family that includes both volumetric defects (porosity, slag inclusions, undercut) and planar defects (lack of fusion, lack of penetration, hot cracks, hydrogen-induced cold cracks). The assessment of weld defects is governed by international standards such as API 1104, ISO 13847 and EN 12732, which specify maximum acceptable dimensions based on workmanship considerations [API 1104, 2018]. For long, narrow planar defects, an Engineering Critical Assessment (ECA) using the FAD or the J-integral approach can be performed to demonstrate fitness for service, provided that the necessary fracture-toughness data and the residual-stress distribution in the weld are properly characterized [BS 7910, 2019; Koçak et al., 2008].

2.3. Inspection and Monitoring Methods

2.3.1 In-Line Inspection (ILI): principles and technologies

In-Line Inspection (ILI), commonly called 'pigging', is the most widely used method for the inspection of long transmission pipelines. An ILI tool, or 'smart pig', is a self-propelled instrumented device that travels inside the pipeline under the pressure of the transported fluid and measures the geometry and the structural condition of the pipe wall along its entire length. Several technologies are deployed depending on the type of defects targeted [Nestleroth & Bubenik, 1999].

Magnetic Flux Leakage (MFL) tools magnetize the pipe wall to near saturation through powerful permanent magnets, and detect the leakage flux produced by the perturbations of the magnetic field caused by metal-loss defects. MFL is the workhorse technology for the detection and sizing of external and internal corrosion, with depth-sizing accuracies of ±10 % of the wall thickness and reliable detection thresholds of 10 % of the wall thickness. Modern MFL tools combine axial and transverse magnetization (TFI/CMFL) to detect both circumferentially-oriented and axially-oriented defects, including narrow axial slits typical of SCC or longitudinal seam-weld cracks.

Ultrasonic Testing (UT) tools, employing either piezoelectric transducers in a liquid couplant (for liquid pipelines) or Electromagnetic Acoustic Transducers (EMAT) (for gas pipelines), measure the wall thickness directly with accuracies of ±0.3 mm and can detect lamination defects, cracks, and SCC colonies. UT tools require careful calibration but provide quantitative information on wall thickness that is superior to MFL in many respects. Modern combined tools (UT-Crack, EMAT-CD, UltraScan WM) combine wall-thickness mapping with crack detection in a single run, optimizing inspection efficiency and reducing the operational impact on the line [Reber et al., 2002].

Geometric inspection tools (caliper or geometry pigs) measure the internal diameter of the pipe with multi-finger arms or laser scanners, and detect dents, ovality, wrinkles and bends with millimetric accuracy. The combination of MFL, UT and geometry data in modern multi-sensor tools provides a comprehensive picture of the pipe condition along the entire length of the inspected section, supporting subsequent integrity-assessment activities [Cordell & Vanzant, 2003].

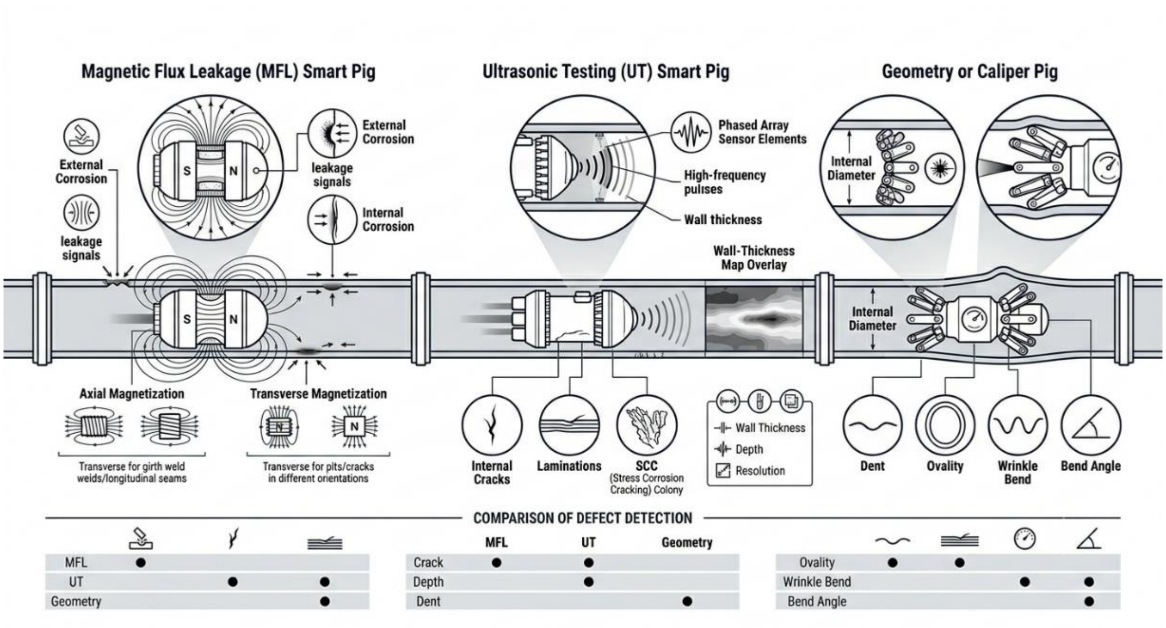

Figure 10: Pipeline Inspection Technologies: MFL, UT, and Geometry Pigs

2.3.2 Surface inspection and non-destructive testing

In addition to in-line inspection, several non-destructive testing (NDT) methods are deployed on the external surface of the pipe during construction, repair, and maintenance operations. Visual Testing (VT) is the most basic but also one of the most important inspection methods, since experienced inspectors can detect surface defects, coating damage, and signs of corrosion that may not yet be visible to instrumented tools. Penetrant Testing (PT) is used to detect surface-breaking discontinuities in welds and machined components, while Magnetic Particle Testing (MT) is suitable for ferromagnetic materials and detects surface and near-surface defects [ASNT, 2016].

Ultrasonic Testing (UT) in its conventional form, with single or twin transducers manually scanned over the surface of the pipe, allows precise sizing of cracks and corrosion defects, and is the workhorse method for the inspection of girth welds. Time-Of-Flight Diffraction (TOFD) and Phased Array Ultrasonic Testing (PAUT) are more advanced versions of UT that provide enhanced detection capability for crack-like defects and improved characterization of complex defect geometries. Automated UT systems, mounted on robotic crawlers, are routinely used for the inspection of girth welds on offshore lay barges and on onshore construction sites [Ginzel, 2006].

Radiographic Testing (RT) provides a permanent record of the inspected weld and is widely used during pipeline construction. Conventional film radiography is being progressively replaced by digital radiography (DR) and computed radiography (CR), which offer faster image acquisition, lower radiation doses and easier archival of inspection records. The new ISO 17636 standard governs the application of RT for fusion welds in metallic materials, including pipeline welds [ISO 17636-1, 2013].

Several specialized methods are dedicated to the detection of specific defect families. The Alternating Current Field Measurement (ACFM) technique is used for surface crack detection without removal of paint or coating; the Eddy Current technique detects surface and near-surface defects in non-magnetic and weakly magnetic materials; the Acoustic Emission technique monitors the elastic waves emitted by growing defects during a controlled pressure test; and the new Guided Wave Ultrasonic Testing (GWUT) sends low-frequency ultrasonic waves along the pipe axis to detect anomalies over distances of tens of meters from a single transducer ring, particularly useful for the inspection of buried or insulated sections [Lowe et al., 1998].

2.3.3 Pressure testing

Hydrostatic pressure testing, originally developed in the 1950s by Battelle and TransCanada Pipelines, consists in pressurizing the pipeline with water to a level higher than the maximum operating pressure (typically 1.25 to 1.50 times the MAOP) and holding this pressure for a specified duration, usually 8 hours. Pressure testing is the most direct demonstration of the structural integrity of a pipeline, because any defect that cannot withstand the test pressure will fail during the test rather than during operation, and any defect that survives the test pressure is guaranteed to be smaller than the critical size at the test pressure level [Kiefner et al., 1973; Rosenfeld, 2002].

The main advantages of hydrostatic pressure testing are the simplicity of the principle, the integrative nature of the test (it tests the entire pipeline at once), and the ability to validate not only the pipe body but also the welds, fittings, and connections. The main drawbacks are the operational disruption (the pipeline must be taken out of service, depressurized, filled with water, then drained, dried and returned to service), the environmental impact (potentially large volumes of water consumed and contaminated), the safety risk during pressurization, and the limited information provided about defect populations below the critical size at the test pressure. Modern integrity-management practice combines periodic ILI runs with focused hydrostatic tests on sections where ILI data indicates the highest defect concentrations.

2.3.4 Continuous monitoring and SCADA

Continuous monitoring of pipeline integrity is achieved through the Supervisory Control And Data Acquisition (SCADA) system, which collects in real time the pressure, flow rate, temperature, and operating data from sensors distributed along the pipeline, and transmits them to a centralized control room. Leak detection systems use the SCADA data to identify anomalies in the pressure-flow relationship that may indicate a leak. The two main families of leak-detection systems are the volume balance and the pressure-wave (Real-Time Transient Modeling, RTTM) methods, with detection thresholds in the range of 0.5 to 2 % of the nominal flow rate for the best-performing systems [Geiger, 2006].

More recent monitoring technologies include Distributed Acoustic Sensing (DAS) and Distributed Temperature Sensing (DTS), which use the optical fiber as a continuous sensor along the pipeline length, providing acoustic and thermal data with spatial resolution of about one meter over distances of tens of kilometers. These technologies allow the detection of small leaks (down to 1-10 liters per minute), of mechanical impacts on the pipe (typical of third-party interference), and of abnormal temperature variations associated with hot spots or insulation failures. The integration of DAS and DTS data with conventional SCADA data is one of the most active areas of pipeline-integrity research, with the promise of substantially improved detection capabilities and reduced false-alarm rates [Sun & Stiles, 2017].

2.4. Structural Integrity Assessment

2.4.1 The Fitness-For-Service (FFS) concept

The Fitness-For-Service (FFS) approach is a multi-disciplinary methodology that evaluates the ability of a component containing one or more defects to continue operating safely until the next inspection or until a predefined operational date. The FFS approach was originally developed in the chemical and petrochemical industries during the 1980s, and was codified in the API 579-1/ASME FFS-1 standard, which is now the reference document used worldwide for the assessment of pressure equipment containing in-service damage [API 579-1, 2021]. The FFS methodology rests on three pillars: characterization of the defect (geometry, location, type, growth mechanism), characterization of the loading (operating conditions, residual stresses, transient events), and characterization of the material (mechanical properties, fracture toughness, environmental susceptibility).

The FFS assessment is organized into three sequential levels of increasing complexity and decreasing conservatism: Level 1 corresponds to a simple screening based on tabulated criteria or conservative formulas, suitable for routine engineering use and applicable in the field; Level 2 corresponds to an intermediate engineering assessment using analytical methods and standard fracture-mechanics formulas, requiring more detailed input data; Level 3 corresponds to an advanced assessment based on detailed finite element analyses, fracture-mechanics tests on actual material, and where appropriate, probabilistic methods accounting for the statistical distribution of input parameters. The choice of the appropriate level depends on the safety significance of the assessment, the available data, and the cost-benefit balance for the operator [API 579-1, 2021; BS 7910, 2019].

2.4.2 Engineering Critical Assessment (ECA)

Engineering Critical Assessment (ECA) is a specific application of the FFS methodology to crack-like defects, with the objective of demonstrating that a given defect, or a defect population obtained from inspection data, will not lead to failure during the operational period considered. The reference standard for ECA is BS 7910, which provides detailed procedures for the construction of Failure Assessment Diagrams (FAD), the determination of stress-intensity factors and limit loads for a wide variety of geometries and loading configurations, and the integration of fatigue crack growth and stress-corrosion crack growth in the assessment [BS 7910, 2019]. The FITNET procedure, developed by an European consortium and published in 2008, provides an alternative framework with similar scope and methodology [Koçak et al., 2008].

In a typical ECA of a pipeline weld, the following steps are performed: definition of the largest credible defect size based on inspection data and on the limitations of the NDT method used; characterization of the applied loading, including the operating pressure, the residual stresses in the weld, and any secondary stresses caused by ground movements; determination of the relevant fracture-toughness parameters of the base metal, weld metal, and heat-affected zone, accounting for the operating temperature and the rate of loading; computation of the assessment point (Lr, Kr) on the FAD; verification that the assessment point lies within the safe region of the FAD with appropriate safety factors on the input variables. The ECA can be performed in a deterministic fashion, or in a probabilistic fashion

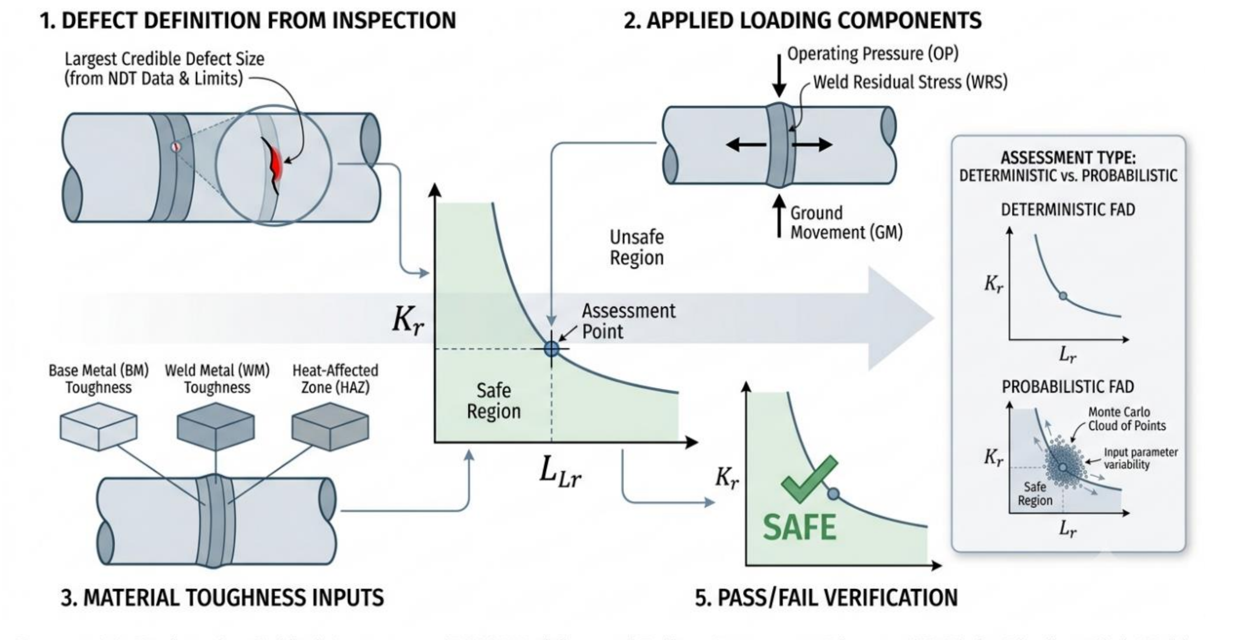

Figure 11: ECA Procedure and FAD-Based Assessment of Pipeline Weld Integrity

using Monte-Carlo simulation or first-order reliability methods (FORM) to compute the probability of failure.

2.4.3 Assessment of corrosion defects

The structural integrity assessment of corrosion defects is governed by a family of semi-empirical equations developed since the 1970s. The original ASME B31G method, published in 1984 and based on full-scale burst tests carried out by Battelle in the 1970s, was the first widely-adopted method, but it was found to be conservative for modern higher-toughness steels [ASME B31G, 1984; Kiefner et al., 1973]. The Modified B31G method, also called RSTRENG 0.85 dL, replaces the parabolic approximation of the defect profile with a 0.85 rectangle and uses a flow stress equal to SMYS plus 69 MPa (10 ksi). The Modified B31G is more accurate than the original method, particularly for defects of intermediate length, and has been widely adopted by the industry [Kiefner & Vieth, 1989].

The DNV-RP-F101 procedure, originally developed by DNV and BG plc in the 1990s on the basis of an extensive program of full-scale burst tests on X52 to X80 steels, is currently considered the state-of-the-art method for the assessment of corrosion defects in modern pipeline steels [DNV-RP-F101, 2019]. The DNV procedure provides two sets of equations, one for the assessment of single defects and one for the assessment of interacting corrosion clusters, and it accounts explicitly for the ultimate tensile strength of the material instead of the flow stress. The procedure also provides probabilistic safety factors that ensure a target probability of failure consistent with the location class and the safety regime of the line.

Other widely used methods include the PCORRC equation developed by Battelle, the LPC-1 method developed by Andrew Cosham at Penspen, and the SHELL92 method. A comprehensive comparison of these methods against full-scale burst tests has been published by Cosham, Hopkins and Macdonald in the framework of the Pipeline Defect Assessment Manual, and shows that the recent methods (PCORRC, LPC-1, DNV-RP-F101) provide predictions of the burst pressure that are typically within ±10 % of the experimental values for ductile pipeline steels, while the original B31G method is conservative by 20-30 % for the same defects [Cosham et al., 2007].

2.4.4 Assessment of mechanical damage

The structural integrity assessment of mechanical damage is significantly more complex than the assessment of corrosion or crack-like defects, because mechanical damage involves a combination of geometric change, residual stresses, strain hardening, and possible microstructural alteration of the steel. For plain dents (without gouge or scratch), the most widely used assessment criterion is the dent-depth limit of 6 % of the outer diameter, originally proposed by ASME B31.4 and B31.8 and supported by decades of operating experience [ASME B31.4, 2019; ASME B31.8, 2020]. Dents deeper than 6 % of the diameter are considered injurious and must be repaired, while dents deeper than 2 % located on a weld or interacting with another defect (corrosion, gouge, scratch) trigger a more detailed assessment.

For dent-gouge combinations, the EPRG criterion (European Pipeline Research Group), validated against more than 100 full-scale burst tests, provides a quantitative failure equation that combines the dent depth, the gouge depth, and the Charpy V-notch toughness of the steel. The application of the EPRG criterion is described in PDAM and in BS 7910, and is one of the few quantitative methods available for this complex defect family [Cosham & Hopkins, 2007; Lyons et al., 2020]. For more general configurations, including the interaction between cracks, dents, and scratches that constitutes the central topic of the present work, detailed three-dimensional finite element simulations with elastic-plastic material behavior are required, with explicit computation of the J-integral along the crack front and comparison to the material's J-R curve.

2.4.5 Probabilistic and reliability-based assessment

Probabilistic and reliability-based assessment methods have been progressively introduced in pipeline integrity management since the 1990s, with the objective of explicitly accounting for the uncertainty in the input parameters (defect dimensions, material properties, operating conditions) and of providing quantitative measures of the probability of failure that can be compared to risk-based target values. The framework of structural reliability analysis, originally developed in the civil engineering community for the design of building structures, is now widely applied to pipelines through methods such as the First-Order Reliability Method (FORM), the Second-Order Reliability Method (SORM), Monte-Carlo simulation, and importance sampling [Melchers & Beck, 2017; Caleyo et al., 2002].

Application of these methods requires the quantification of the statistical distributions of all relevant random variables, which is one of the most challenging aspects of the analysis. For corrosion defects, the statistical distributions of the depth and length of the defects detected by ILI must be combined with the uncertainty of the ILI measurement itself (typically expressed as a confidence interval on the reported defect size), and with the corrosion-growth rate distribution that describes the evolution of the defect over time. For crack-like defects, similar uncertainties must be addressed for the initial defect size, the Paris-law parameters, the threshold stress-intensity factor range, and the fracture toughness of the material. Recent developments include Bayesian updating of the corrosion-rate distribution based on successive ILI runs, and the integration of advanced machine-learning techniques for the prediction of defect-growth rates from operational data [Shuai et al., 2017; Xie & Tian, 2018].

2.5. Repair and Maintenance Techniques

2.5.1 Hierarchy of repair decisions

When a defect is detected by inspection and judged unacceptable on the basis of a fitness-for-service assessment, the pipeline operator must select an appropriate repair method. The choice depends on the type of defect, on its severity (depth, length, location), on the operational constraints (need to depressurize, possibility of shutdown), and on the economic and safety considerations. The decision process is hierarchical: the first option is always to do nothing if the defect is within acceptable limits; the second option is to reduce the operating pressure (de-rating) to ensure that the defect remains stable until a more permanent repair can be implemented; the third option is to install a temporary repair (such as a clamp or a pressure-containing sleeve); and the fourth option is to perform a permanent repair (replacement of the damaged section, full-encirclement reinforcing sleeve, or composite wrap) [ASME PCC-2, 2018; Bruce, 2014].

The relative ranking of repair methods is governed by the principles of permanence, structural reliability, cost-effectiveness, and minimization of operational impact. A permanent repair restores the original structural integrity of the pipeline and allows operation at the maximum allowable operating pressure indefinitely, while a temporary repair is intended only as a short-term solution until a permanent repair can be implemented. The selection of the appropriate repair method is a complex engineering decision that requires the integration of fitness-for-service assessment, knowledge of the available repair technologies, and consideration of operational constraints.

2.5.2 Section replacement (cut-out)

Section replacement, also called cut-out, is considered the most reliable repair method since it physically removes the defective section and replaces it with a new, defect-free section. The procedure involves draining and purging the pipeline section, cutting out the defective length, and welding in a new pipe segment with two girth welds (or installing a flanged spool in particular cases). Section replacement is the only acceptable repair method for some categories of defects, such as cracks longer than acceptable thresholds, dents on welds with co-located gouges, or arc burns that cannot be removed by grinding [ASME B31.8, 2020; ASME PCC-2, 2018].

The main drawback of section replacement is the operational impact: the pipeline must be taken out of service, depressurized, drained or purged, and re-commissioned after the repair, which can take several days for a major line. For gas pipelines, the venting of the gas inventory in the isolated section is an environmental and economic concern, although modern operators can transfer the gas to adjacent sections or to a buffer tank using mobile compression equipment. Hot-tap and stopple operations, originally developed in the 1950s, allow some types of repairs to be performed without taking the pipeline out of service, but their applicability is limited to specific defect geometries and operating conditions.

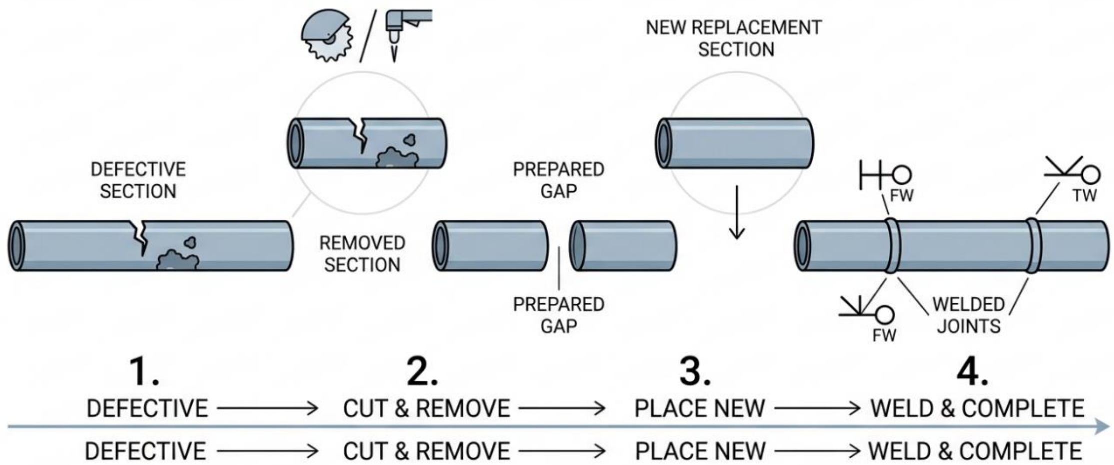

Figure 12: Pipeline Section Replacement Repair Procedure

2.5.3 Full-encirclement steel sleeves

Full-encirclement steel sleeves, also called Type-A and Type-B sleeves depending on the welding configuration, are the most widely used permanent repair method for pipelines in service. A Type-A sleeve consists of two half-shells of steel placed around the defective section and welded together along their longitudinal seams, without circumferential welds to the carrier pipe. The Type-A sleeve provides mechanical reinforcement of the defective area, allowing it to share the hoop stress with the underlying defect, but does not seal the pipeline if the defect leaks through the wall. The Type-A sleeve is therefore applicable to non-leaking defects such as corrosion patches, dents, gouges, or non-through-wall cracks [ASME PCC-2, 2018; Bruce, 2014].

A Type-B sleeve, by contrast, includes both longitudinal welds (between the two half-shells) and circumferential fillet welds to the carrier pipe, creating a pressure-tight enclosure around the defect. Type-B sleeves can therefore repair leaking defects as well as non-leaking ones. The fillet welds, however, introduce additional stresses and metallurgical complications, and must be designed and qualified with great care, in particular for thin-walled high-grade steels. The application of full-encirclement sleeves is governed by detailed procedures and qualification requirements specified in ASME PCC-2 and in the operating company's own standards.

2.5.4 Composite repair systems

Composite repair systems, introduced in the 1990s and widely deployed since the 2000s, use high-strength fibers (carbon, glass, aramid) embedded in a polymer matrix (epoxy, vinylester, polyurethane) to wrap the defective area of the pipe and provide mechanical reinforcement. The two main families of composite repair systems are the rigid pre-cured systems (such as Clock Spring), in which a stack of pre-cured composite layers is bonded to the pipe surface with a filler material, and the flexible wet-lay systems (such as Armor Plate Pipe Wrap), in which dry fabric is impregnated with resin and applied to the pipe in successive layers that cure in situ [ISO 24817, 2017; ASME PCC-2, 2018].

Composite repairs offer several advantages compared to steel sleeves: they can be installed without welding, eliminating concerns related to hot work on a pressurized line; they are corrosion-resistant by nature, providing a durable repair for external corrosion problems; they conform easily to complex pipe geometries such as bends, tees, and reducers; and they are typically lighter and less expensive than steel sleeves of equivalent strength. The qualification of composite repairs is governed by the ISO 24817 and the ASME PCC-2 Article 4.1 standards, which specify the structural design procedures, the material qualification tests, the installation procedures, and the long-term durability assessments. The performance of composite repairs has been confirmed by full-scale burst tests, by long-term creep tests, and by the satisfactory operating experience accumulated over more than two decades on tens of thousands of installations worldwide [Alexander, 2007].

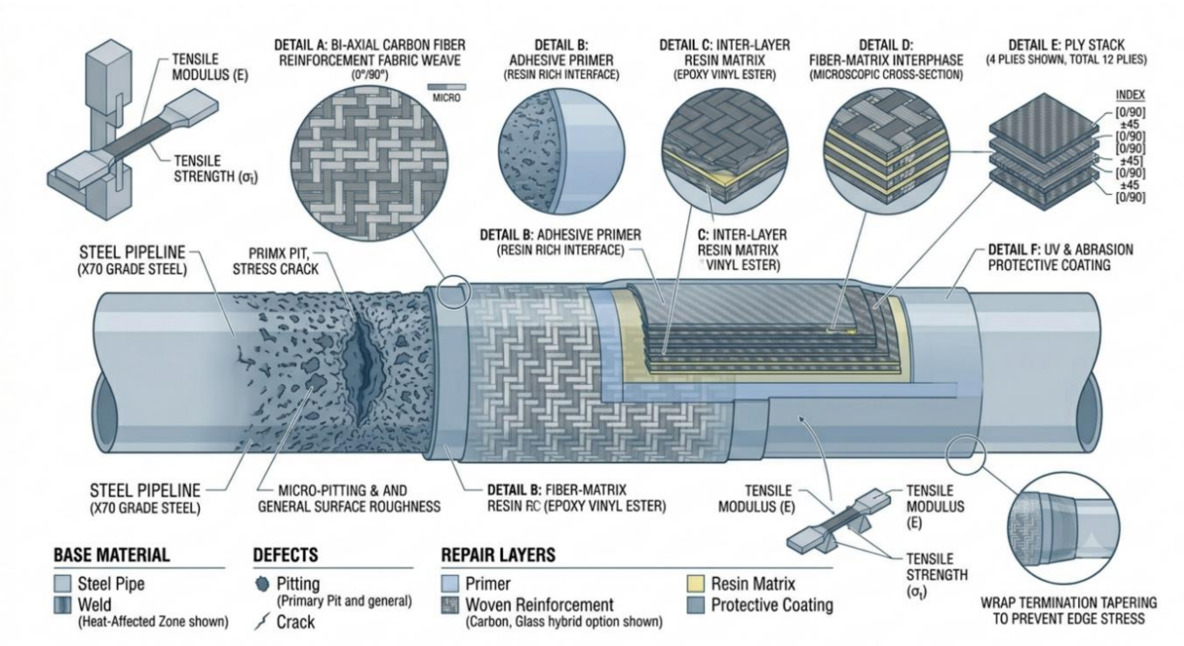

Figure 13: Composite Pipeline Repair Wrap for Surface Defects and Cracks

2.5.5 Hot taps and in-service welding

Hot tapping is the practice of installing a new branch connection on a pipeline that is in service, without interrupting the flow of the transported fluid. The hot-tap procedure involves welding a reinforcing fitting (a saddle or a split-tee) to the carrier pipe, attaching a valve and a drilling machine, and drilling through the carrier pipe wall to create the new opening. The technique was developed in the 1950s and has been used millions of times around the world since then, with an excellent safety record when performed by qualified personnel in accordance with the relevant procedures [API 2201, 2003; CSA Z662, 2019].

In-service welding, of which hot-tap welding is a particular case, refers to the welding of an in-service pipeline carrying a transported fluid. The main technical challenges are the rapid quenching of the weld pool by the flowing fluid, which can lead to the formation of brittle martensitic microstructures and to hydrogen-induced cold cracking, and the risk of burn-through when welding on thin walls or at low flow velocities. Specific procedures, qualified by the Battelle thermal-analysis model (PRCI welding model) or by validated finite element simulations, are used to determine the safe parameter envelope (current, voltage, travel speed, electrode type) for each combination of carrier pipe, transported fluid, and weld configuration [Bruce, 2014].

2.5.6 Defect grinding and preventive maintenance

For shallow surface defects such as small corrosion patches, scratches, or grinding marks, the simplest repair method is to remove the defect by grinding, provided that the residual wall thickness remains above the minimum acceptable value determined by fitness-for-service assessment. The grinding operation must be performed by qualified personnel, using appropriate grinding wheels and techniques, to avoid the introduction of new defects (overheating, thermal cracks, additional metal loss). After grinding, the area is inspected by non-destructive methods to confirm the complete removal of the original defect and the absence of new defects, and the residual wall thickness is measured to verify compliance with the integrity assessment.

Preventive maintenance activities encompass the regular inspection of cathodic protection systems, the renewal of damaged coatings, the surveillance of right-of-ways to detect unauthorized excavations or land-use changes, the cleaning of internal pipe surfaces by mechanical or chemical pigging, the calibration of pressure-relief and flow-measurement devices, and the training of operating and maintenance personnel. The cumulative effect of these preventive activities is the main contributor to the high reliability achieved by the modern pipeline industry, and the maintenance of safety records that compare favorably with most other modes of long-distance energy transportation.

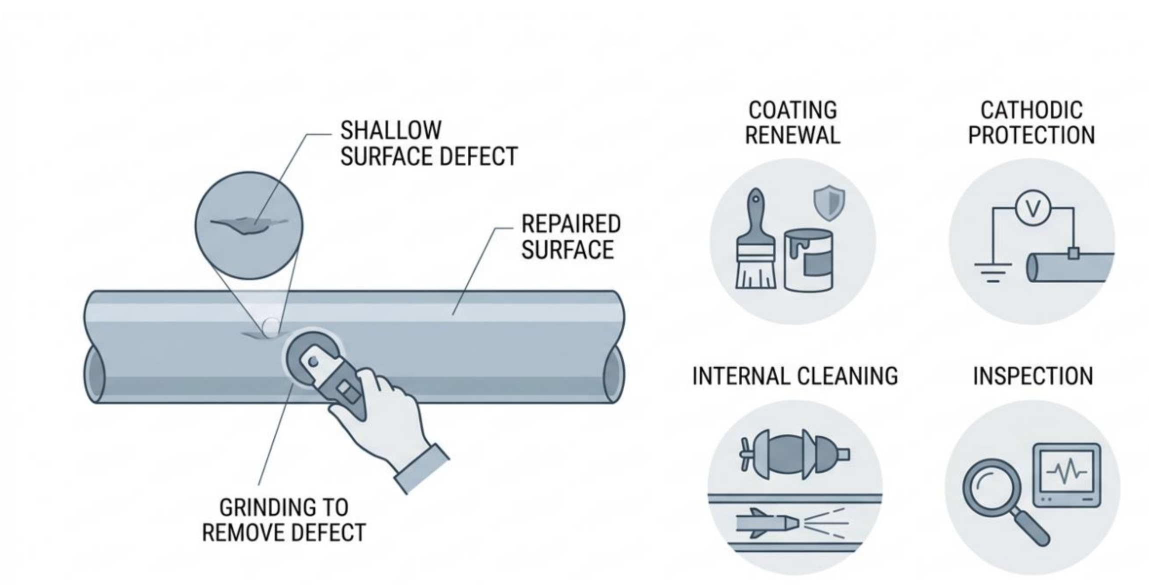

Figure 14: Pipeline Surface Defect Grinding and Preventive Maintenance

2.5.7 Conclusion: integration of inspection, assessment and repair

The three components of pipeline integrity management — inspection, assessment, and repair — must be tightly integrated within a coherent Integrity Management Program to achieve the safety, reliability, and economic-performance objectives that society expects from modern pipeline systems. The inspection technologies provide the raw data on the type, location, dimensions, and growth rate of the defects; the assessment methods translate these data into quantitative measures of the structural reliability and remaining life of each defective section; and the repair technologies restore the structural integrity where the assessment indicates that the current condition is unacceptable for safe operation. The feedback loop between repair effectiveness and subsequent inspection data, combined with the continuous improvement of the assessment models, is the cornerstone of the modern risk-based approach to pipeline integrity management.

This integrated approach is now embodied in the international standards governing pipeline integrity (API 1160, ASME B31.8S, CSA Z662, ISO 16708), in the operating procedures of the major pipeline operators worldwide, and in the regulatory frameworks of the countries hosting major pipeline networks. It is also the framework within which the present numerical study should be understood: by providing a refined quantitative description of the interaction between a crack, a co-located dent, and a remote scratch in an API X80 transmission pipeline, the present work contributes to the improvement of the assessment methods used for complex multi-defect configurations, and ultimately to the safe and economical operation of the world transmission-pipeline network.

2.5.8 Practical case studies and lessons learned

The application of fitness-for-service assessment procedures to real pipeline cases has accumulated over the past four decades a substantial body of experience that constitutes a valuable resource for practicing integrity engineers. Several case studies have been documented in the open literature, including the assessment of corrosion defects in offshore export pipelines, the evaluation of stress-corrosion-cracking colonies on transmission gas lines, the analysis of dent-gouge combinations on cross-country oil pipelines, and the assessment of girth-weld defects detected during construction. These case studies illustrate the systematic methodology that integrates field data, laboratory testing, analytical computations, and finite element simulations into a coherent assessment chain.

A notable example is the integrity assessment of the Trans-Alaska Pipeline System (TAPS), an 800-mile crude-oil pipeline operating in extreme arctic conditions, where a comprehensive integrity-management program has been developed over more than four decades. The assessment of corrosion defects detected by ILI on TAPS combines the application of B31G/Modified B31G with detailed elastic-plastic finite element analyses for the most critical defects, and is integrated with a long-term reliability model that accounts for the soil-pipe interaction under permafrost-degradation scenarios [Sotberg et al., 1997]. Another example is the integrity-management program of the Norwegian gas-export pipelines, where probabilistic methods based on Bayesian updating of corrosion-rate distributions are used to optimize the schedule of ILI campaigns and to support the operating decisions [Bjørnøy et al., 2001; DNV-RP-F101, 2019].

From these case studies, several general lessons can be drawn. First, the quality of the input data — defect dimensions, material properties, operating conditions — is at least as important as the sophistication of the assessment method; an excellent method applied with poor data leads to unreliable results. Second, the integration of multiple sources of information (inspection data, monitoring data, historical operating records, material certificates) provides a more robust basis for decision-making than reliance on a single data source. Third, the assessment should be calibrated against full-scale tests or operating experience whenever possible, since the empirical and semi-empirical methods used in routine engineering practice have inherent limitations of validity that must be respected. Fourth, the assessment is a continuous process that should be revisited at regular intervals as new data become available, in order to reflect the evolution of the defect population and the operational conditions over time.

2.6. Complementary Considerations: Multi-Defect Assessment and Modern Trends

2.6.1 Specific assessment of crack-dent-scratch interactions

The interaction between a crack and one or more other defects in its vicinity (a dent, a gouge, a scratch, a corrosion patch, or a girth weld) constitutes one of the most challenging configurations encountered in pipeline integrity assessment. Unlike isolated defects, for which well-established empirical and semi-empirical methods are available, multi-defect configurations call for case-by-case analyses, generally based on detailed three-dimensional finite element simulations including elastic-plastic material behavior. The complexity of these analyses stems from the coupled effects that may take place between the defects: a dent introduces residual stresses, strain hardening, and a local change of curvature that all modify the stress state acting on a co-located crack; a scratch acts as a stress raiser that can amplify the effective driving force on a nearby crack; and a corrosion patch reduces the load-bearing section and redistributes the stress field on a larger scale [Allouti et al., 2012, 2014].

Several experimental and numerical studies have been published in the last two decades on the interaction of cracks with dents in pipeline steels. Allouti et al. carried out full-scale tests on X52 pipes containing artificial dent-gouge defects of controlled geometry, and showed that the burst pressure decreases monotonically with both the dent depth and the gouge depth, with a strong coupling between the two parameters [Allouti et al., 2012]. Pluvinage and co-workers developed a notch fracture mechanics approach based on the volumetric method to assess the failure pressure of dented pipelines with co-located cracks [Pluvinage et al., 2014; Hadj Meliani et al., 2010]. Other contributions by Capelle, Bouledroua and their teams have specifically addressed the case of X65 and X70 steels under sour service conditions [Capelle et al., 2008; Bouledroua et al., 2017].

From the methodological standpoint, two complementary approaches are used to quantify the interaction between defects. The first approach is based on the comparison of the failure pressure or the limit load of the combined-defect configuration with the failure pressure of the same components considered in isolation: an interaction factor IF = Pf,combined / min(Pf,individual,i) is defined, and values smaller than 1 indicate a detrimental interaction. The second approach, more refined, is based on the comparison of the J-integral or CTOD at the crack tip in the combined configuration with the same fracture parameter in the isolated-crack configuration: an amplification ratio is defined as J_combined / J_isolated, and values greater than 1 indicate amplification of the driving force on the crack by the secondary defects. This second approach is the one adopted in the present work and provides finer quantitative information on the underlying mechanical mechanisms.

2.6.2 Performance evaluation of inspection technologies

The performance of inspection technologies — both in-line and on-surface — is characterized by three main figures of merit: the Probability of Detection (POD), which is the probability that a defect of given dimensions is detected by the inspection tool; the Probability of False Calls (POFC), which is the probability that the tool reports a defect that does not actually exist; and the sizing accuracy, which is the statistical distribution of the difference between the reported and the actual defect dimensions, usually expressed as a confidence interval around a mean value. The POD curves of modern ILI tools for metal-loss defects exhibit a sigmoid shape with 50 % POD at depths around 5-10 % of the wall thickness and 90 % POD at depths of 15-20 % of the wall thickness, with marked variability depending on the defect geometry, the wall thickness, and the inspection conditions [Nestleroth & Bubenik, 1999; API 1163, 2013].

The qualification of ILI tools is governed by the API 1163 standard, which specifies the procedures for the determination of POD, POFC and sizing accuracy from controlled tests on pre-characterized pipe samples [API 1163, 2013]. The qualification results are reported in the form of performance specifications that quantify the tool capabilities in well-defined inspection conditions, and that constitute the basis for the integration of ILI data into integrity-management decisions. The choice of the appropriate ILI tool for a given inspection campaign depends on the expected defect population, on the structural significance of the defects, and on the cost-benefit analysis of inspection accuracy versus inspection cost. Modern integrity-management programs combine periodic ILI runs of different technologies (MFL, UT, geometry, EMAT) to obtain a comprehensive picture of the defect population on the inspected line.

2.6.3 The role of the J-integral in multi-defect assessments

The J-integral plays a central role in the assessment of multi-defect configurations because it provides a single quantitative measure of the driving force at the crack tip that integrates all the effects of geometry, material non-linearity, and loading distribution. In a finite element analysis of a pipeline containing a crack and one or more secondary defects, the J-integral is computed along the crack front as a function of the applied internal pressure, of the dimensions of the primary crack, and of the dimensions and locations of the secondary defects. The variation of J with these parameters constitutes the main output of the analysis and provides the basis for the comparison with the material's J-R curve to predict the onset of stable crack growth and the eventual failure of the section.

For the configurations of interest in the present work — a crack co-located with a dent or interacting with a remote scratch in an X80 pipeline — the parametric study of the J-integral as a function of the dent depth, the scratch depth, the distance between the defects, and the internal pressure leads to a series of interaction maps that quantify the conditions under which the secondary defects significantly amplify the driving force on the primary crack. These interaction maps can be subsequently used in engineering practice to identify the configurations that require detailed assessment and the configurations that can be safely assessed using simpler methods based on the isolated-defect approach. The construction of such interaction maps is one of the main objectives of the simulations described in the subsequent chapters.

Recent literature on the subject has emphasized the importance of the relative orientation of the defects (axial, circumferential, or oblique) and of the relative position with respect to the welds. For circumferential cracks (typical of girth-weld defects) interacting with adjacent axial scratches, the amplification of the J-integral can be moderate (less than 30 %) for most realistic configurations, while for axial cracks (typical of seam-weld or SCC defects) interacting with co-located dents, the amplification can be much larger (up to 100-200 %) when the crack is located at the position of maximum tensile stress in the dent. These findings underline the importance of an accurate three-dimensional analysis for any non-trivial multi-defect configuration, and they motivate the methodological approach adopted in the present work [Allouti et al., 2014; Pluvinage et al., 2018].

2.6.4 Long-term durability of repairs and post-repair monitoring

The long-term durability of pipeline repairs is a crucial concern for integrity-management programs, since a repair that fails prematurely can lead to a serious incident on a section that was believed to have been brought back to satisfactory condition. Several factors influence the long-term durability of repairs: the quality of the surface preparation and of the installation procedure; the mechanical and environmental loading applied to the repair throughout its service life; the long-term aging and degradation of the repair materials (steel, polymer, composite); and the effectiveness of the bond between the repair and the underlying pipe. The qualification of repair systems for long-term service is governed by accelerated aging tests, full-scale fatigue tests, and field validation programs.

Post-repair monitoring is performed to verify that the repaired section behaves as designed during its operational life. The monitoring can be passive (periodic inspection of the repair by visual, ultrasonic or radiographic methods) or active (instrumentation of the repair with strain gauges, fiber-optic sensors, or acoustic-emission sensors that continuously transmit data to the control room). The integration of post-repair monitoring into the overall integrity-management program closes the loop between defect detection, assessment, repair, and verification, and contributes to the continuous improvement of the integrity practices of the operator. Recent developments in distributed fiber-optic sensing have opened new possibilities for the continuous monitoring of strain and temperature along the entire length of a repair, providing high-resolution data for the verification of repair performance and for the early detection of any anomalies [Sun & Stiles, 2017].

2.6.5 Towards a digital twin of the pipeline

The most recent trend in pipeline integrity management is the development of digital twins — virtual replicas of the physical pipeline that integrate three-dimensional geometric models, finite element simulations, sensor data, and probabilistic models within a unified computational framework. A pipeline digital twin allows the operator to evaluate in real time the structural status of any section of the line, to predict the evolution of defects under expected operating conditions, to evaluate the consequences of operating decisions (pressure increase, transient events), and to optimize the schedule of inspection and repair activities. The integration of artificial-intelligence and machine-learning techniques further enables the extraction of meaningful patterns from large datasets of operating and inspection data, and the prediction of failure probabilities with improved accuracy [Hassani & Tian, 2018; Xie & Tian, 2018].

The successful implementation of a digital twin requires a multi-disciplinary effort that combines mechanical engineering, materials science, electronics, computer science, and data analytics. The present work, focused on the detailed finite element analysis of multi-defect configurations in an X80 pipeline, can be seen as a contribution to one of the building blocks of a future pipeline digital twin: the mechanistic component that translates defect geometries into quantitative measures of the structural reliability. The integration of this component with sensor data, with operational data, and with probabilistic models of defect growth is the natural extension of the present research, and one of the most promising research directions for the next decade of pipeline integrity management.

2.6.6 Closure

In summary, the safe and economical operation of modern pipeline systems requires the continuous interplay between inspection technologies that detect and characterize defects, assessment methods that translate these data into quantitative structural-reliability measures, and repair techniques that restore the integrity of the affected sections. The present work, by providing detailed three-dimensional finite element analyses of the J-integral behavior in the presence of interacting crack/dent/scratch defects in an API X80 pipeline, contributes to the second pillar of this triad and provides a methodological framework that can be applied to similar multi-defect configurations encountered in practice. The conclusions drawn from the parametric analyses presented in the following chapters are expected to enrich the assessment toolkit of pipeline-integrity engineers and to support the development of refined acceptance criteria for multi-defect configurations in modern high-grade transmission pipelines.

2.6.7 Emerging regulatory frameworks and harmonization efforts

The regulatory framework governing pipeline integrity has undergone significant evolution over the past two decades, driven by the lessons learned from major accidents, by the developments in inspection and assessment technologies, and by the growing public concern for safety and environmental protection. In the United States, the issuance of 49 CFR Part 192 and Part 195 by the Department of Transportation, and the periodic updates of the integrity-management rules by PHMSA, have progressively tightened the regulatory requirements for inspection frequencies, assessment methods, and management-system performance. The Mega Rule of 2019 and 2020 extended the scope of integrity-management programs to a broader range of pipelines, including gas gathering lines and underground natural gas storage facilities [PHMSA, 2019].

In Europe, the harmonization of pipeline integrity practices has been promoted by the European Gas Pipeline Incident Data Group (EGIG), by the Pipeline Operators Forum (POF), and by the European Pipeline Research Group (EPRG), through the development of common databases, of shared research programs, and of consensus-based assessment guidelines. The EN 1594 and EN 12007 standards specify the design and operating requirements for gas transmission and distribution pipelines, while the EN 14161 standard covers oil transportation pipelines. National regulations supplement these European standards in each member state, leading to a complex multi-layered regulatory landscape that the operators must navigate.

At the international level, the ISO Technical Committee 67/Subcommittee 2 (TC 67/SC 2) develops and maintains the ISO 13623 standard on pipeline transportation systems, which serves as a reference for many national codes around the world. The recently published ISO 19345 standard provides specific guidance on pipeline integrity management, while ISO 16708 covers reliability-based limit-state methods for pipeline design. These international standards converge with the practices codified in API 1160, API 1163, ASME B31.4, B31.8 and B31.8S, and with the Canadian Standards Association Z662, providing a relatively consistent technical foundation across the major pipeline-operating jurisdictions [ISO 13623, 2017; ISO 19345, 2019].

The increasing globalization of the pipeline industry, with operating companies present across multiple regulatory jurisdictions and with project consortia involving partners from various countries, has reinforced the need for further harmonization of the technical standards and of the regulatory frameworks. Joint industry projects (JIPs) coordinated by PRCI, by DNV, or by the EPRG have played a key role in this harmonization, by producing consensus-based technical reports that are subsequently incorporated into the international standards. The present work, by contributing detailed quantitative data on the J-integral behavior of multi-defect configurations in X80 pipelines, is intended to feed into this collective effort of technical harmonization and to support the development of refined acceptance criteria that can be incorporated into the next generation of international standards.

2.7. Chapter Summary and Conclusions

This second chapter has presented the broader framework of pipeline integrity within which the present numerical study should be understood. Starting from the definition of pipeline integrity as the ability of a pipeline system to safely and reliably perform its intended function, the chapter has reviewed the regulatory and standard-based foundations of modern integrity-management programs, the types of defects and degradation mechanisms encountered in operation, the inspection and monitoring methods available for their detection and characterization, the structural integrity assessment procedures, and the repair and maintenance techniques used to restore the integrity of defective sections.

The classification of pipeline defects has been examined in three categories — manufacturing, construction, and in-service defects — and in three main families relevant to integrity assessment: metal-loss defects (external and internal corrosion, erosion), crack-like defects (stress corrosion cracking, fatigue, hydrogen damage, weld defects), and mechanical damage (dents, gouges, scratches, arc burns). Each family has been characterized in terms of its degradation mechanism, its detection methods, its assessment procedures, and its repair options. Particular attention has been given to the interaction between crack-like defects and mechanical damage, which constitutes the central topic of the present work and is one of the most challenging configurations in modern pipeline integrity assessment.

The inspection and monitoring methods available for pipeline integrity assessment have been reviewed at three levels: in-line inspection (ILI) with magnetic flux leakage, ultrasonic, and geometry technologies that provide comprehensive defect mapping along the pipeline length; non-destructive surface testing with conventional and advanced ultrasonic, radiographic, magnetic-particle, and emerging methods such as ACFM and guided-wave UT for specific applications; and continuous monitoring through SCADA systems, real-time transient modeling, and distributed fiber-optic sensing technologies. The integration of these multiple data sources within modern integrity-management programs has been emphasized as a key element of the defense-in-depth approach to pipeline safety.

The structural integrity assessment procedures have been organized according to the multi-level approach codified in API 579-1, BS 7910 and the FITNET procedure, with progressively increasing levels of refinement and decreasing levels of conservatism. The assessment of corrosion defects through the B31G/Modified B31G, DNV-RP-F101, PCORRC and LPC-1 methods has been reviewed, as has the assessment of crack-like defects through Engineering Critical Assessment (ECA) based on the Failure Assessment Diagram and J-integral methods. The specific assessment of dent-gouge combinations using the EPRG criterion has been described, and the role of probabilistic and reliability-based methods (FORM, SORM, Monte-Carlo simulation, Bayesian updating) in modern integrity-management has been highlighted.

The repair and maintenance techniques available to restore the integrity of defective pipeline sections have been reviewed in their hierarchy of decision: section replacement as the most reliable but most disruptive option; full-encirclement steel sleeves (Type A and Type B) as the workhorse permanent repair method; composite repair systems (rigid pre-cured and flexible wet-lay) as a lighter and corrosion-resistant alternative; hot taps and in-service welding for repairs without service interruption; and defect grinding combined with preventive maintenance for shallow surface defects. The long-term durability of the repairs and the post-repair monitoring strategies have been discussed, and the emerging concept of pipeline digital twins has been introduced as the natural evolution of integrity management toward fully integrated and data-driven decision support systems.

Section 2.6 has provided complementary considerations specifically relevant to the present research: the assessment of crack-dent-scratch interactions through interaction factors and J-integral amplification ratios, the performance evaluation of inspection technologies through Probability of Detection curves, the central role of the J-integral in multi-defect assessments, the long-term durability of repairs, and the emerging concept of pipeline digital twins. These considerations frame the present numerical work as a contribution to the mechanistic component of a future integrated integrity-management framework.

On the basis of this review, several observations can be made that motivate and orient the subsequent numerical study. First, multi-defect configurations involving a crack and one or more co-located mechanical-damage defects are not adequately covered by the existing semi-empirical assessment methods, and call for detailed three-dimensional finite element analyses based on elastic-plastic fracture mechanics. Second, the relevant fracture-mechanics parameter for the assessment of these configurations is the J-integral computed along the crack front, with explicit consideration of the path-independence verification and of the constraint corrections. Third, the most informative output of the analysis is a non-dimensional amplification ratio that quantifies the increase of the driving force on the crack due to the secondary defects, and that can be subsequently used to develop refined acceptance criteria for engineering practice. Fourth, the numerical analysis should explore a parameter space that is representative of the configurations encountered in service, including realistic ranges for the crack dimensions, the dent depths, the scratch geometries, the internal pressure levels, and the soil-pipe interaction effects.

With these methodological foundations established, the subsequent chapters of this work will present in detail the numerical model developed for the parametric finite element analysis (geometric and material modeling, mesh refinement, contact algorithms, boundary conditions), the results of the systematic parameter studies (J-integral profiles along the crack front, sensitivity to the geometric parameters, comparison with reference cases), and the engineering interpretation of the results in terms of interaction maps and proposed acceptance criteria. The contribution of this work to the broader discipline of pipeline integrity assessment, and its implications for the safe operation of the Algerian and international transmission networks, will be the subject of the final concluding chapter.

3. Chapter III MODELISATION ET SIMULATION NUMERIQUE

3.1. Introduction and objectives

This chapter presents the numerical investigation of scratched and cracked specimens using the finite element software ABAQUS. The main objective is to reproduce an existing experimental study [Xiao Tian∗, n.d.] and then extend it by a systematic parametric analysis of defect geometry and repair configurations. The numerical model is first validated by comparison with published experimental results under the same geometry, material, loading, and boundary conditions. After validation, the model is used to study the influence of scratch and crack parameters on the local stress and strain fields, as well as on the J-integral at the crack tip.

The first part of the chapter is devoted to describing the geometry of the studied specimens, the material properties, and the boundary conditions used in the simulations. The finite element modeling strategy implemented in ABAQUS is then detailed, including element type, mesh refinement, and loading procedure. A comparison between numerical and experimental responses is presented to demonstrate the reliability of the model.

Once the model is validated, a parametric study is carried out on scratch defects by varying successively the scratch depth, width, and orientation angle. For each configuration, von Mises stress and equivalent plastic strain (PEEQ) distributions are extracted in order to evaluate the severity of the defect. A second parametric study addresses crack defects, where different crack depths and widths are analyzed, and von Mises stress, PEEQ, and J-integral values are obtained for each case.

Finally, three different repair configurations are modeled: a cracked and scratched specimen reinforced with a composite material, a cracked specimen with composite repair only, and a scratched and cracked specimen repaired using mastic. The J-integral is used as the main parameter to compare these configurations and to assess the effectiveness of the different repair strategies on the reduction of the crack driving force. The results of these analyses provide a basis for discussing the structural integrity of defective pipelines and the contribution of repair techniques

3.2. ABAQUS presentation

ABAQUS/Standard is a finite element code dedicated to nonlinear static and quasi-static analyses of structures. It allows 3D modelling of complex geometries, definition of elastic–plastic material behavior, contact between bodies, and evaluation of advanced fracture mechanics quantities such as the J-integral. In this study, ABAQUS/Standard is used to simulate the tensile behavior of the CT80 steel specimen with scratch and crack defects, and to extract global responses (force–displacement) as well as local fields (von Mises stress, PEEQ, J-integral).

3.2.1. Geometry (Part)

- Create the geometry of the structure (2D or 3D) using sketches and solid features.
- The numerical study is carried out on a flat tensile specimen with the same geometry as in the reference experimental work. The specimen has a total length of 190 mm, a grip

width of 16 mm and a constant thickness of 3.18 mm. The central reduced section, where the defect is introduced, has a parallel width of 10 mm and a length of 50 mm, connected to the grip zones by shoulders of radius 75 mm. The transition between the grip and the reduced section is defined by a 24 mm straight part followed by a 21 mm curved shoulder on each side, as shown in the specimen drawing. The scratch and crack defects are always located at the mid-length of the specimen, in the center of the reduced section

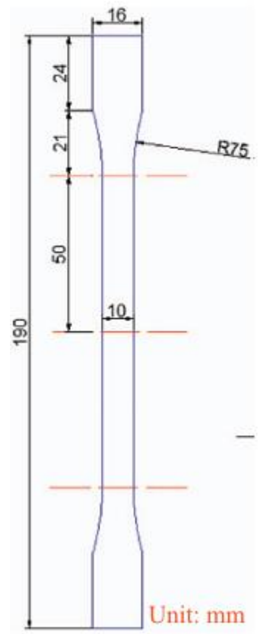

Figure 15: tensile specimen geometry [Xiao Tian∗, n.d.]

3.2.2. Material and section definition

The material of the tensile specimen is assumed to be identical to the CT80 steel used in the experimental reference study. An isotropic elastic–plastic behavior with isotropic hardening is adopted in ABAQUS in order to correctly reproduce the large plastic deformations observed before fracture. The Young's modulus is taken as 186 GPa and the Poisson's ratio as 0.3. The yield strength is 580 MPa, while the nominal tensile strength and true tensile strength are 715 MPa and 787 MPa, respectively. The true fracture strain is 0.1867, as reported in the experimental campaign.

The plastic part of the stress–strain curve is implemented in the form of a true stress–true strain relationship, obtained from the tensile test data of CT80 steel. This curve is introduced into ABAQUS as a series of $(\sigma_{\text{true}}, \varepsilon_{\text{plastic}})$ points, allowing the code to interpolate the hardening behavior up to large strains. This constitutive model ensures a consistent description of yielding and strain hardening in the vicinity of the defects, which is essential for accurately capturing von Mises stress, equivalent plastic strain and J-integral values.

Elastic modulus E/GPa	Yield strength σy/MPa	Nominal tensil strength σu/MPa	True tensil strength σ'u/MPa	True fracture strain εf
186	**580**	**715**	**787**	**0.1867**

Table 1: Material properties of CT80

The scratch defect is introduced on the tensile specimen after machining the final geometry. The specimen is positioned so that the scratch is created at the centre of the reduced gauge section, along the specimen width. The tool is guided in the transverse direction in order to obtain a straight notch with a nearly constant width of about 0.8 mm, while the scratch depth is adjusted according to the test matrix. In this configuration, the scratched zone coincides with the region of maximum axial stress during tensile loading, ensuring that the defect governs the fracture behaviour of the specimen.

3.2.3. Interaction definition (optional)

- Define contact between surfaces

In the finite element model, the interaction between the reference point (RP) and the upper surface of the tensile specimen is defined by a surface-based coupling. The RP is created outside the specimen and kinematically linked to all nodes of the upper loading surface, so that any imposed traction or displacement at the RP is uniformly transmitted to this surface. In this way, the applied load is controlled through the RP, while the coupling constraint ensures a consistent distribution of the boundary conditions over the loaded area, reproducing the experimental tensile loading configuration.

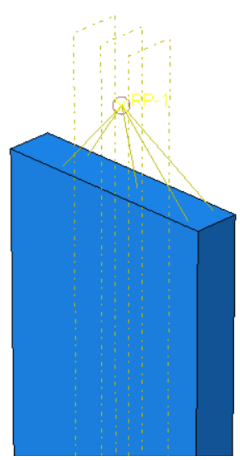

Figure 16: the reference point (RP) and the upper surface of the tensile specimen

3.2.4. Step creation

- Choose the type of step: static, dynamic, modal, thermal, etc. ABAQUS/Standard is typically used for static and quasi-static problems.

3.2.5. Loads and boundary conditions

In the tensile simulation, the load is applied in a displacement-controlled manner through the reference point (RP) associated with the upper surface of the specimen. A prescribed displacement is imposed on the RP in the axial y-direction, while all other translational degrees of freedom at this point are constrained to ensure a pure tensile loading. The bottom surface of the specimen is fully fixed, with all translational degrees of freedom set to zero, in order to reproduce the clamping conditions of the experimental setup. The entire specimen is modeled without using any symmetry conditions, so that the global deformation and the local response in the defected region are directly captured over the full geometry.

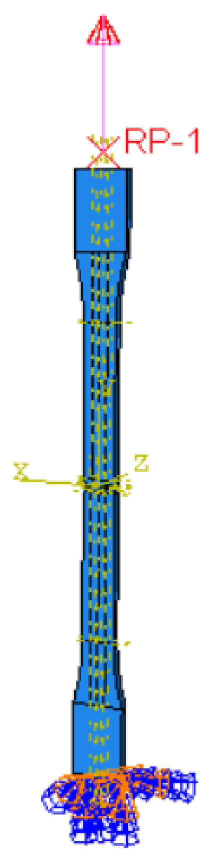

Figure 17: Loads and boundary conditions

3.2.6. Meshing

A full three-dimensional finite element model of the tensile specimen is developed in ABAQUS in order to capture the three-dimensional stress and strain fields in the vicinity of the defects. The model reproduces the exact specimen geometry described in Section 3.2, including the reduced gauge section where the scratch and crack are introduced. The overall mesh size in the bulk of the specimen is taken as 2.5 mm, which is sufficient to represent the global stiffness and load–displacement response with reasonable computational cost.

A strong mesh refinement is applied in the defect region to correctly resolve the high stress and strain gradients. Around the scratch, the characteristic element size is reduced to 0.5 mm in all directions, ensuring a smooth description of the U-shaped groove geometry. In the crack tip region, an even finer mesh is adopted, with a minimum element size of 0.012 mm at the vicinity of the crack front. This refinement is necessary to obtain accurate evaluations of von Mises stress, equivalent plastic strain and J-integral along the crack front. Solid elements with reduced integration are used throughout the model, which are well suited for large deformation and contact problems in metallic materials.

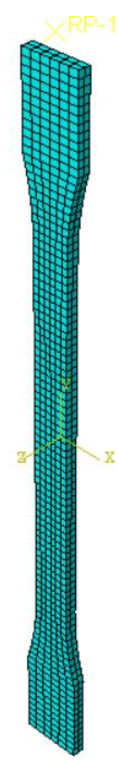

Figure 18: meshing of the spiceman

3.2.7. Job creation and submission

- Create a “job” that points to the model, set numerical options (number of processors, memory limits).

- Submit the job for analysis. ABAQUS writes an input file, solves the finite element problem, and produces output databases.

3.2.8. Field output viewing

During post-processing, the field output is examined in terms of the Von Mises equivalent stress and the equivalent plastic strain (PEEQ) over the entire specimen. The contour plots of these quantities are first viewed on the full model to identify the global deformation pattern and the overall stress distribution. Particular attention is then paid to the scratched zone located at the middle of the reduced section, where detailed zoomed views are used to evaluate the local concentration of stress and plastic strain and to correlate these fields with the observed fracture behavior.

3.2.9. History output and curves

In addition to the field output, several quantities are extracted through history output requests in order to construct global and local response curves. The reaction force and the imposed displacement at the reference point (RP) are recorded throughout the tensile step, allowing the global force–displacement curve of the specimen to be plotted and compared for different defect configurations. At the same time, the evolution of the Von Mises equivalent stress and the equivalent plastic strain is monitored at a selected element located in the scratched region, which provides insight into the local stress and strain concentration near the defect. Furthermore, the J-integral is evaluated along contours surrounding the crack tip during loading, and its variation with the applied displacement is used as a fracture parameter to characterize the interaction between the defect geometry and the overall load-carrying capacity of the specimen.

3.3. Scratch defect study

3.3.1. Scratch geometry and studied configurations

In this part, the specimen contains a single surface scratch located at the center of the gauge section, where the cross-section is 10 mm × 3.18 mm. The scratch is machined on one face of the specimen and is fully contained within the reduced section, so that its influence is not perturbed by the grip zones. Its center coincides with the intersection of the specimen mid-length and mid-width axes, ensuring a symmetric stress field with respect to the specimen geometry.

The scratch is modeled as a U-shaped groove, defined by three parameters: depth a, surface width w and orientation angle θ

The depth a is measured from the original specimen surface towards the interior, along the thickness direction, while the width w corresponds to the opening of the groove at the surface. Two orientations are considered: θ=90 , θ=45

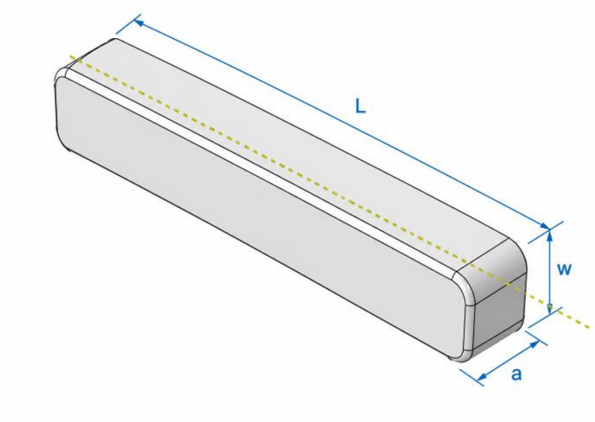

Figure 19: Scratch geometry

3.3.2. Validation and comparison for scratched specimens

The numerical model in the presence of a scratch is validated by reproducing the experimental configurations studied by X. Tian and H. Zhang in their work on the failure criterion of steel plates with dent and scratch defects. In that study, the authors tested CT80 steel specimens containing only a surface scratch of different depths and reported the corresponding tensile strength as a function of scratch depth. To be consistent, the present finite element model uses the same specimen geometry, material properties and loading conditions.

A first series of simulations is performed by varying only the scratch depth a, while keeping the scratch perpendicular to the loading direction and centred in the gauge section. The considered depths are 0.2, 0.4, 0.6 and 0.8 mm, which correspond to the experimental configurations of Tian and Zhang. For each depth, a displacement-controlled tensile test is simulated, and the fracture load is taken from the peak of the global reaction force–displacement curve at the loaded end.

The numerical evolution of fracture load with scratch depth is directly compared to the experimental curve of Tian and Zhang (Figure 20). Both sets of results show the same trend: the tensile strength decreases as the scratch depth increases, with a modest reduction for shallow defects (around 0.2 mm) and a marked drop when the depth exceeds about 0.6 mm. The quantitative difference between the simulated and experimental fracture loads remains limited across the whole range of depths, which confirms that the present FE model faithfully reproduces the behavior observed experimentally by Tian and Zhang and can therefore be used confidently for the subsequent extended parametric studies.

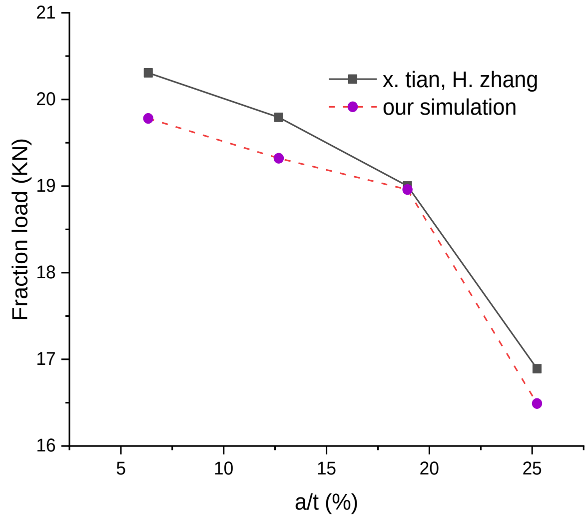

Figure 20: Validation and comparison for scratched specimens

3.3.3. Effect of scratch *depth on von Mises stress*

In this first parametric study, only the scratch depth *a* is varied, while the scratch width and orientation are kept constant (figure 21) . The scratch is located at the centre of the gauge section and oriented perpendicular to the loading direction. Depth values between 0.2 mm and 0.8 mm are considered. For each configuration, a displacement-controlled tensile simulation is performed and the von Mises stress distribution in a region surrounding the scratch is extracted.

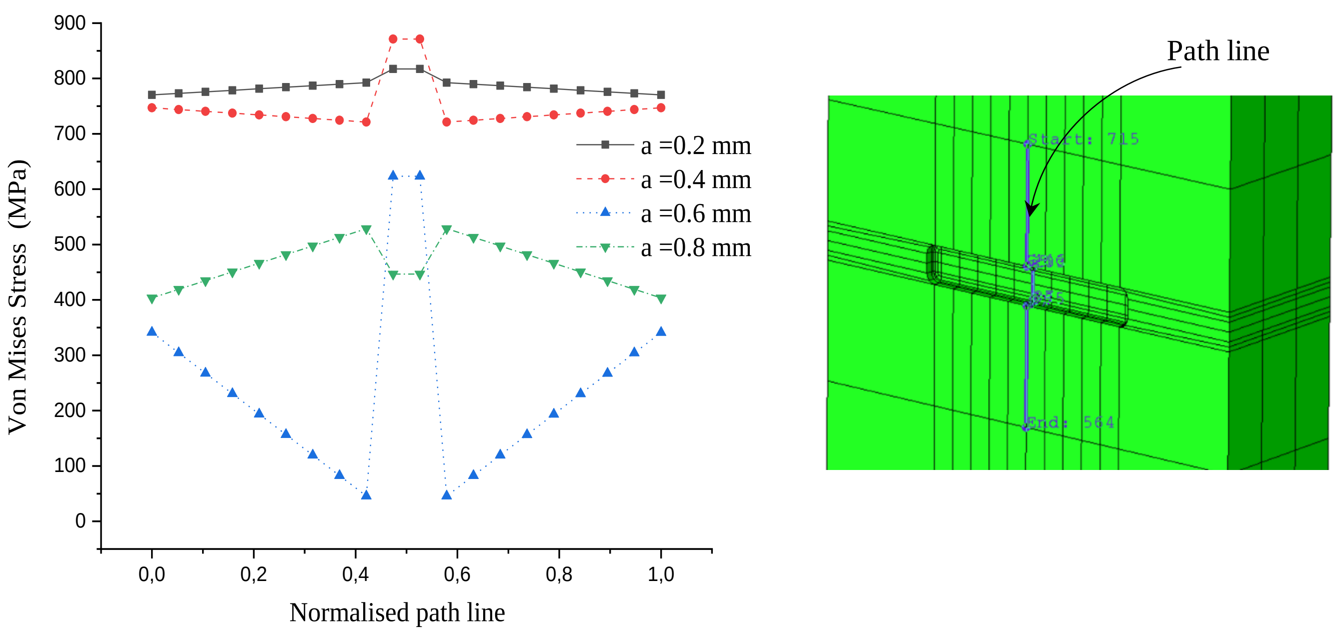

Figure 21: distribution of the Von Mises stress along of the path line

The results show that increasing the scratch depth causes a marked rise in the maximum von Mises stress at the root of the groove. Shallow scratches produce a relatively moderate stress concentration, with the high-stress zone confined close to the surface. As the depth increases, the stress concentration factor K_T rises and the zone of high von Mises stress extends progressively towards the interior of the specimen. Deep scratches therefore generate a more severe local loading state, which is expected to reduce the load-bearing capacity of the section.

3.3.4. Effect of scratch depth on equivalent plastic strain (PEEQ)

The influence of scratch depth on the equivalent plastic strain is analyzed using the same set of simulations (figure 22). For each depth, the PEEQ field is recorded at the end of the tensile loading, and the maximum value at the scratch root, as well as the spatial extent of the plastically deformed region, are examined.

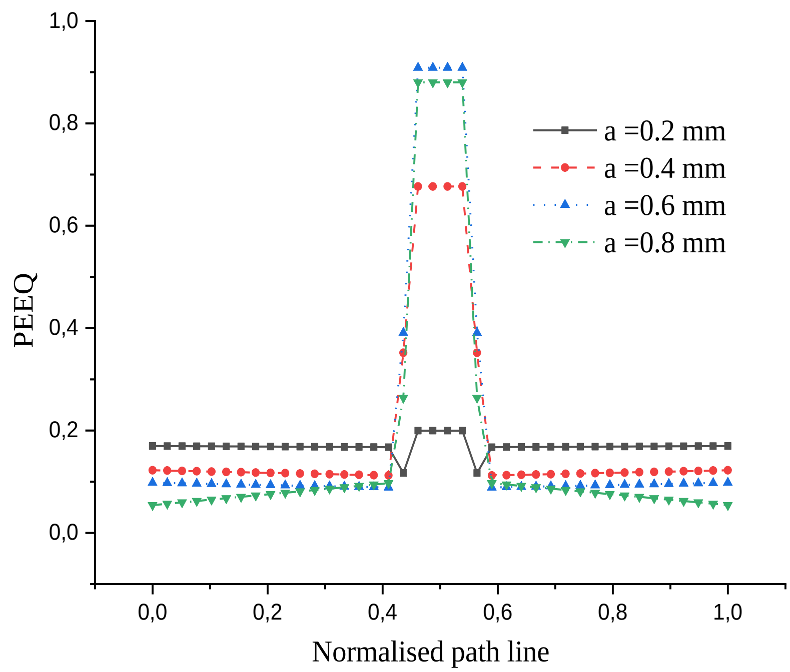

Figure 22: variation of equivalent plastic deformation (PEEQ) along the path line

The numerical results indicate that the PEEQ level and the size of the plastic zone both increase with scratch depth. For small depths, plastic deformation remains localized in a small region close to the bottom of the groove and decays rapidly through the thickness. When the depth becomes larger, the maximum PEEQ value increases significantly and the plastic zone penetrates deeper into the specimen, occupying a larger volume around the defect. This behavior confirms that deeper scratches promote earlier and more extensive plastic yielding in the critical region

3.3.5. *Effect of scratch width on von Mises stress*

In a second series of simulations, the influence of scratch width w on the stress state is investigated (figure 23). The scratch remains located at the centre of the gauge section and oriented perpendicular to the loading direction, while the depth a is kept constant. (a=0.8 mm) Several surface widths w are considered by changing the length of the rectangular groove cut on the specimen surface, as illustrated in the ABAQUS model. For each width, a displacement-controlled tensile test is simulated and the von Mises stress distribution in the vicinity of the scratch is analyzed.

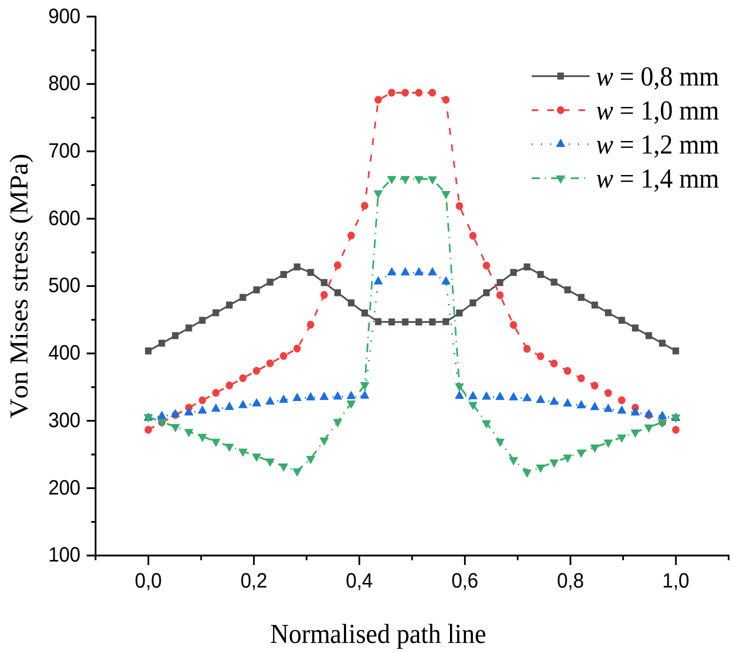

Figure 23: distribution of the Von Mises stress along of the path line for different scratch width

The results show that increasing the scratch width causes the high-stress region to extend over a larger area along the specimen surface, while the absolute maximum von Mises stress at the groove root may either remain nearly constant or slightly increase, depending on the chosen depth. Narrow scratches concentrate the stresses in a small zone immediately around the defect, whereas wider scratches spread the stress concentration over a longer portion of the gauge section. This effect modifies the overall stiffness reduction and can influence the onset of macroscopic yielding.

3.3.6. *Effect of scratch width on equivalent plastic strain (PEEQ)*

The corresponding equivalent plastic strain fields are examined for the same set of scratch widths (figure 24). For each configuration, the maximum PEEQ value near the scratch and the size of the plastic zone along the surface and through the thickness are evaluated.

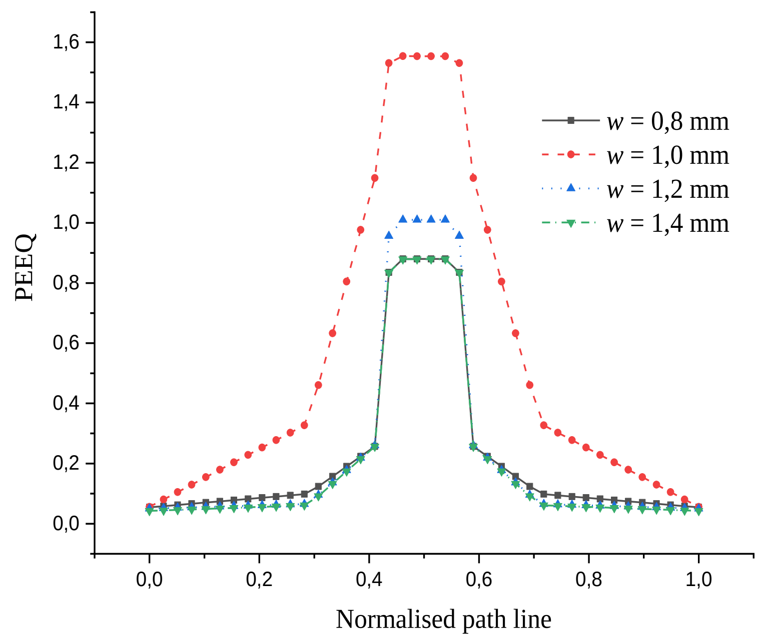

Figure 24: Distribution of equivalent plastic deformation (PEEQ) along the path line

The numerical results indicate that, for a fixed depth, increasing the scratch width tends to enlarge the plastically deformed region along the specimen surface, while the peak PEEQ at the groove root may remain close to the same level. This means that wider scratches mobilize plastic deformation over a longer length of the gauge section, which contributes to a greater loss of effective cross-section and can reduce the remaining ductility of the specimen.

3.3.7. Influence of Scratch orientation

In addition to depth and width, the orientation of the scratch with respect to the loading direction is also considered as a variable parameter. The scratch remains centred in the gauge section with fixed depth (a=0.8 mm) and the width at (w=1 mm) while its axis is rotated in the specimen plane (figure 25) . Two orientations are studied:

- $\theta = 90°$: the scratch is horizontal, parallel to the specimen width and perpendicular to the tensile axis (figure 25B).
- $\theta = 45°$: the scratch is inclined, forming a 45° angle with the tensile axis (figure 25A).

For each orientation, the same displacement-controlled tensile loading is applied and the fields of von Mises stress and equivalent plastic strain (PEEQ) in the vicinity of the defect are recorded. These simulations provide the basis for a detailed comparison of the effect of orientation on local stress and plasticity once the corresponding numerical maps and curves are analyzed.

The effect of scratch orientation on the mechanical response is evaluated by comparing the time evolution of the maximum von Mises stress and maximum equivalent plastic strain for the two angles, 45° and 90°, while keeping depth and width constant. The corresponding curves are shown in Figures (figure 27).

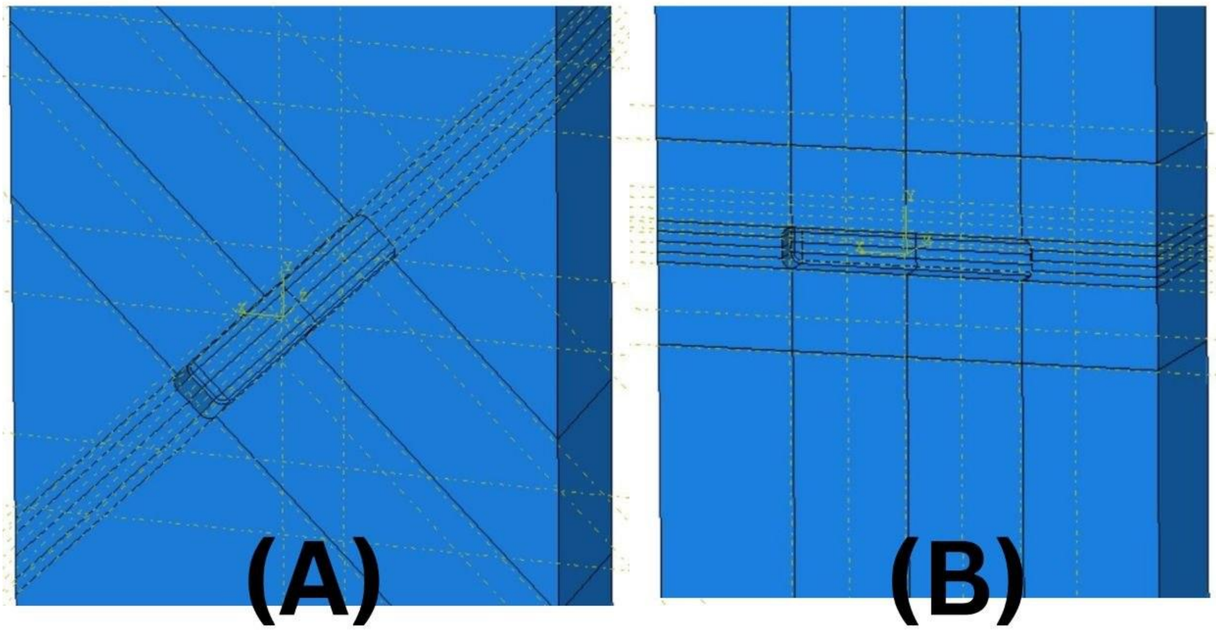

Figure 25: scratch orientation

(A):45° ; (B):90°

The von Mises (figure 26a) curves indicate that the 45° scratch generates higher stress levels than the 90° scratch during most of the loading history. The peak von Mises stress for the 45° configuration reaches approximately the material tensile strength, whereas the 90° configuration remains noticeably below this value. This means that the inclined scratch produces a more severe stress concentration, making the material around the defect more prone to damage and crack initiation.

The PEEQ evolution (figure 26b) confirms this trend. Both orientations lead to similar maximum plastic strain values at peak loading, but the 45° scratch reaches high PEEQ levels earlier and maintains them over a wider time interval. In contrast, the 90° scratch shows a more localized plastic response in time. This behaviour suggests that an inclined scratch promotes earlier and more sustained plastic yielding in the critical region, which can accelerate the initiation and growth of cracks from the defect.

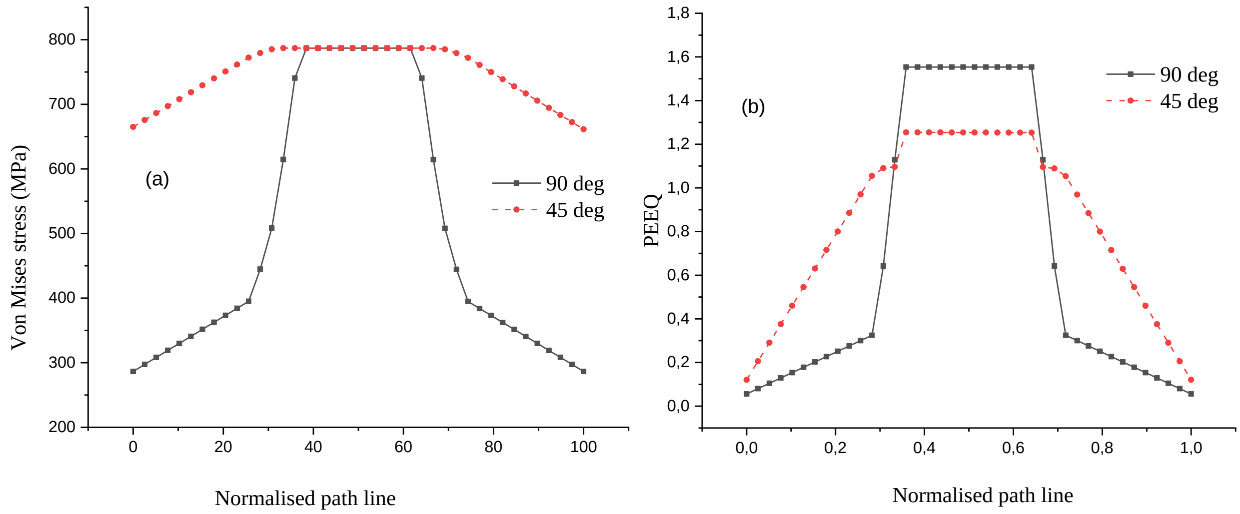

Figure 26: Distribution of Von Mises stress (a) and the equivalent plastic deformation (b) along the path line

3.4. Study of semi-elliptical crack defects

In the second part of the numerical investigation, the tensile specimen contains a crack instead of a scratch. The crack is introduced at the center of the gauge section, at the same location previously used for the scratch, so that it lies in the region of maximum axial stress. It is oriented perpendicular to the loading direction and normal to the specimen surface, which corresponds to a pure opening (mode I) configuration.

The crack geometry is defined in (figure 27). In the present study, several crack depths are considered (C= 0.4, 0.5, 0.6 and 0.8 mm) together with several crack widths (D = 2.8, 3.0, 3.2 and 3.4 mm), while all other parameters of the model remain unchanged. For each combination of depth and width, a displacement-controlled tensile test is simulated, and the corresponding fields of Von Mises stress, equivalent plastic strain and J-integral at the crack front are evaluated.

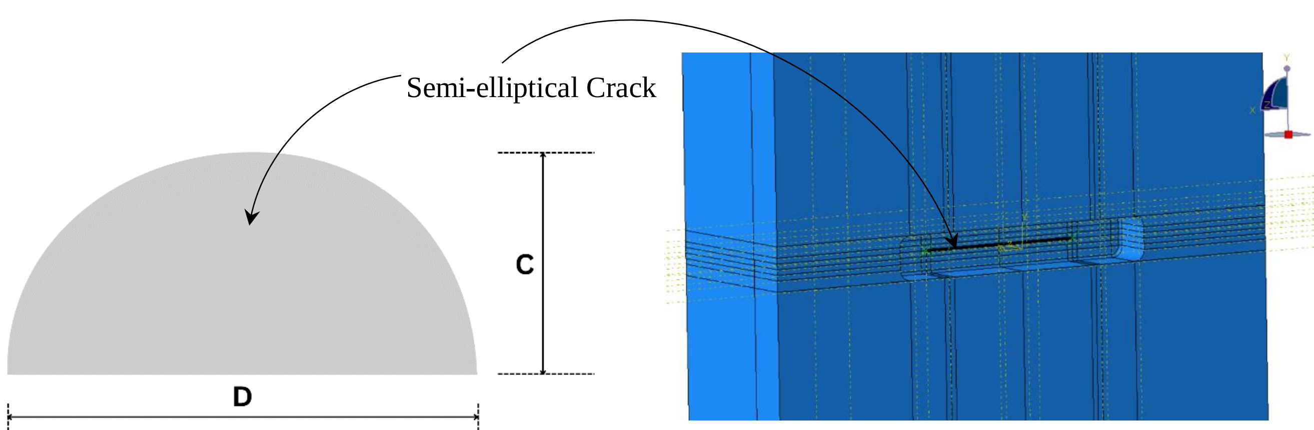

Figure 27: semi-elliptical crack geometry

3.4.1. Study of semi-elliptical crack depth

In this subsection, only the crack depth C varies, while its width D = 3 mm and its position remain constant. The depth values studied are 0.4, 0.5, 0.6, and 0.8 mm. For each depth, a displacement-controlled tensile simulation is performed. During each analysis, the distributions of the maximum von Mises stress in the vicinity of the crack, the maximum equivalent plastic strain (PEEQ), and the integral J along the crack front are extracted.

In this section, the influence of crack depth on the von Mises stress is investigated. The corresponding stress contour curves and maps are presented to compare how crack depth modifies the level and distribution of the von Mises stress around the defect (figure 28).

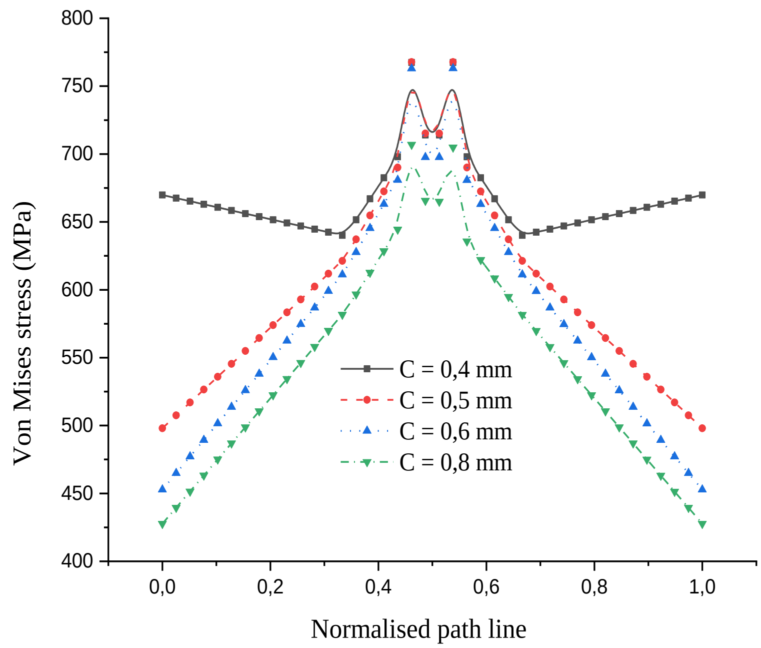

Figure 28: Distribution of Von Mises stress along the path line for different crack depth

The figure highlights a symmetrical distribution of Von Mises stresses along the normalized path around the crack, with stress peaks localized at the crack edges, indicating a high geometric concentration. Inside the crack, stress values decrease from these maxima but remain higher than the levels measured outside the damaged area, suggesting that the crack tip continues to bear a significant portion of the load. Furthermore, increasing the depth C leads to an overall decrease in stress levels along the path, a phenomenon interpreted as energy absorption and dissipation at the crack tip, partially quantifiable by the energy integral J . These observations suggest that local geometry and dissipative mechanisms control both the location of stress maxima and the evolution of the stress state with crack depth, with direct implications for crack initiation and propagation as well as for reinforcement and monitoring strategies.

The same simulations will be used to study the effect of crack depth on the equivalent plastic strain (figure 29) For each value of C, the maximum PEEQ near the crack front will be extracted at each time increment. The results will be shown as PEEQ–time curves together with contour maps at selected load levels. This will make it possible to examine how the size and intensity of the plastic zone around the crack evolve when the depth increases.

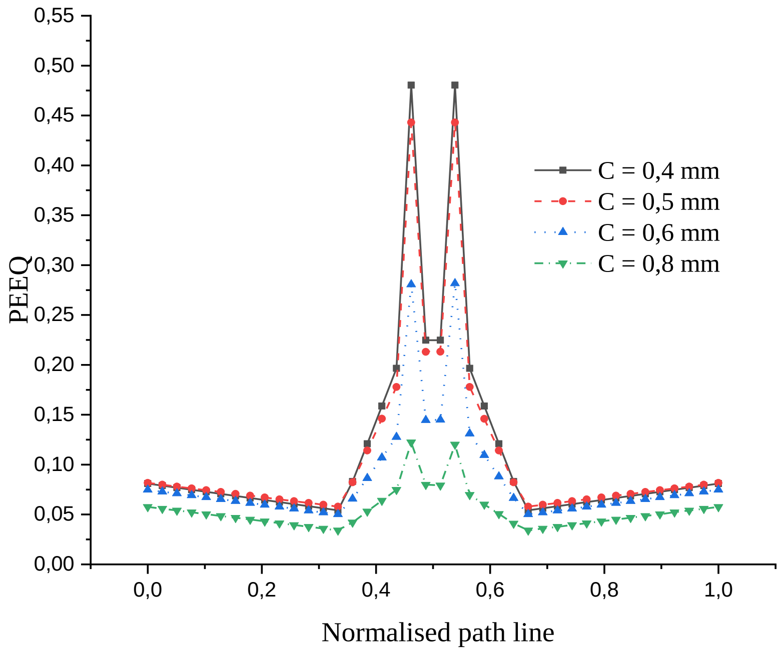

Figure 29: Distribution of equivalent plastic strain (PEEQ) along the path line for different crack depth (C)

The figure illustrates the evolution of the equivalent plastic strain (PEEQ) along a normalized path as a function of crack depth C. The distribution exhibits a marked peak near the center of the path, indicating that plasticity is concentrated in the most stressed area. The maximum PEEQ value is obtained for a low crack depth (C = 0.4 mm), indicating a high concentration of plastic strain when the crack is small. As the depth C increases, the intensity of the peak gradually decreases, reflecting a redistribution and dissipation of plastic energy towards the crack tip. This behavior is consistent with the role of the integral J, which expresses the energy available for crack propagation: some of this energy is absorbed by dissipative mechanisms (local plasticity, microcracking), thus reducing the PEEQ value measured along the path. Consequently, crack depth acts as a regulating factor of equivalent plasticity, with direct implications for predicting crack initiation and propagation in stressed structures.

3.4.2. Study of semi-elliptical crack width

In this subsection, only the crack width D will be modified, while its depth C = 0.5 mm and all other parameters will remain constant. The crack widths considered are 2.8, 3.0, 3.2, and 3.4 mm. For each width, a displacement-controlled tensile simulation will be performed, and the same quantities as before will be calculated: maximum von Mises stress, maximum PEEQ in the vicinity of the crack, and the integral J along the crack front and the path line.

During the analysis, the maximum von Mises stress in the vicinity of the crack will be recorded along the path (Figure 30). Von Mises stress curves will be presented for the different crack widths to compare the influence of D on the level and spatial distribution of the von Mises stress around the crack.

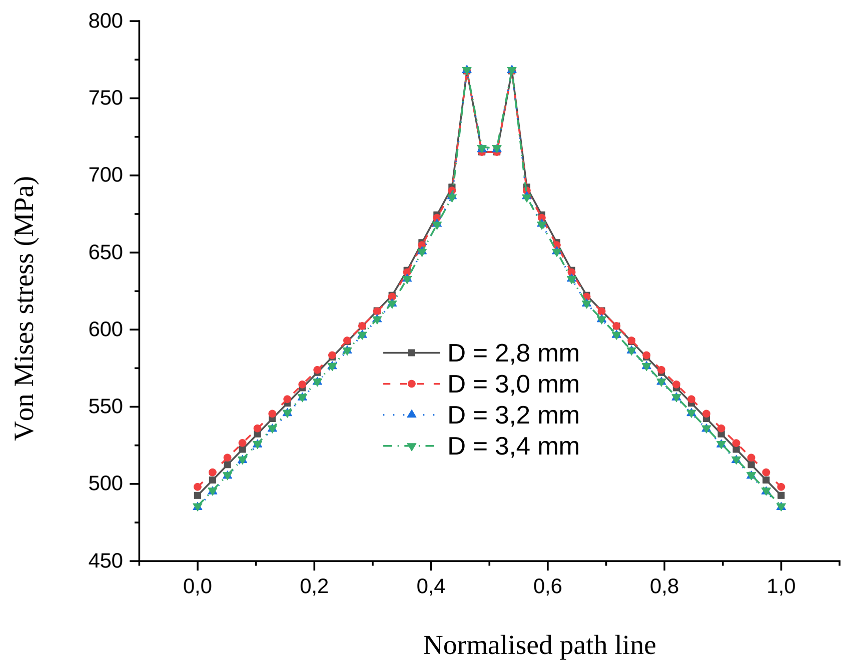

Figure 30: Distribution of Von Mises stress along the path line for different crack width

The same simulations will be used to evaluate the influence of crack width on the equivalent plastic strain (figure 31) For each width, the maximum PEEQ near the crack front will be extracted at each load increment.

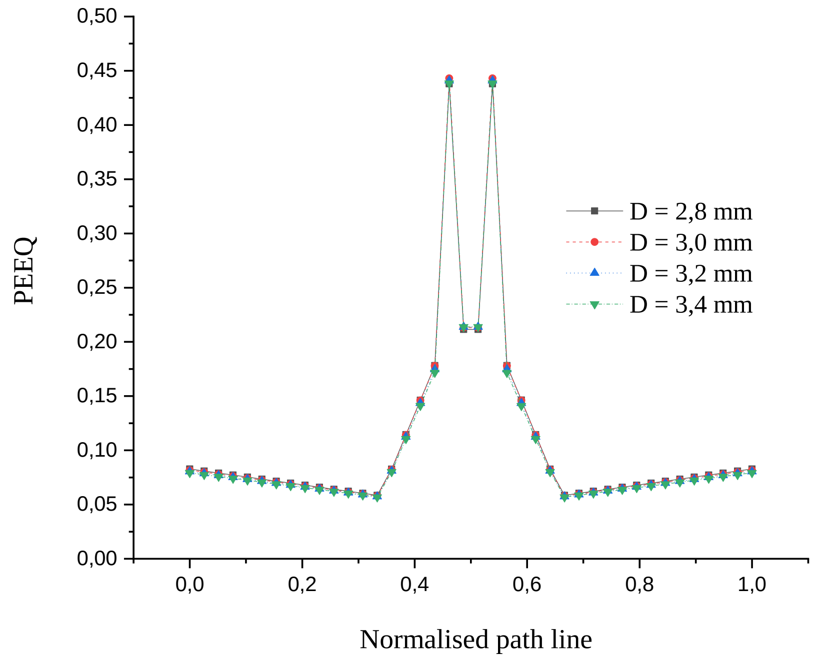

Figure 31: Distribution of equivalent plastic strain (PEEQ) along the path line for different crack width

The results show that the Von Mises stress and the PEEQ index evolve consistently along the normalized path for different crack widths D. The Von Mises stress exhibits a marked peak at the center of the path, reaching high values for narrow cracks (D = 2.8 mm), indicating strong mechanical concentration as the crack width decreases. As D increases, the intensity of the peak decreases, indicating better stress distribution and a reduction in local singularities. Complementarily, the PEEQ distribution reveals two symmetrical peaks around the center, corresponding to areas of high plastic energy dissipation. These peaks are also more pronounced for narrow cracks and gradually diminish with increasing D, reflecting an increased capacity of the structure to absorb and redistribute energy without concentrating plasticity in limited areas. Thus, the joint analysis highlights that crack width acts as a regulating parameter: a wider crack simultaneously limits stress concentration and plasticity localization, improving the stability and overall resistance of the structure to stresses.

3.5.J-Integral and Fracture Mechanics Law

The J-integral is a fundamental parameter in fracture mechanics used to characterize the energy release rate associated with crack growth in elastic–plastic materials. It provides a measure of the intensity of the stress and strain field near the crack tip and is widely used for evaluating fracture resistance in ductile materials such as steel pipelines.

The concept of the J-integral was introduced by Rice and is defined as a contour integral surrounding the crack tip. It represents the rate of change of potential energy with respect to crack extension and is path-independent under certain conditions. The mathematical expression of the J-integral is given by:

$$J = \int_{\Gamma} \left(W\, dy - T_i \frac{\partial u_i}{\partial x} ds \right) \quad (11)$$

where $W$is the strain energy density, $T_i$represents the traction vector, $u_i$is the displacement vector, and $\Gamma$is a contour surrounding the crack tip.

In linear elastic fracture mechanics, the J-integral is equivalent to the energy release rate G, which defines the amount of energy available for crack propagation per unit crack surface area. When the material exhibits plastic behavior, the J-integral extends this concept by accounting for plastic deformation at the crack tip, making it suitable for ductile fracture analysis.

Crack propagation occurs when the calculated J-integral reaches a critical value J_{IC}, known as the material's fracture toughness. This condition defines the onset of unstable crack growth and failure.

In numerical simulations using Abaqus, the J-integral is evaluated around the crack tip using a domain integral method. Multiple contours are typically used to ensure path independence and improve the accuracy of the results. The variation of the J-integral with respect to crack geometry provides important insight into the fracture resistance of the pipeline under different defect configurations.

3.5.1. J-integral for crack depth variation

The first study of the J integral focuses on the influence of crack depth. The width and position of the crack are kept constant, while its depth C varies between 0.4, 0.5, 0.6, and 0.8 mm. For each depth, a tensile simulation with imposed displacement is performed, and the J integral along the crack front is calculated at each increment (figure 32).

The curves reveal that the J-integral reaches its maximum near the middle of the crack front before slightly decreasing, reflecting a non-uniform distribution of fracture energy with a central zone that is more highly solicited. As crack depth increases (C=0.4 mm→0.8 mm), the values of J rise, indicating that the deeper the crack, the greater the energy available for its propagation.

A shallow crack (C=0.4 mm) exhibits lower J values and therefore a reduced tendency to propagate, whereas a deeper crack concentrates more energy, increasing the risk of unstable growth. The localization of the J maxima at the center of the crack front suggests that preferential propagation will occur in this critical region, where fracture energy is highest. The increase in J with depth confirms that the crack acts as an energy reservoir: the deeper it penetrates, the more mechanical energy it accumulates and makes available for damage.

This behavior is consistent with the observations made for Von Mises stress and PEEQ: while a deeper crack reduces local stress levels, it simultaneously increases the overall fracture energy, thereby altering both the mode and stability of crack propagation.

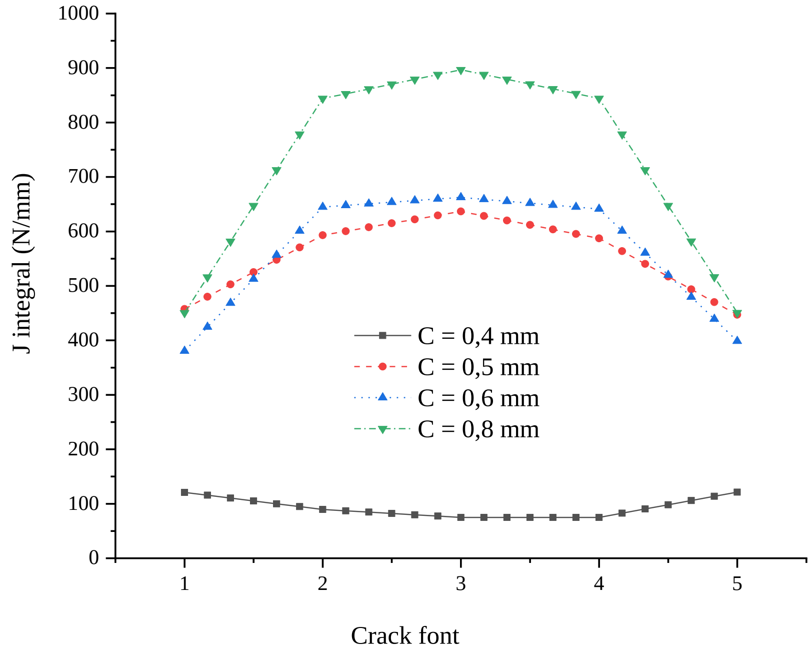

Figure 32: Distribution of J integral along the crack front for crack depth variation

3.5.2. J-integral for crack width variation

In the second study, the effect of crack width D on the integral J is examined (Figure 33). The crack depth C = 0.5 mm is kept constant, while its width varies between 2.8, 3.0, 3.2, and 3.4 mm. For each width, the integral J is calculated along the crack front during tensile loading, using the same domain integration procedure.

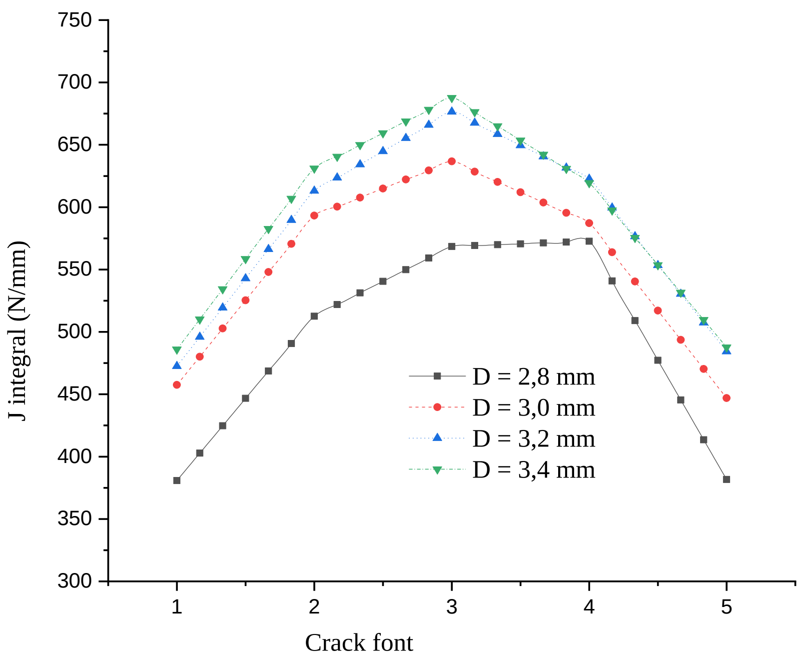

Figure 33: Distribution of J integral along the crack front for crack width variation

The curves show that the J-integral reaches its maximum at the center of the crack front before decreasing toward the edges same remark as for the effect of crack depth, reflecting a non-uniform distribution of fracture energy with increased solicitation in the central zone. For narrow cracks (D=2.8 mm), the J values are higher, revealing a strong energy concentration and a greater tendency for propagation. Conversely, as the crack width increases (D=3.4 mm), the J values decrease, indicating a more homogeneous distribution of energy and a reduced risk of unstable propagation. The comparison of the curves confirms that widening the crack reduces the energy available for growth, thereby improving the overall stability of the structure. The localization of the J maxima at the center of the front suggests that preferential propagation will occur in this critical zone. The opposite trend between narrow and wide cracks demonstrates that crack width acts as a regulating parameter: a narrow crack concentrates energy and promotes instability, whereas a wider crack dissipates energy and limits propagation. This behavior is consistent with the observations related to Von Mises stress and PEEQ, showing that crack width simultaneously influences mechanical concentration and plastic dissipation, thereby altering both the mode and stability of crack propagation.

3.6. J-Integral Variation for Repair Models

In this final part of the study, the main objective is to evaluate the interaction of defects (scratch cracks) in the presence of different modeled repair configurations. To this end, several repair models were developed and analyzed. The first model corresponds to the repair of a cracked plate (C = 0.5 mm and D = 3.0 mm) at the base of the scratch (a/t = 25%) with putty applied within the scratch. The second model presents a composite repair on a cracked plate (C = 0.5 mm and D = 3.0 mm) without scratch. The third model considers the composite repair applied to the case of a crack and a scratch (a/t = 25%) without putty (figure 34).

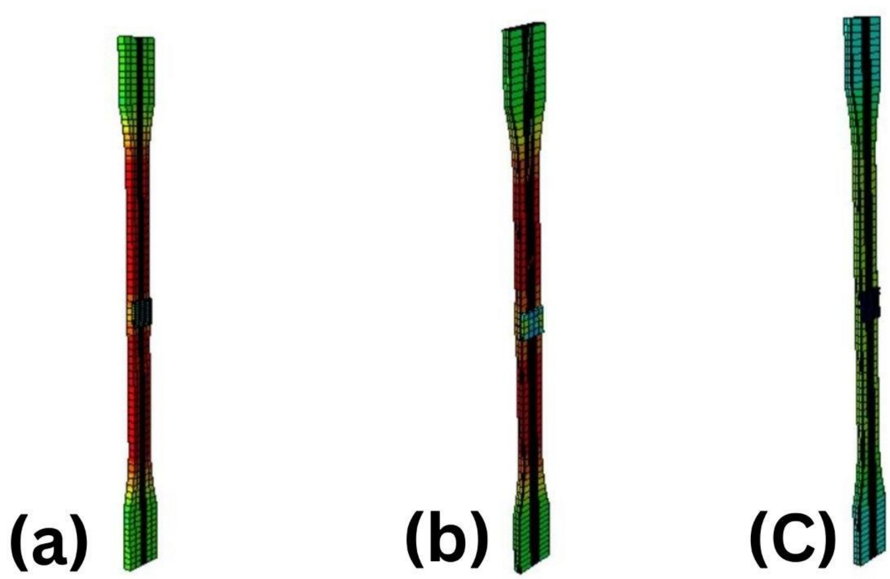

Figure 34: Variation for Repair Models

(a) cracked plate + scratch with putty
(b) cracked plate + scratch repaired with composite
(c) cracked plate + no scratch repaired with composite

This comparison is important because it provides a clear indication of how the repair material and the damaged condition affect the structural response. In particular, it helps highlight the differences between mastic and composite repairs, as well as the influence of the presence of scratch damage on the overall fracture behavior.

Proprieties of material:

Material	Linear (below yield)	Nonlinear (above yield)
Putty (Thickened Epoxy)	Young's Modulus E = 1.74 GPa Poisson's Ratio ν = 0.45	Yield Stress σY = 33 MPa Tangent Modulus Etan = 0.87 GPa
Colle (FM37 Elastique)	Young's Modulus E = 2.21 GPa Poisson's Ratio ν = 0.43	N/A
Composite (Boron/Epoxy)	Ex = 200 GPa Ey = 25 GPa Ez = 25 GPa νxy = 0.21 νxz = 0.21 νyz = 0.21 Gxy = 7.2 GPa Gxz = 5.5 GPa Gyz = 5.5 GPa	N/A

Table 2: Proprieties of material

The (figure 35) compares the distribution of the J-integral along the crack front for three repair configurations, highlighting the impact of treatments (putty, composite repair, absence of scratch) on the energy available for crack propagation.

The relative J levels differ markedly by configuration: the “scratch with putty” case exhibits the highest J values, the composite repair without putty shows intermediate values, and the plate without an initial scratch but repaired with composite displays the lowest values. For each configuration, J reaches one or more localized maxima—generally near the central region of the front—then decreases toward the edges, indicating a non-uniform loading of the front. The use of putty appears to leave zones where fracture energy remains concentrated, whereas the composite alone partially mitigates this concentration; the absence of an initial defect (or a fully effective repair) minimizes J overall.

The J-integral quantifies the elastic–plastic energy available for crack growth: locally high values indicate an increased risk of crack initiation and propagation. Putty can introduce mechanical discontinuities or residual stresses that sustain elevated J levels near the defect, which explains the observed peaks. The composite, by covering and reinforcing the area, reduces the energy concentration but does not necessarily eliminate all critical zones if the interface or adhesion are imperfect. The most favorable configuration is therefore the one that lowers and homogenizes J along the front, thereby reducing preferential initiation sites.

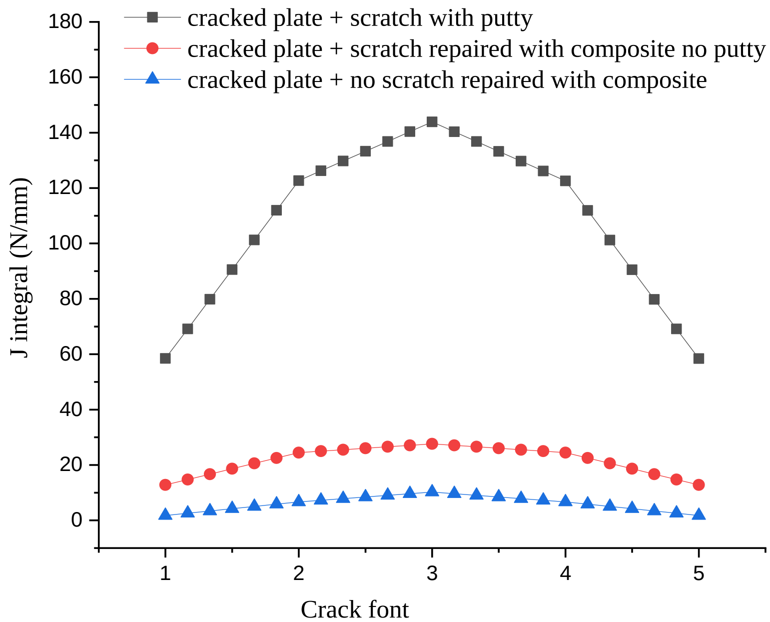

Figure 35: Distribution of J integral along the crack front for different repair configuration

In conclusion, the extent and nature of the repair directly influence the energy distribution along the crack front. To limit propagation risk, repairs that restore mechanical continuity and improve adhesion should be favored over isolated filling, and non-destructive inspections should be focused on the regions identified by the J maximal.

General Conclusion

The transportation of oil and natural gas through pipelines represents one of the most efficient and economical methods for meeting the growing global energy demand. Because these infrastructures operate under high internal pressures and often in harsh environmental conditions, maintaining their structural integrity is essential for ensuring safety, reliability, and uninterrupted service. However, pipelines are frequently exposed to various degradation mechanisms, including corrosion, fatigue, manufacturing defects, and mechanical damage. Among these, crack-like defects and surface scratches are particularly critical because of their ability to generate significant stress concentrations and promote fracture initiation and propagation.

The present work focused on the numerical investigation of the interaction between crack and scratch defects in a buried API 5L X80 steel pipeline. The study was conducted using the Finite Element Method implemented in ABAQUS, which provides a powerful and reliable tool for analyzing complex defect geometries and evaluating their influence on pipeline behavior. The main objective was to understand how the geometric characteristics of cracks and scratches affect stress distribution, plastic deformation, and fracture parameters, thereby influencing the overall integrity of the structure.

A comprehensive review of fracture mechanics principles and pipeline integrity assessment methods was first presented. Particular attention was given to the concepts of stress concentration, crack initiation and propagation, fracture toughness, and the J-integral, which constitutes one of the most important parameters for evaluating crack-driving forces in elastic-plastic materials. The study also examined the main causes of pipeline deterioration and the engineering approaches commonly used to assess defect severity and structural safety.

The numerical analyses demonstrated that the presence of defects significantly modifies the local mechanical response of the pipeline. The results revealed that increasing the dimensions of cracks and scratches leads to higher levels of Von Mises stress and equivalent plastic strain in the vicinity of the defect region. These stress concentrations create favorable conditions for crack growth and may accelerate the deterioration process under operational loading conditions.

The evaluation of the J-integral showed that defect geometry plays a crucial role in fracture behavior. Larger crack dimensions produced higher J-integral values, indicating a greater tendency for crack propagation and a reduction in the safety margin of the pipeline. Furthermore, the interaction between crack and scratch defects was found to amplify local stress and strain fields, demonstrating that combined defects may be more critical than isolated defects. This observation highlights the importance of considering defect interaction effects during pipeline integrity assessments rather than evaluating each defect independently.

The numerical simulations also provided valuable information regarding repair configurations and their effectiveness in reducing fracture severity. The obtained results indicate that suitable repair solutions can decrease the crack-driving force and improve the structural performance of the damaged pipeline. Such findings are particularly important for maintenance planning and for extending the service life of aging pipeline systems while maintaining acceptable safety levels.

From an engineering perspective, the results obtained in this work contribute to a better understanding of the mechanical behavior of high-strength API 5L X80 steel pipelines containing interacting defects. The study confirms the usefulness of finite element analysis as an advanced tool for structural integrity assessment and demonstrates the relevance of fracture mechanics parameters, especially the J-integral, for evaluating defect severity and predicting failure risks.

Bibliography

Allouti, M., Schmitt, C., Pluvinage, G., Gilgert, J., & Hariri, S. (2012). Study of the influence of dent depth on the critical pressure of pipeline. Engineering Failure Analysis, 21, 40-51.

Allouti, M., Schmitt, C., & Pluvinage, G. (2014). Assessment of a gouge and dent defect in a pipeline by a combined criterion. Engineering Failure Analysis, 36, 1-13.

Anderson, T. L. (2017). Fracture Mechanics: Fundamentals and Applications (4th ed.). CRC Press, Boca Raton.

ANSI/NACE MR0175/ISO 15156 (2015). Petroleum and natural gas industries — Materials for use in H2S-containing environments in oil and gas production. NACE International.

API 5L (2018). Specification for Line Pipe (46th ed.). American Petroleum Institute, Washington, D.C.

API 579-1/ASME FFS-1 (2021). Fitness-For-Service. American Petroleum Institute / American Society of Mechanical Engineers.

ASME B31.4 (2019). Pipeline Transportation Systems for Liquids and Slurries. ASME, New York.

ASME B31.8 (2020). Gas Transmission and Distribution Piping Systems. ASME, New York.

ASME B31G (1984, revised 2012). Manual for Determining the Remaining Strength of Corroded Pipelines. ASME, New York.

ASTM E399 (2020). Standard Test Method for Linear-Elastic Plane-Strain Fracture Toughness KIC of Metallic Materials. ASTM International, West Conshohocken, PA.

ASTM E1820 (2021). Standard Test Method for Measurement of Fracture Toughness. ASTM International, West Conshohocken, PA.

ASTM E1921 (2021). Standard Test Method for Determination of Reference Temperature T0, for Ferritic Steels in the Transition Range. ASTM International.

Beavers, J. A., & Harle, B. A. (2001). Mechanisms of high-pH and near-neutral-pH SCC of underground pipelines. Journal of Offshore Mechanics and Arctic Engineering, 123(3), 147-151.

Beretta, S., Carboni, M., & Conte, A. L. (2013). Fatigue propagation and threshold for shallow cracks in a railway axle of API X70 steel. Engineering Fracture Mechanics, 110, 165-179.

BS 7910 (2019). Guide to methods for assessing the acceptability of flaws in metallic structures. British Standards Institution, London.

Carneiro, R. A., Ratnapuli, R. C., & Lins, V. F. C. (2003). The influence of chemical composition and microstructure of API line pipe steels on hydrogen induced cracking and sulfide stress corrosion cracking. Materials Science and Engineering A, 357(1-2), 104-110.

Chen, W., Kania, R., Worthingham, R., & Boven, G. V. (2007). Crack growth model of pipeline steels in near-neutral pH soil environments. Corrosion, 63(7), 696-707.

Cosham, A., & Hopkins, P. (2007). The pipeline defect assessment manual (PDAM): A report to the PDAM joint industry project. Penspen Integrity, Newcastle upon Tyne.

Bibliography

Cosham, A., Hopkins, P., & Macdonald, K. A. (2007). Best practice for the assessment of defects in pipelines — Corrosion. Engineering Failure Analysis, 14(7), 1245-1265.

CSA Z662 (2019). Oil and gas pipeline systems. Canadian Standards Association, Mississauga.

DeArdo, A. J. (2003). Niobium in modern steels. International Materials Reviews, 48(6), 371-402.

DNV-RP-F101 (2019). Corroded pipelines. Det Norske Veritas Recommended Practice, Høvik.

EGIG (2018). 10th Report of the European Gas Pipeline Incident Data Group (1970-2016). EGIG, Doc. 18.R.0431.

EIA (2021). Annual Energy Outlook. U.S. Energy Information Administration, Washington, D.C.

Eiber, R. J., Bubenik, T. A., & Maxey, W. A. (2004). GASDECOM: Computer code for the calculation of gas decompression speed. Pipeline Research Council International, Houston.

Folias, E. S. (1965). An axial crack in a pressurized cylindrical shell. International Journal of Fracture Mechanics, 1(2), 104-113.

Glover, A., Horsley, D., Dorling, D., & Takehara, J. (2003). Construction and installation of X100 pipelines. In Proceedings of the International Pipeline Conference, IPC2002-27073.

Gray, J. M. (2002). HSLA steels and microalloying. International Symposium on Niobium 2001, TMS, Warrendale, PA.

Griffith, A. A. (1921). The phenomena of rupture and flow in solids. Philosophical Transactions of the Royal Society of London A, 221, 163-198.

Hashemi, S. H. (2011). Strength-hardness statistical correlation in API X65 steel. Materials Science and Engineering A, 528(3), 1648-1655.

Hillenbrand, H. G., Kalwa, C., & Liessem, A. (2002). High strength line pipe steels for sour service and arctic applications. In Proceedings of the International Pipeline Conference, Calgary.

Hopkins, P. (2007). Pipelines: Past, present, and future. The 5th Asian Pacific IIW International Congress, Sydney.

Hutchinson, J. W. (1968). Singular behaviour at the end of a tensile crack in a hardening material. Journal of the Mechanics and Physics of Solids, 16(1), 13-31.

Hwang, B., Lee, S., Kim, Y. M., Kim, N. J., & Yoo, J. Y. (2011). Analysis of abnormal fracture occurring during drop-weight tear test of high-toughness line-pipe steel. Materials Science and Engineering A, 368(1-2), 18-27.

Irwin, G. R. (1957). Analysis of stresses and strains near the end of a crack traversing a plate. Journal of Applied Mechanics, 24, 361-364.

Kiefner, J. F., & Vieth, P. H. (1989). A modified criterion for evaluating the remaining strength of corroded pipe. Final Report PR-3-805 to the Pipeline Research Committee of the AGA, Battelle Memorial Institute, Columbus, OH.

Bibliography

Kim, Y. J., Shim, D. J., Lim, H., & Kim, Y. J. (2007). Numerical investigation on plastic limit loads and J-integral estimates of axial surface cracked pipes. International Journal of Pressure Vessels and Piping, 84(7), 433-451.

Koçak, M., Webster, S., Janosch, J. J., Ainsworth, R. A., & Koers, R. (2008). FITNET Fitness-for-Service Procedure - Final Draft. GKSS Research Centre, Geesthacht.

Krauss, G. (2005). Steels: Processing, Structure, and Performance. ASM International, Materials Park, OH.

Liessem, A., & Erdelen-Peppler, M. (2004). A critical view on the significance of HAZ toughness testing. In Proceedings of the International Pipeline Conference IPC2004-0315.

Lyons, C. J., Race, J. M., Wetenhall, B., Chang, E., Hopkins, H. F., & Barnett, J. (2020). Validation of the EPRG dent-gouge fatigue failure equation for modern high-toughness pipeline steels. International Journal of Pressure Vessels and Piping, 188, 104224.

Macdonald, K. A., & Cosham, A. (2005). Best practice for the assessment of defects in pipelines — gouges and dents. Engineering Failure Analysis, 12(5), 720-745.

Maxey, W. A. (1974). Fracture initiation, propagation and arrest. In Proceedings of the 5th Symposium on Line Pipe Research, AGA, Houston, paper J.

Mohitpour, M., Golshan, H., & Murray, A. (2003). Pipeline Design and Construction: A Practical Approach (2nd ed.). ASME Press, New York.

Murakami, Y. (1987). Stress Intensity Factors Handbook. Pergamon Press, Oxford.

O'Dowd, N. P., & Shih, C. F. (1991). Family of crack-tip fields characterized by a triaxiality parameter - I: Structure of fields. Journal of the Mechanics and Physics of Solids, 39(8), 989-1015.

O'Rourke, M. J., & Liu, X. (2012). Seismic Design of Buried and Offshore Pipelines. MCEER Monograph No. 4, Buffalo.

Oh, C. K., Kim, Y. J., Baek, J. H., Kim, Y. P., & Kim, W. S. (2007). A phenomenological model of ductile fracture for API X65 steel. International Journal of Mechanical Sciences, 49(12), 1399-1412.

Paris, P. C., & Erdogan, F. (1963). A critical analysis of crack propagation laws. Journal of Basic Engineering, 85(4), 528-533.

Parkins, R. N. (2000). A review of stress corrosion cracking of high pressure gas pipelines. NACE Corrosion 2000, paper 363.

Parkins, R. N., Blanchard, W. K., & Delanty, B. S. (2003). Transgranular stress corrosion cracking of high-pressure pipelines in contact with solutions of near neutral pH. Corrosion, 50(5), 394-408.

PHMSA (2020). Pipeline Incident Statistics. Pipeline and Hazardous Materials Safety Administration, U.S. Department of Transportation.

Bibliography

Pluvinage, G., Capelle, J., & Schmitt, C. (2014). Methods for assessing defects leading to gas pipe failure. In Handbook of Materials Failure Analysis with Case Studies from the Oil and Gas Industry, Elsevier, 55-89.

Pluvinage, G., Bouledroua, O., Hadj Meliani, M., & Suleiman, R. (2018). Corrosion defect analysis using domain failure assessment diagram. International Journal of Pressure Vessels and Piping, 165, 126-134.

R6 (2013). Assessment of the Integrity of Structures Containing Defects, Revision 4. EDF Energy, Gloucester.

Rice, J. R. (1968). A path independent integral and the approximate analysis of strain concentration by notches and cracks. Journal of Applied Mechanics, 35(2), 379-386.

Rice, J. R., & Rosengren, G. F. (1968). Plane strain deformation near a crack tip in a power-law hardening material. Journal of the Mechanics and Physics of Solids, 16(1), 1-12.

Rice, J. R., & Tracey, D. M. (1969). On the ductile enlargement of voids in triaxial stress fields. Journal of the Mechanics and Physics of Solids, 17(3), 201-217.

Shih, C. F., Moran, B., & Nakamura, T. (1986). Energy release rate along a three-dimensional crack front in a thermally stressed body. International Journal of Fracture, 30(2), 79-102.

Shin, S. Y., Hwang, B., Kim, S., & Lee, S. (2007). Fracture toughness analysis in transition temperature region of API X70 and X80 line pipe steels. Materials Science and Engineering A, 458(1-2), 281-289.

Sonatrach (2020). Sonatrach Annual Report 2019. Algerian National Oil and Gas Company, Algiers.

Stephens, D. R., & Leis, B. N. (2000). Development of an alternative criterion for residual strength of corrosion defects in moderate- to high-toughness pipe. In Proceedings of the International Pipeline Conference, ASME, 781-792.

Sumpter, J. D. G., & Forbes, A. T. (1992). Constraint based analysis of shallow cracks in mild steel. In Proceedings of TWI/EWI/IS International Conference on Shallow Crack Fracture Mechanics, TWI, Cambridge.

Tada, H., Paris, P. C., & Irwin, G. R. (2000). The Stress Analysis of Cracks Handbook (3rd ed.). ASME Press, New York.

Tvergaard, V., & Needleman, A. (1984). Analysis of the cup-cone fracture in a round tensile bar. Acta Metallurgica, 32(1), 157-169.

Wallin, K. (1991). Statistical aspects of constraint with emphasis on testing and analysis of laboratory specimens in the transition region. ASTM STP 1171, 264-288.

Wells, A. A. (1961). Unstable crack propagation in metals: cleavage and fast fracture. In Proceedings of the Crack Propagation Symposium, Cranfield, 1, 210-230.

Westergaard, H. M. (1939). Bearing pressures and cracks. Journal of Applied Mechanics, 6, A49-A53.

Bibliography

Yang, S., Chao, Y. J., & Sutton, M. A. (1993). Higher order asymptotic crack tip fields in a power-law hardening material. Engineering Fracture Mechanics, 45(1), 1-20.

Zhou, W., & Nessim, M. A. (2011). Optimal design of onshore natural gas pipelines. Journal of Pressure Vessel Technology, 133(3), 031702.

Atluri, S. N. (1986). Energetic approaches and path-independent integrals in fracture mechanics. In Computational Methods in the Mechanics of Fracture (S. N. Atluri, Ed.), Elsevier, 121-165.

Bouledroua, O., Hadj Meliani, M., Azari, Z., Sorour, A. A., Merah, N., & Pluvinage, G. (2017). Effect of sandblasting on tensile properties, hardness and fracture resistance of a line pipe steel used in Algeria for oil transport. Journal of Failure Analysis and Prevention, 17(5), 890-904.

Brocks, W., & Scheider, I. (2003). Reliable J-values: Numerical aspects of the path-dependence of the J-integral in incremental plasticity. Materialprüfung, 45(6), 264-275.

CER (2019). Pipeline performance reports. Canada Energy Regulator (formerly NEB), Calgary.

Concawe (2020). Performance of European cross-country oil pipelines: Statistical summary of reported spillages in 2019 and since 1971. Concawe Report 6/20, Brussels.

Hadj Meliani, M., Matvienko, Yu. G., & Pluvinage, G. (2010). Two-parameter fracture criterion (Kρ,c-Tef,c) based on notch fracture mechanics. International Journal of Fracture, 167(2), 173-182.

Moran, B., & Shih, C. F. (1987). Crack tip and associated domain integrals from momentum and energy balance. Engineering Fracture Mechanics, 27(6), 615-642.

Nikishkov, G. P., & Atluri, S. N. (1987). Calculation of fracture mechanics parameters for an arbitrary three-dimensional crack, by the equivalent domain integral method. International Journal for Numerical Methods in Engineering, 24(9), 1801-1821.

Rolfe, S. T., & Barsom, J. M. (1999). Fracture and Fatigue Control in Structures: Applications of Fracture Mechanics (3rd ed.). ASTM, Philadelphia.

Wilkowski, G. (2000). Leak-before-break: What does it really mean? Journal of Pressure Vessel Technology, 122(3), 267-272.

Newman, J. C., & Raju, I. S. (1981). An empirical stress-intensity factor equation for the surface crack. Engineering Fracture Mechanics, 15(1-2), 185-192.

San Marchi, C., & Somerday, B. P. (2012). Technical Reference for Hydrogen Compatibility of Materials. Sandia National Laboratories Report SAND2012-7321.

Slifka, A. J., Drexler, E. S., Amaro, R. L., Hayden, L. E., Stalheim, D. G., Lauria, D. S., & Hrabe, N. W. (2018). Fatigue measurement of pipeline steels for the application of transporting gaseous hydrogen. Journal of Pressure Vessel Technology, 140(1), 011407.

Anon., AVRIL 2022. SONATRACH-SPA and ARH. Pipeline Transport Network Code.

Anon., n.d. CAE Assistant. Fracture & Damage Mechanics. [Online]

Available at: 882392105-Fracture-and-Damage-Machanics.pdf

Bibliography

Sir Rashid Fiaz, C.-0., 26 April 2011. Imtisal-e-Noor. Classification of Steel, s.l.: s.n.

API 1163 (2013). In-line Inspection Systems Qualification (2nd ed.). American Petroleum Institute, Washington, D.C.

Capelle, J., Gilgert, J., & Pluvinage, G. (2008). A fatigue initiation parameter for gas pipe steel submitted to hydrogen absorption. International Journal of Hydrogen Energy, 35(2), 833-843.

Hassani, H., & Tian, Z. (2018). Application of artificial neural networks in pipeline integrity management. ASME International Pipeline Conference, IPC2018-78437.

Bjørnøy, O. H., Sigurdsson, G., & Marley, M. J. (2001). Background and development of DNV RP-F101 'Corroded Pipelines'. International Society of Offshore and Polar Engineers Conference, ISOPE-I-01-179.

Sotberg, T., Moan, T., Bruschi, R., Jiao, G., & Mørk, K. J. (1997). The SUPERB project: Wall thickness design guideline for pressure containment of offshore pipelines. Proceedings of OMAE 1997, Vol. V, 145-155.

ISO 13623 (2017). Petroleum and natural gas industries — Pipeline transportation systems. International Organization for Standardization, Geneva.

ISO 19345 (2019). Petroleum and natural gas industry — Pipeline transportation systems — Pipeline integrity management specification. ISO, Geneva.

PHMSA (2019). Pipeline Safety: Safety of Gas Transmission Pipelines, MAOP Reconfirmation, Expansion of Assessment Requirements, and Other Related Amendments (Mega Rule Part 1). 49 CFR Parts 191 and 192, U.S. Department of Transportation.

Alexander, C. R. (2007). Development of standards for the use of composite materials in repairing high-pressure transmission pipelines. In Proceedings of the ASME Pressure Vessels and Piping Conference, PVP2007-26023.

API 1104 (2018). Welding of Pipelines and Related Facilities (22nd ed.). American Petroleum Institute, Washington, D.C.

API 1160 (2019). Managing System Integrity for Hazardous Liquid Pipelines (3rd ed.). American Petroleum Institute, Washington, D.C.

API 2201 (2003). Safe Hot Tapping Practices in the Petroleum and Petrochemical Industries (5th ed.). American Petroleum Institute, Washington, D.C.

API 579-1/ASME FFS-1 (2021). Fitness-For-Service. American Petroleum Institute / American Society of Mechanical Engineers.

ASME B31.4 (2019). Pipeline Transportation Systems for Liquids and Slurries. ASME, New York.

ASME B31.8 (2020). Gas Transmission and Distribution Piping Systems. ASME, New York.

ASME B31.8S (2018). Managing System Integrity of Gas Pipelines. ASME, New York.

Bibliography

ASME B31G (1984, revised 2012). Manual for Determining the Remaining Strength of Corroded Pipelines. ASME, New York.

ASME PCC-2 (2018). Repair of Pressure Equipment and Piping. ASME, New York.

ASNT (2016). Nondestructive Testing Handbook (3rd ed.), Vols. 1-10. American Society for Nondestructive Testing, Columbus, OH.

Beavers, J. A. (2014). Integrity management of natural gas and petroleum pipelines subject to stress corrosion cracking. Corrosion, 70(1), 3-18.

Beavers, J. A., & Thompson, N. G. (2006). External corrosion of oil and natural gas pipelines. In ASM Handbook, Vol. 13C: Corrosion: Environments and Industries, ASM International, 1015-1025.

Beretta, S., Carboni, M., & Conte, A. L. (2013). Fatigue propagation and threshold for shallow cracks in a railway axle of API X70 steel. Engineering Fracture Mechanics, 110, 165-179.

Bruce, W. A. (2014). Welding onto in-service pipelines: Avoiding burn-through and hydrogen cracking. Welding Journal, 93(10), 24-30.

BS 7910 (2019). Guide to methods for assessing the acceptability of flaws in metallic structures. British Standards Institution, London.

Caleyo, F., Gonzalez, J. L., & Hallen, J. M. (2002). A study on the reliability assessment methodology for pipelines with active corrosion defects. International Journal of Pressure Vessels and Piping, 79(1), 77-86.

Carneiro, R. A., Ratnapuli, R. C., & Lins, V. F. C. (2003). The influence of chemical composition and microstructure of API line pipe steels on hydrogen induced cracking and sulfide stress corrosion cracking. Materials Science and Engineering A, 357(1-2), 104-110.

Chen, W., Kania, R., Worthingham, R., & Boven, G. V. (2007). Crack growth model of pipeline steels in near-neutral pH soil environments. Corrosion, 63(7), 696-707.

Cordell, J., & Vanzant, H. (2003). The Pipeline Pigging Handbook (3rd ed.). Clarion Technical Publishers, Houston.

Cosham, A., & Hopkins, P. (2007). The pipeline defect assessment manual (PDAM): A report to the PDAM joint industry project. Penspen Integrity, Newcastle upon Tyne.

Cosham, A., Hopkins, P., & Macdonald, K. A. (2007). Best practice for the assessment of defects in pipelines — Corrosion. Engineering Failure Analysis, 14(7), 1245-1265.

CSA Z662 (2019). Oil and gas pipeline systems. Canadian Standards Association, Mississauga.

de Waard, C., & Lotz, U. (1993). Prediction of CO2 corrosion of carbon steel. Corrosion 93, paper 69, NACE International.

DNV-RP-F101 (2019). Corroded pipelines. Det Norske Veritas Recommended Practice, Høvik.

EGIG (2018). 10th Report of the European Gas Pipeline Incident Data Group (1970-2016). EGIG, Doc. 18.R.0431.

Bibliography

Geiger, G. (2006). State-of-the-art in leak detection and localization. Pipeline Technology Conference, Hannover.

Ginzel, E. A. (2006). Mentor Ultrasonic Testing in the Pipeline Industry. Materials Research Institute, Waterloo.

IEA (2019). World Energy Outlook 2019. International Energy Agency, Paris.

ISO 17636-1 (2013). Non-destructive testing of welds — Radiographic testing — Part 1: X- and gamma-ray techniques with film. ISO, Geneva.

ISO 24817 (2017). Petroleum, petrochemical and natural gas industries — Composite repairs for pipework — Qualification and design, installation, testing and inspection. ISO, Geneva.

Kiefner, J. F., Maxey, W. A., Eiber, R. J., & Duffy, A. R. (1973). Failure stress levels of flaws in pressurized cylinders. ASTM STP 536, 461-481.

Kiefner, J. F., & Vieth, P. H. (1989). A modified criterion for evaluating the remaining strength of corroded pipe. Final Report PR-3-805 to the Pipeline Research Committee of the AGA, Battelle Memorial Institute, Columbus, OH.

Koçak, M., Webster, S., Janosch, J. J., Ainsworth, R. A., & Koers, R. (2008). FITNET Fitness-for-Service Procedure - Final Draft. GKSS Research Centre, Geesthacht.

Lam, C., & Zhou, W. (2016). Statistical analyses of incidents on onshore gas transmission pipelines based on PHMSA database. International Journal of Pressure Vessels and Piping, 145, 29-40.

Leis, B. N., & Thomas, J. (2001). Linepipe property issues in pipeline design and re-establishing MAOP. Pipeline Engineering Magazine, 4, 23-31.

Lowe, M. J. S., Alleyne, D. N., & Cawley, P. (1998). Defect detection in pipes using guided waves. Ultrasonics, 36(1-5), 147-154.

Lyons, C. J., Race, J. M., Wetenhall, B., Chang, E., Hopkins, H. F., & Barnett, J. (2020). Validation of the EPRG dent-gouge fatigue failure equation for modern high-toughness pipeline steels. International Journal of Pressure Vessels and Piping, 188, 104224.

Macdonald, K. A., & Cosham, A. (2005). Best practice for the assessment of defects in pipelines — gouges and dents. Engineering Failure Analysis, 12(5), 720-745.

Melchers, R. E., & Beck, A. T. (2017). Structural Reliability Analysis and Prediction (3rd ed.). John Wiley & Sons, Chichester.

Nestleroth, J. B., & Bubenik, T. A. (1999). Magnetic flux leakage (MFL) technology for natural gas pipeline inspection. Battelle Memorial Institute, Columbus, OH.

NTSB (2011). Pacific Gas and Electric Company natural gas transmission pipeline rupture and fire, San Bruno, California, September 9, 2010. National Transportation Safety Board Report PAR-11/01.

Bibliography

NTSB (2012). Enbridge Incorporated hazardous liquid pipeline rupture and release, Marshall, Michigan, July 25, 2010. National Transportation Safety Board Report PAR-12/01.

Parkins, R. N. (2000). A review of stress corrosion cracking of high pressure gas pipelines. NACE Corrosion 2000, paper 363.

PHMSA (2002). 49 CFR Part 192: Transportation of Natural and Other Gas by Pipeline: Minimum Federal Safety Standards. U.S. Department of Transportation.

Reber, K., Beller, M., Willems, H., & Barbian, O. A. (2002). A new generation of ultrasonic in-line inspection tools for detecting, sizing and locating metal loss and cracks. ASME International Pipeline Conference, IPC2002-27267.

Rosenfeld, M. J. (2002). Pipeline integrity management & risk evaluation: A review of methodologies. Pipeline Pigging, Integrity Assessment and Repair Conference, Houston.

Shuai, Y., Shuai, J., & Xu, K. (2017). Probabilistic analysis of corroded pipelines based on a new failure pressure model. Engineering Failure Analysis, 81, 216-233.

Souza, L. T., & Murray, D. W. (1999). Prediction of wrinkling in pipelines with girth welds. Structural Engineering Report No. 222, University of Alberta, Edmonton.

Sun, Q., & Stiles, J. (2017). Distributed fiber-optic sensors for pipeline monitoring: A review. Optical Engineering, 56(3), 030901.

Xie, M., & Tian, Z. (2018). Risk-based pipeline re-assessment optimization considering corrosion defects. Sustainable Cities and Society, 38, 746-757.

Xiao Tian*, H. Z., s.d. College of Mechanical and Transportation Engineering, China University of Petroleum, Beijing 102249, China. *Engineering Failure Analysis.*